

Alexander Steiner, BSc

Scalable Photochemistry using LEDs

Implementing Hydrogen Atom Transfer Catalysis for Rapid and Selective
Reductive Photoredox Transformations in Continuous Flow

MASTER'S THESIS

to achieve the university degree of

Master of Science

Master's degree programme: Chemistry

Submitted to

Graz University of Technology

Supervisor:

Univ.-Prof. Mag. Dr.rer.nat. C. Oliver Kappe

University of Graz, Institute of Chemistry

Center for Continuous Flow Synthesis and Processing (CC FLOW)

Graz, August 2019

This work has been published in:

European Journal of Organic Chemistry

**Implementing Hydrogen Atom Transfer (HAT) Catalysis for Rapid and Selective
Reductive Photoredox Transformations in Continuous Flow**

Alexander Steiner, Jason D. Williams, Juan A. Rincon, Oscar De Frutos, Carlos
Mateos, and C. Oliver Kappe

DOI: [10.1002/ejoc.201900952](https://doi.org/10.1002/ejoc.201900952)

AFFIDAVIT

I declare that I have authored this thesis independently, that I have not used other than the declared sources/resources, and that I have explicitly indicated all material which has been quoted either literally or by content from the sources used.

The text document uploaded to TUGRAZonline is identical to the present master's thesis.

Date

Signature

Acknowledgment

The CCFLOW Project (Austrian Research Promotion Agency FFG No. 862766) is funded through the Austrian COMET Program by the Austrian Federal Ministry of Transport, Innovation and Technology (BMVIT), the Austrian Federal Ministry of Science, Research and Economy (BMWFW), and by State of Styria (Styrian Funding Agency (SFG)).

Content

1. Abstract	1
2. Introduction	2
2.1 The Early Days of Photochemistry	2
2.2 Photochemical Transformations	3
2.2.1 Photophysical processes	4
2.2.2 Light Sources	5
2.3 Photochemistry in Flow	6
2.3.1 Light Penetration	6
2.3.2 Further advantages of flow chemistry	7
2.4 Photoredox Transformations.....	9
2.4.1 Photoredox Catalysts	11
2.4.2 Formation and Use of Aryl Radicals	12
2.5 Aim of the Thesis.....	14
3. Results and Discussion.....	15
3.1 Combining PC and HAT Catalysis	15
3.2 Reaction Optimisation	17
3.2.1 Design of Experiment (DoE) Study	19
3.3 Substrate Scope Dehalogenations	24
3.3.1 Mono Dehalogenations.....	24
3.3.2 Comparison of the Photocatalysts: PTH vs Np-PTH	29
3.3.3 Double Dehalogenations.....	30
3.4 Further Reactions	34
3.4.1 Pinacol couplings.....	34
3.4.2 Reductive styrene coupling	35
3.5 Mechanistic Studies	36

3.5.1	Fluorescence Quenching Studies.....	36
3.5.2	Deuterium Incorporation	39
3.5.3	Kinetic Isotope Effect.....	40
3.5.4	Proposed Mechanism.....	41
4.	Conclusion.....	43
5.	Experimental	44
5.1	General Information.....	44
5.1.1	Flow Reactor Setup	45
5.1.2	General Procedure 1 for Scoping Experiments in Flow	47
5.1.3	General Procedure 2 for Isolation Experiments in Flow	48
5.1.4	General Procedure 3 for Batch Reactions	49
5.2	Catalyst Synthesis	50
5.3	Substrate Synthesis	51
5.4	Pinacol Coupling Reactions.....	52
5.5	Reductive Styrene Coupling	54
6.	References	55
7.	Appendix	59
7.1	Abbreviations.....	59
7.2	Calibration Data for HPLC Assays.....	60
7.3	NMR Spectra	64

1. Abstract

Aryl radicals are key intermediates in many synthetic transformations and their formation is a crucial step in the reaction protocols. Aryl halides are readily available and stable precursors, but require strongly reducing conditions. A photoredox catalytic approach, using an organic dye as photocatalyst, is favourable due to mild reaction conditions and a metal free protocol. Continuous flow technology enables the scale up of photochemical transformation but still requires sufficiently short reaction times in order to be practically useful. Since the currently available batch protocols for reductive transformations of aryl halides require reaction times of hours to days, a thiol-based hydrogen atom transfer catalyst was combined with the highly reducing photocatalyst. The resulting reactions were rapid and highly selective, reducing aryl bromides and even aryl chlorides in reaction times as short as 1 minute. Additionally, selectivity between mono- and di-dehalogenation could be achieved by modification of residence time and light intensity. Furthermore, aromatic aldehydes, ketones and imines were shown to readily undergo pinacol couplings when applying this photocatalytic reductive protocol. Finally, a coupling of an aryl chloride with a styrene was also successful.

Aryl Radikale sind wichtige Zwischenprodukte in vielen Synthesen und die Bildung dieser ist dabei ein entscheidender Schritt in den Reaktionsprotokollen. Arylhalogenide sind stabile und leicht verfügbare Ausgangsmaterialien, allerdings sind stark reduzierende Bedingungen notwendig, um daraus Radikale zu bilden. Ein photoredoxkatalytischer Ansatz, bei dem organische Farbstoffe als Katalysatoren verwendet werden, ist im Hinblick auf mildere Reaktionsbedingungen und ein metallfreies Protokoll von Vorteil. Durchflusschemie ermöglicht die Skalierung der photochemischen Umwandlung, es sind jedoch ausreichend schnelle Reaktionszeiten notwendig, damit diese praktisch nützlich sein kann. Die derzeit verfügbaren Batchprotokolle für reduktive Umwandlungen von halogenierten Aromaten erfordern Reaktionszeiten von Stunden bis Tagen. Daher wurde ein Wasserstoffatomtransferkatalysator auf Basis eines Thiols mit dem stark reduzierenden Photokatalysator kombiniert. Das Ergebnis sind schnelle und hochselektive Reaktionen, bei denen bromierte und sogar chlorierte Aromaten in Reaktionszeiten von nur 1 Minute reduziert wurden. Durch Modifikation von Verweilzeit und Lichtintensität konnte eine Selektivität zwischen einfacher und vollständiger Dehalogenierung erreicht werden. Das photochemische Protokoll ermöglichte darüber hinaus die Pinakol-Kupplung von aromatischen Aldehyden, Ketonen und Iminen. Mit Hilfe dieser Methode gelang außerdem eine bislang literaturunbekannte Kupplung zwischen einem Arylchlorid und einem Styrol.

2. Introduction

2.1 The Early Days of Photochemistry

About 3 400 000 EJ of solar energy reach the earth's surface per year, and the sun has directed all forms of life since its beginnings.^[1,2] Plants and some other organisms have mastered transforming the harvested light energy into chemical energy via photosynthesis, nature's most significant light-driven process. However, mankind still has to seek ways for using solar energy -and other renewable sources of energy- more efficiently and to a larger extent.^[1,3]

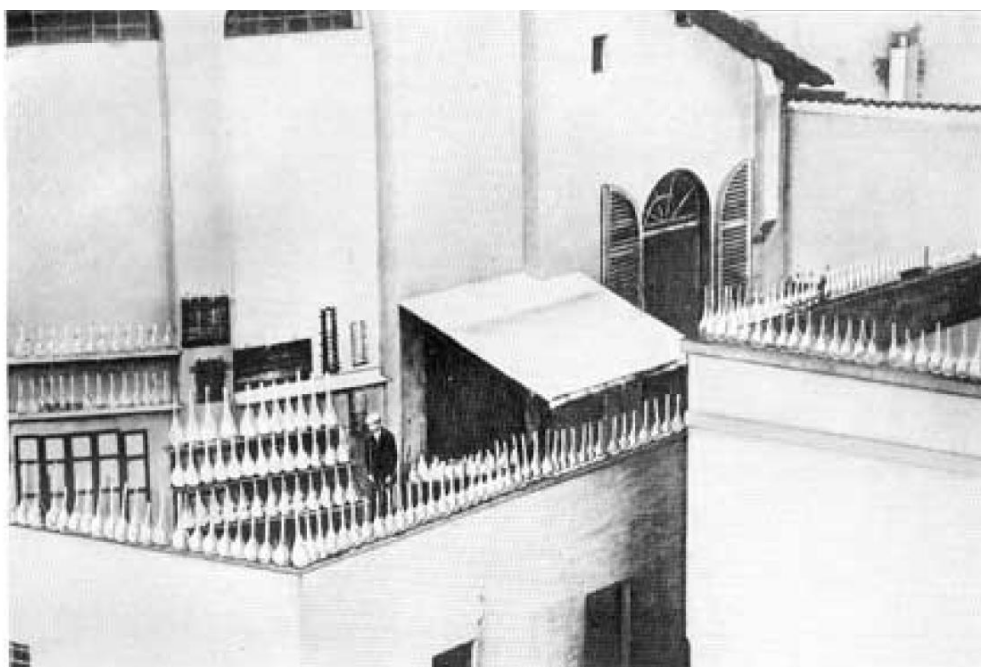


Figure 1. Giacomo Ciamician on his "rooftop laboratory" in Bologna.^[4]

In organic chemistry, light has only relatively recently been used to drive reactions.^[5] Heinrich Klinger was the first chemist to observe and further investigate such a reaction, which he published in 1886. He noticed the formation of a crystalline precipitate in a solution of benzil in ether when the solution was exposed to sunlight, whilst that did not happen if kept in the dark.^[6] He was also the first to observe a wavelength dependence of light driven reactions, by filtering the incident light with solutions of coloured inorganic salts, such as dichromate or copper(II) solutions.^[7] Another early example is the publication by Julian Schramm,^[8] who investigated the bromination of aromatic hydrocarbons, where bromination of the ring or the side chain can occur. He found, that exposing the reaction mixture to bright sunlight has the

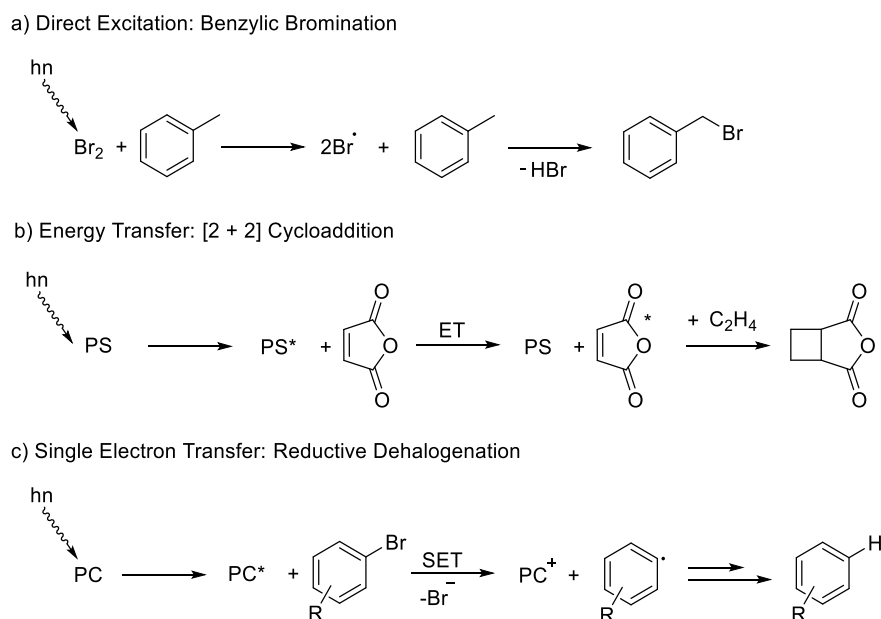
same effect as refluxing it, in both cases sidechain bromination takes place, whereas if the reaction is kept cold and not exposed to light, the aromatic ring is brominated.

As the last pioneer Giacomo Ciamician, who is shown in Figure 1, should be mentioned. He and Paul Silber investigated photochemical reactions very systematically and published them in a series of 37 articles in *Gazzetta Chimica Italiana* under the title “Azione Chimiche della Luce” and in *Berichte der Deutschen Chemischen Gesellschaft* under the title “Chemische Lichtwirkungen”. In 1912, in his famous lecture before the International Congress of Applied Chemistry in New York^[9] Ciamician did not only summarize the results of his photochemical investigations, but also addressed solar energy as an important and renewable source of energy in times where coal was the main energy source. He even ranked solar energy second after nuclear energy, which was at that time not yet accessible for mankind.

2.2 Photochemical Transformations

Meanwhile, more than 100 years after Ciamician’s visionary lecture, photochemistry has evolved as an important part of organic chemistry. A large number of valuable transformations have been discovered and therefore photochemistry is now established as a useful tool in complex synthetic plans. The general prerequisite for a photochemical transformation is that the incident photons must be absorbed by a photoactive species in the reaction mixture, thus the irradiation wavelength must overlap with the absorption spectrum of this species.^[10] This species could be a substrate (e.g. in a cycloaddition reactions^[11–13]) or a reagent, for example bromine in benzylic brominations as shown in Scheme 1a.^[14]

However, in many photochemical reactions, light is not absorbed directly by the reagent, because few organic chemicals absorb in the visible light range and the use of high energy UV light is in many cases detrimental. The higher the photon energy is, the more likely it is that side reactions are induced, and fouling might take place. Therefore, photocatalysts are often employed. Those photocatalysts are characterized by a very efficient photon absorption in the UV-VIS, or even in the infrared region.^[15] The absorbed photon energy is then used to activate the reagent or substrate, either by directly transferring the energy (Scheme 1b) to the reagent (energy transfer, ET) in which case the catalyst is often referred to as photosensitizer (PS), or via a single electron transfer (Scheme 1c) in which case it is called photoredox catalyst (PC).^[10,16] The latter mechanism will be discussed in more detail in chapter 2.4.



Scheme 1. Selected examples of photochemical reactions. a^[14], b^[17], c^[18]

2.2.1 Photophysical processes

The photophysical processes behind a catalysed photochemical reaction are shown in the state energy diagram (Jablonski diagram) in Figure 2. At the beginning of the process, the photocatalyst is in its ground state S_0 , and the highest occupied molecular orbital (HOMO) is occupied by two electrons. Upon absorption of a photon whose energy matches the HOMO-LUMO gap, the PC gets to its excited state S_1 where one electron is promoted to the LUMO. This electron can then fall back to the HOMO emitting light (fluorescence) or via the non-radiative internal conversion (IC) process. However, those two processes are not useful if we want to use the photon's energy for a chemical transformation. If the excited state has a long enough lifetime for the PC to interact with the substrate, the photochemical reaction can proceed. Alternatively, by intersystem crossing (ISC), when the spin configuration of one electron changes, the PC can also get into the triplet state. From there it again can fall back into the ground state via the radiative (phosphorescence) and non-radiative (IC) pathway, but it can also interact with a substrate to drive the reaction, although having a different energy and redox potential.^[19]

By knowing the properties of the photocatalyst, one can design a photochemical systems which permits unique reaction pathways that would not be possible under thermal control.^[16] Important characteristics are the absorption spectrum, the lifetime of the singlet and triplet

excited states, as well as the rate and quantum yield of ISC (τ_{ISC} and ϕ_{ISC}), and the corresponding redox potentials of the excited states.

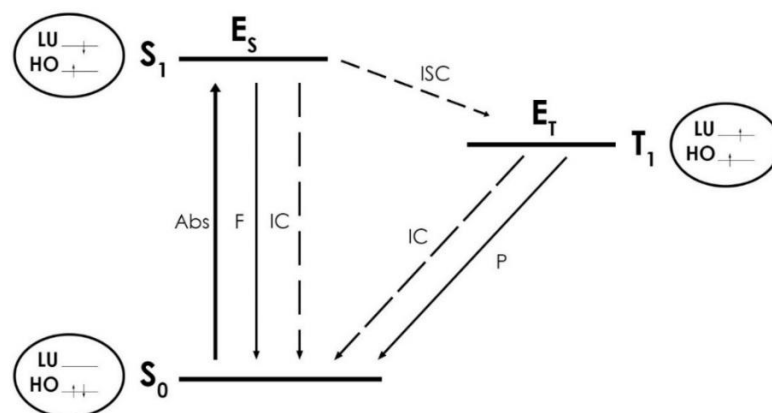


Figure 2. Simplified Energy State (Jablonski) diagram showing ground state (S_0), singlet (S_1) and triplet (T_1) excited state with their corresponding energies E_S and E_T as well as the electron configurations ($HO = HOMO$, $LU = LUMO$). The transitions between those states are radiative (solid lines): absorption of a photon (**Abs**), fluorescence (**F**) and phosphorescence (**P**) or non-radiative (dashed lines): internal conversion (**IC**) and intersystem crossing (**ISC**).^[19,20]

2.2.2 Light Sources

Compared to the early days of photochemistry, a broad variety of different light sources is now available. Photochemists can now choose which wavelengths and intensities they want to irradiate their reaction mixtures with, and they are no longer dependent on the sun's emission spectrum as well as the weather and seasonal changes. Nevertheless, the sun remains the greenest source of photons and chemists and engineers have found ways to even use sunlight in larger scale production of fine chemicals.^[21]

Table 1 gives an overview of the different available light sources used in photochemistry, with their emission wavelength and some properties. LEDs as photon sources should be especially highlighted. They are characterised as a narrow-band pseudo-monochromatic light source with a long lifetime. They are a very rapidly developing technology,^[22] LEDs emitting lower wavelengths at higher power enter the market frequently and they are starting to replace traditionally used light sources in photochemistry.^[14,23–27]

Table 1. Characterisation of various light sources used in photochemistry.^[28]

Light source	Emission wavelength λ	Note
Low pressure Hg Arc	> 90% emission at 254 nm, small fraction at 185 nm	
Medium pressure Hg Arc	prominent emission lines: 313, 366, 405, 550 nm	10-fold more intense than low pressure Hg arc
High pressure Hg Arc	continuum between 360-600 nm	expensive, short lifetime
Black light	360 nm (broad)	cheap
Lasers	discrete wavelengths	high intensity, expensive
UV-LEDs	400 nm and down to 310-320 nm ^[a]	high energy efficiency, long lifetime, expensive
Vis-LEDs	variety of wavelengths between 400-700 nm	high energy efficiency, long lifetime, cheap
Sunlight	5% UV, 43% Vis, 52% NIR	low and variable intensity, diffuse irradiation

^[a]Efficiency / radiant power drops off substantially below 365 nm.

2.3 Photochemistry in Flow

Although photochemical transformations are a versatile tool in organic synthesis, they come with a multitude of challenges, which may explain why the uptake of synthetic photochemistry in chemical research labs and industrial production has been fairly slow. Using photons in reactions increases the process complexity, requiring proper reactor design, which takes into account the compatibility of the light source and solvents as well as a more challenging scale-up.^[28,29]

2.3.1 Light Penetration

The main hurdle in scaling up a batch photochemical reaction is light penetration. Figure 3 illustrates how light is attenuated in a solution of different concentrations of $[\text{Ru}(\text{bpy})_3]\text{Cl}_2$, a

frequently used PC. In a solution containing 1 mM catalyst, the Beer-Lambert law estimates that 97% of the light is absorbed within the first millimetre, and more than 99.9% if the concentration is increased to 2.5 mM. This shows that even in a very small scale batch reaction most of the reaction mixture is not being irradiated. However, decreasing the catalyst concentration in many cases also reduces the reaction rate significantly. The solution to this problem can often be found by using flow technology.^[30]

For example the photoreactor used in this study (details see chapter 5.1.1, p.45) contains a reaction plate with a channel width (irradiated path length) of 0.3 mm and a total irradiated volume of 2.8 mL. Since the LEDs are mounted on both sides of the transparent plate, the effective irradiated path length to consider is only 0.15 mm. This means, that in the case of higher catalyst concentration (2.5 mM) about 28% of the incident light is being transmitted, ensuring that in most photochemical applications the reaction is not limited by inhomogeneous absorption of light.

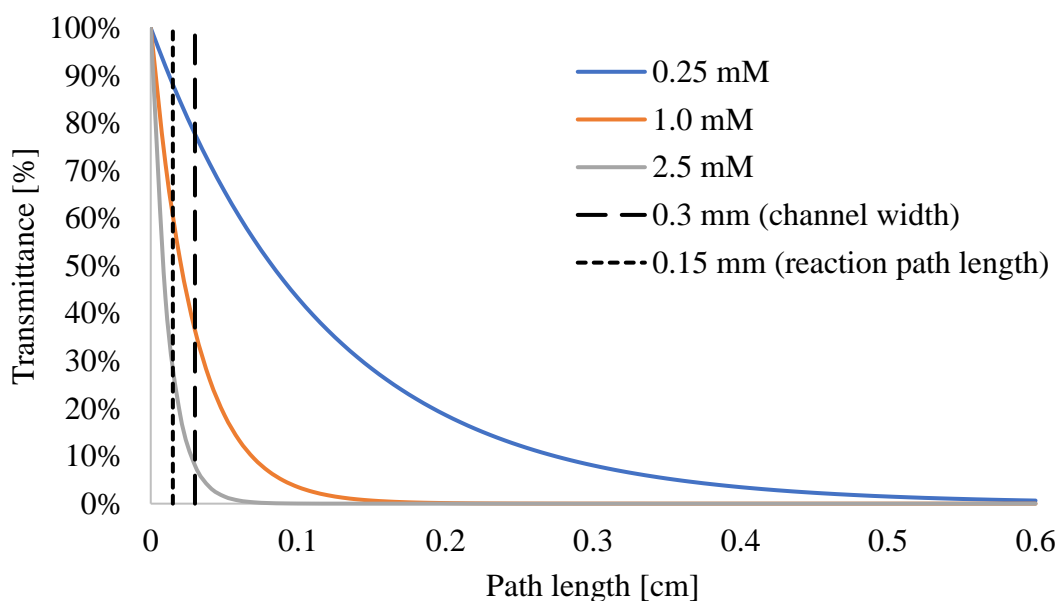


Figure 3. Transmittance of light in solutions of $[\text{Ru}(\text{bpy})_3]\text{Cl}_2$ in methanol ($\epsilon = 14600 \text{ M}^{-1} \text{ cm}^{-1}$)^[31] as a function of the path length l and concentration c , calculated using the Beer-Lambert law: $T = 10^{-\epsilon c l}$.

2.3.2 Further advantages of flow chemistry

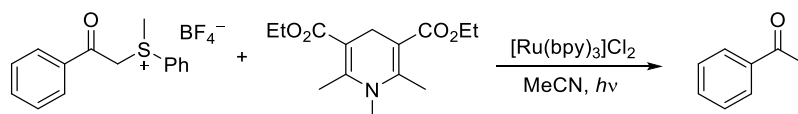
Aside from the excellent light penetrations properties, such a plate-based flow photoreactor comes with all the other advantages of flow chemistry as well. The reaction plate might contain mixing elements, such as the heart-shaped elements in the Corning® reactor (used in this study,

Figure 4). This is especially useful if biphasic reactions under photochemical conditions are performed. The interfacial area between the two phases, and therefore the mass transport, is significantly increased in such microfluidic systems, not only in liquid-liquid reactions but also gaseous reagents such as oxygen^[32] or ethylene^[17] can be easily handled and improved reactivity are often observed.^[30] Other advantages are the improved heat transfer and precise temperature control by using a thermostat and a heat transfer medium in such a plate. By applying pressure with a back pressure regulator (BPR) the solubility of gases can be increased and higher temperatures can be reached, even above the solvent boiling point.^[28] Scale-up of a photochemical reaction, even to production scale, is possible in continuous flow reactors. Corning for example produces, apart from the lab photoreactor reactor used in this study, two larger photoreactors, which combine the concepts of numbering up (using more modules) as well as increasing the size of the reaction plates. This scalability principle has previously been demonstrated for a photoreaction within the Kappe group.^[17]



Figure 4. Photograph of the reaction plate with heart-shaped mixing elements. Reaction channels highlighted in orange using aq. bromine solution.

2.4 Photoredox Transformations



Scheme 2. First organic reaction accelerated by a photoredox catalyst by Kellogg in 1978.^[33]

Although first publications on photoredox chemistry date back to 1978, when Kellogg showed that dyes such as Eosin Y and $[\text{Ru}(\text{bpy})_3]\text{Cl}_2$ accelerate the reductive desulfuration shown in Scheme 2, only in the late 2000s more chemists began to do investigations in this field (Figure 5).^[16] A broad variety of ruthenium and iridium based PCs have been developed as well as many different organic dyes which will be shown in chapter 2.4.1.

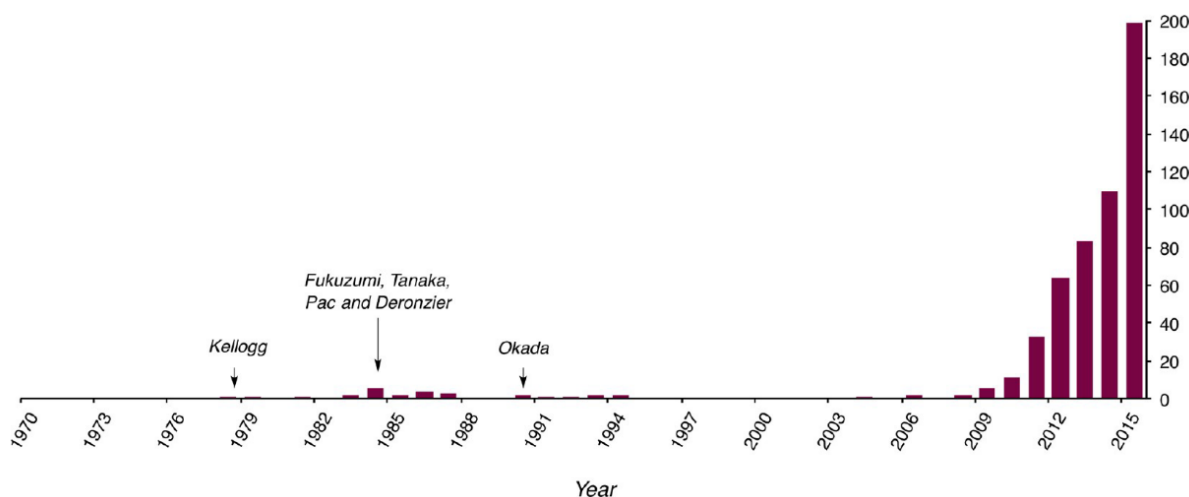
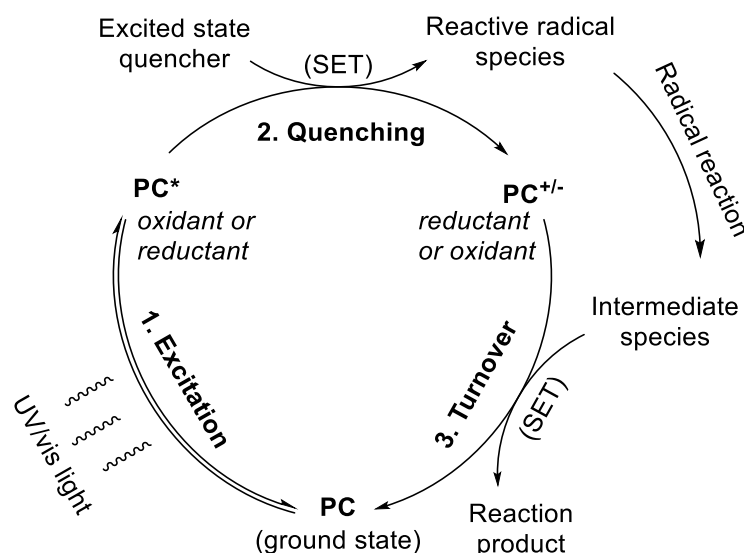


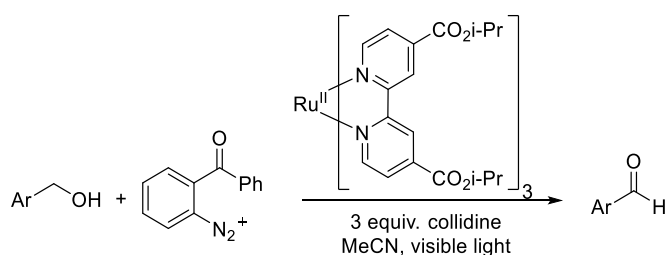
Figure 5. Publications about organic photoredox chemistry per year, reprinted from ACS Publications.^[16]

The catalytic cycle as illustrated in Scheme 3 consists of three different elementary reaction steps: **1.** Excitation of the PC by absorption of a photon, **2.** single electron transfer (SET) from or to the excited state of the PC (oxidative or reductive quenching) and **3.** the turnover step where the PC is reduced or oxidised back to its ground state. If the PC is being oxidised in the second step, by donating an electron to the excited state quencher (the substrate or an oxidant), the photocatalytic transformation proceeds via oxidative quenching and the PC is an excited state reductant. If the PC is being reduced in this step, by accepting an electron from the excited state quencher, the cycle proceeds via reductive quenching and the PC is an excited state oxidant.^[20]



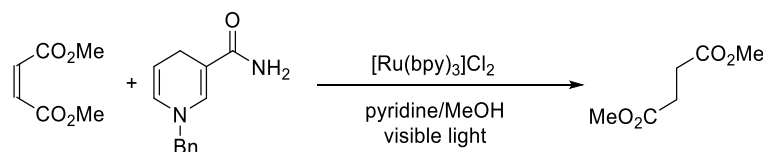
Scheme 3. Catalytic cycle of a photoredox catalyst including excitation (1) of the PC, quenching (2, either oxidative or reductive) and the turnover step (3) to bring the PC back to its ground state.^[20]

One can also distinguish by the overall outcome of the redox reaction between net reductive, net oxidative and net redox-neutral reactions.^[20,34] As shown in Scheme 3, if the substrate is being oxidised in either the quenching or the turnover step, and stoichiometric amounts of an oxidant are necessary, the reaction is net oxidative. One early example by Deronzier from 1984 is shown in Scheme 4, where the diazonium salt is used as the stoichiometric oxidant to oxidise a benzylic alcohol to the corresponding aldehyde employing a Ru(II) catalyst under visible light irradiation.^[35]



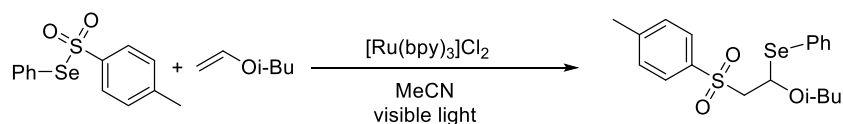
Scheme 4. Example of a net oxidative reaction: photocatalytic oxidation of a benzylic alcohol to the corresponding aldehyde.^[35]

In the second type of redox reactions, net reductive reactions, a stoichiometric reductant is used, and the PC transfers an electron in the quenching or the turnover step onto the substrate. In 1981, Pac and co-workers reduced electron poor olefins such as dimethyl maleate with $[\text{Ru}(\text{bpy})_3]\text{Cl}_2$ and a 1,4-dihydronicotinamide derivative as the reductant under visible light irradiation in analogy to nature's reducing agent NADH.^[36]



Scheme 5. Example of a net reductive reaction: reduction of dimethyl maleate using $[\text{Ru}(\text{bpy})_3]\text{Cl}_2$ and 1-benzyl-1,4-dihydropyridin-2(1H)-one to yield dimethyl succinate.^[36]

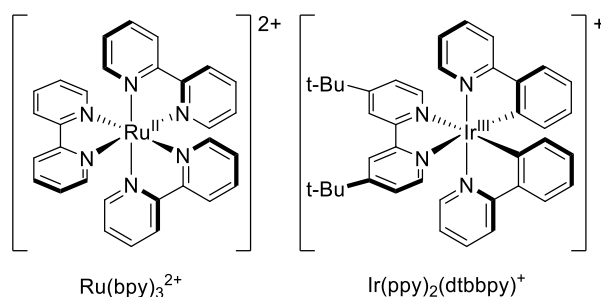
In net redox-neutral reactions, the substrate exchanges an electron in the quenching, then a subsequently formed intermediate undergoes the complimentary redox process in the turnover step. One example is the atom transfer radical addition (ATRA reaction). Barton and co-workers showed in 1994 that tosylphenyl selenide can be added to alkyl vinyl ethers using $[\text{Ru}(\text{bpy})_3]\text{Cl}_2$ under visible light irradiation as shown in Scheme 6.^[37]



Scheme 6. Example of a net redox-neutral reaction: ATRA of tosylphenyl selenide to vinyl isobutyl ether.^[37]

2.4.1 Photoredox Catalysts

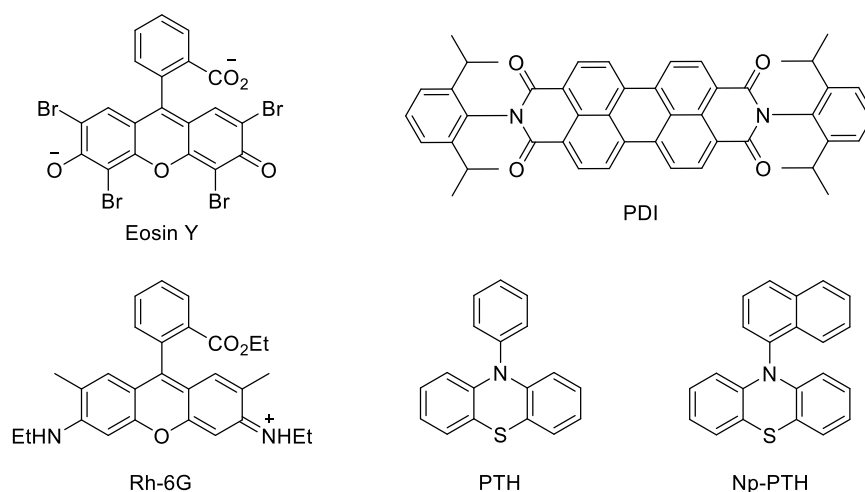
Photoredox catalysts (PCs) can be divided in two different classes: metal-based and organic PCs. The transition metals ruthenium and iridium are most common and polypyridyl ligands, most prominently bipyridyl or 2-phenylpyridyl ligands, can easily be derivatised to fine tune their photochemical properties. Scheme 7 shows two examples of metal-based PCs, first the extensively used $[\text{Ru}(\text{bpy})_3]^{2+}$, and second an iridium catalyst containing a derivatised bipyridyl ligand as well as two 2-phenylpyridyl ligands.^[34]



Scheme 7. Examples of two metal-based PCs, $[\text{Ru}(\text{bpy})_3]^{2+}$ and $[\text{Ir}(\text{ppy})_2(\text{dtbbpy})]^+$.

Organic PCs, on the other hand, are not only a metal-free alternative, they also possess potent reactivity enabling unique transformations by reacting with a wide range of substrates that

might not be accessible in other chemical contexts. Organocatalysts are generally significantly cheaper than their metal counterparts, however, their excited state lifetimes are often shorter and they are more prone to side reactions. There is a broad variety of organic dyes available: xanthene dyes such as Eosin Y and Rhodamine 6G, perylene diimide (PDI) derivatives and phenothiazine based catalysts, for example *N*-phenylphenothiazine (PTH) and *N*-(1-naphthyl)-phenothiazine (Np-PTH) as shown in Scheme 8.^[20]



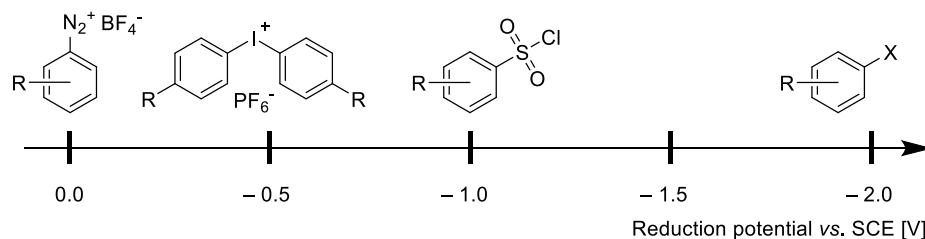
Scheme 8. Examples of organic PCs: Eosin Y, Rhodamine 6G (Rh-6G), 2,6-diisopropylperylene diimide (PDI), *N*-phenylphenothiazine (PTH) and *N*-(1-naphthyl)-phenothiazine (Np-PTH).

2.4.2 Formation and Use of Aryl Radicals

A frequently used key step in organic synthesis is the introduction of (hetero)aryl groups and in 2010 Heck, Negishi and Suzuki were honoured with the Nobel Prize in Chemistry “for palladium-catalysed cross couplings in organic synthesis”.^[38] Nevertheless, the required metal catalysts, ligands and higher temperatures can sometimes be problematic. Hence, photocatalytic protocols employing organic dyes under mild conditions have received significant attention as a complementary synthetic method.^[39,40]

Table 2. Excited state reduction potentials of the PCs shown in Scheme 8.^[20,41,42]

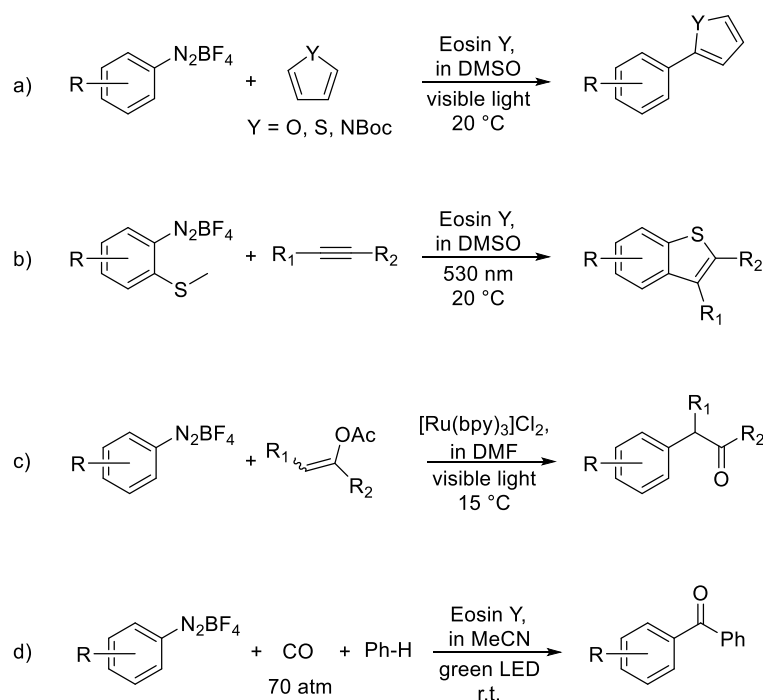
PC	Eosin Y	Rh-6G	PDI	PTH	Np-PTH
$E_{1/2}(\text{PC}^+/\text{PC}^*)$ [V] vs SCE	-1.15	-1.09	-0.72	-2.10	-2.23



Scheme 9. Precursors for the reductive formation of aryl radicals according to their redox potential.^[39]

The formation of (hetero)aryl radicals through reduction of suitable precursors is sometimes necessary to perform such arylation reactions. Various precursors have been studied already, most commonly diazonium salts.^[39,43] Diazonium salts can be reduced easily by a variety of different metal and organic catalysts (compare Table 2) due to their low redox potential close to 0 V vs SCE.^[20,44] However, their highly reactive nature can also be problematic: the starting materials themselves can be unstable, and radical chain mechanisms are often believed to be at play, potentially harming reaction selectivity. Diazonium salts are commercially available but expensive and are usually synthesized in the laboratory and stored at low temperature. Selected examples of photoredox reactions starting from diazonium salts are shown in Scheme 10. König et al. for example reported the direct C–H arylation of various heteroarenes using Eosin Y under visible light irradiation shown in Scheme 10a.^[45] Benzothiophenes (Scheme 10b) can be prepared by trapping the aryl radical with an alkyne, followed by the intramolecular reaction of the intermediate vinyl radical with the sulfur atom which, upon oxidation and demethylation, gives the final product.^[46] Ketones can be formed, for example, by addition of the aryl radical to terminal enol acetates as in Scheme 10c^[47] or by trapping the aryl radical with carbon monoxide to form an acyl radical which further reacts with different (hetero)arenes as shown in Scheme 10d.^{[48][39]}

Molecules containing other functional groups, such as diaryliodonium salts, triarylsulfonium salts, or arylsulfonyl chlorides, can also be used as starting materials, but are often not commercially available.^[39] Aryl halides, on the other hand, are bench stable and readily available reaction precursors. The challenge for using them is their much higher reduction potential^[49] as illustrated in Scheme 9, and in most cases more complex systems are required. König et al. take advantage of catalyst activation by two consecutive photoinduced electron transfer (PET) events^[50–54] using PDI or Rh-6G as PCs, additional hydrocarbon “energy acceptor”^[55] or catalyst complexation by lanthanide salts^[56].



Scheme 10. Selected examples of photoredox reactions starting from diazonium salts: a) Direct C–H arylation of heteroarenes;^[45] b) Synthesis of benzothiophenes by photoannulation;^[46] c) Formation of ketones from terminal enol acetates;^[47] d) Formation of ketones using carbon monoxide^[48].

2.5 Aim of the Thesis

Recently, highly reducing organic photocatalysts have been synthesised, which are capable of directly reducing aryl halides.^[18,57] The phenothiazine based catalyst PTH reaches an excited state reduction potential of -2.1 V vs SCE,^[18,42,58] enabling reactions that were previously unachievable by the most reducing catalysts available.^[59,60] The problem still remains that these transformations are generally extremely slow, often requiring reaction times of several days.

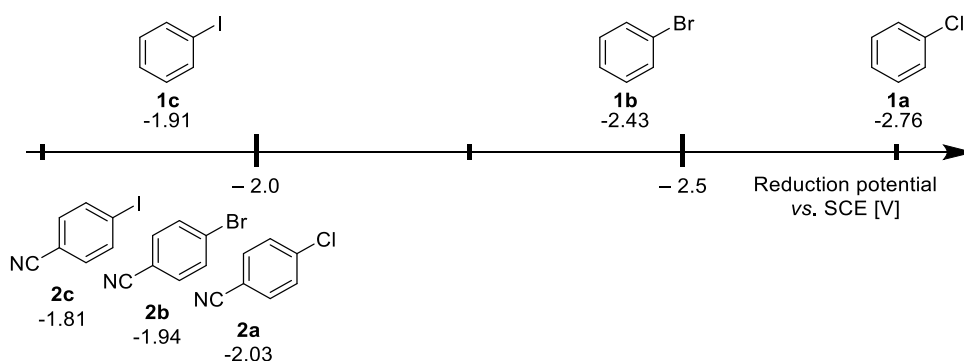
As discussed in the previous chapters, flow chemistry has been demonstrated as a valuable tool for photochemical transformations enabling the scale-up of photochemistry, which is unachievable in batch. To achieve a usable level of productivity, though, relatively short residence times are required, highlighting the importance of fast reaction kinetics.^[17,61–63]

Therefore, the aim of this thesis is the development and continuous flow application of an organic photoredox catalyst system, by combining PTH, a highly reducing organic photoredox catalyst and cyclohexanethiol, a hydrogen atom transfer (HAT) catalyst, to enable reductive transformations of aryl halides and carbonyls with high selectivity and reaction rate.

3. Results and Discussion

3.1 Combining PC and HAT Catalysis

Photocatalytic reductions of aryl halides are usually very slow. The general trend of reactivity, that aryl iodides are much easier to reduce than aryl bromides and chlorides, is reflected in their reduction potential as illustrated in Scheme 11. From an economic point of view however, chlorides are favoured as precursors due to their lower cost as well as the lower mass of waste produced (atomic mass of Cl: 35/37 u vs. Br: 79/81 u and I: 127 u).



Scheme 11. Reduction potential of selected aryl halides vs. SCE [V].^[64]

De Alaniz and co-workers published the reduction of aryl iodides in 1 to 24 hours, aryl bromides in 9 to 48 hours and aryl chlorides in 24 to 72 hours.^[18] Such long reaction times for aryl chloride reductions are impractical in continuous flow processes and a hydrogen atom transfer (HAT) catalyst was implemented to accelerate the reaction, analogous to what has been shown by the group of Jui.^[59,65] Indeed, as Figure 6 shows, the reaction is complete within 30 min, whereas without the HAT catalyst it takes more than 4 hours to complete. Moreover, the initial rate is five times higher upon addition of 5 mol% of cyclohexanethiol (CySH). This enhanced reaction was then transferred into a continuous flow protocol. Since gas formation was observed (presumably CO₂ formed from the formic acid), a back pressure of 3.5 bar was applied to keep the CO₂ in solution, avoiding cavitation which would lead to shortened and unknown reaction times and irreproducible results.

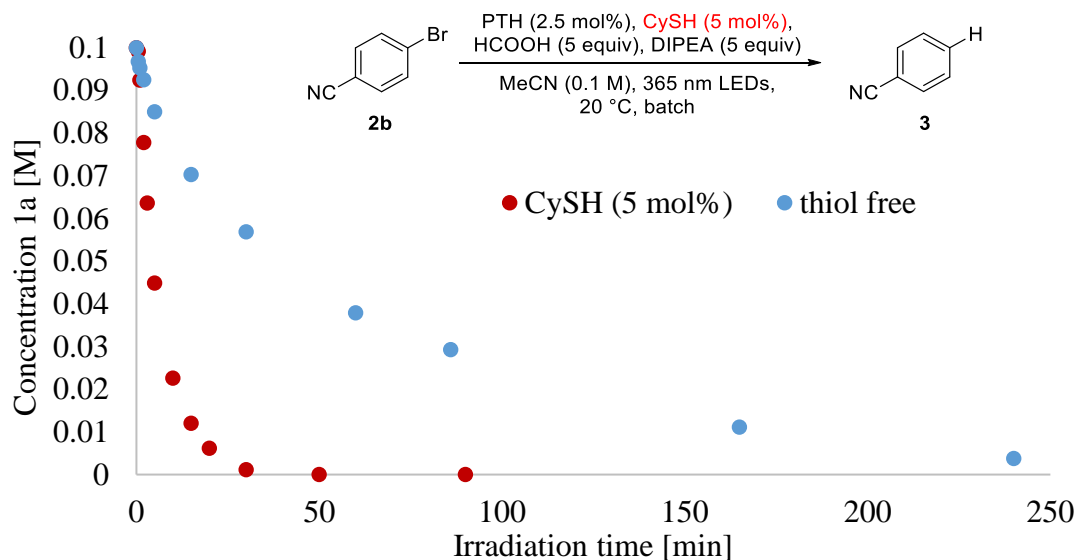


Figure 6. Time course demonstrating the increase in rate observed upon incorporating CySH (5 mol%) into the reaction mixture.

Comparing the reduction of 4-bromobenzonitrile **2b** under differing conditions (Table 3, entries 1 vs. 3 and 2 vs. 4) the reactions were significantly faster in flow than in the batch protocol. This improvement can be explained by the advantages of flow chemistry as described in chapter 2.3, especially by the enhanced light penetration. While the batch reactions yielded 98% product in 30 minutes, the reaction was complete in only 1 minute in the flow reactor, giving 97% yield. The reaction without the HAT catalyst was also accelerated, from 96% yield in 4 hours to 87% yield in 30 minutes. All yields were determined by HPLC analysis vs an internal standard, calibration curves are given in the appendix. Changing to the more challenging substrate, 4-chlorobenzonitrile **2a**, again a significantly faster reaction was observed. Without the CySH the reaction reached a yield of only 74% within 28 min residence time, which is the maximum achievable reaction time in the used flow reactor set-up (minimum accurate flow rate = 0.1 mL/min). With CySH, 96% yield was obtained in only 3 minutes residence time. This reaction took 72 hours to yield 94% in the literature protocol.^[18] Comparing the catalyst loading (entries 7 - 9) no significant reduction of yield was observed when the PTH loading was reduced from 5 to 2.5 mol%, but further reduction to 1 mol% decreased the yield to 57%. Therefore, 2.5 mM concentration of photocatalyst was chosen for the further optimisation experiments.

Table 3. Comparison of reductive dehalogenation using **2a** and **2b** with and without cyclohexanethiol (CySH) under batch and continuous flow conditions.

Entry	Compound	Reaction time [min]	Deviation from standard conditions	Yield 3a ^[a] [%]
1	2b	30	batch ^[b]	98
2	2b	240	batch, no CySH ^[b]	96
3	2b	1	none	97
4	2b	15	No CySH	87
5	2a	3	none	96
6	2a	28	No CySH	74
7	2a	1	none	78
8	2a	1	2.5 mol% PTH	75
9	2a	1	1 mol% PTH	57

^[a]Reported yields were determined by HPLC, calibrated against an internal standard. ^[b]Reaction carried out with 2.5 mol% PTH photocatalyst.

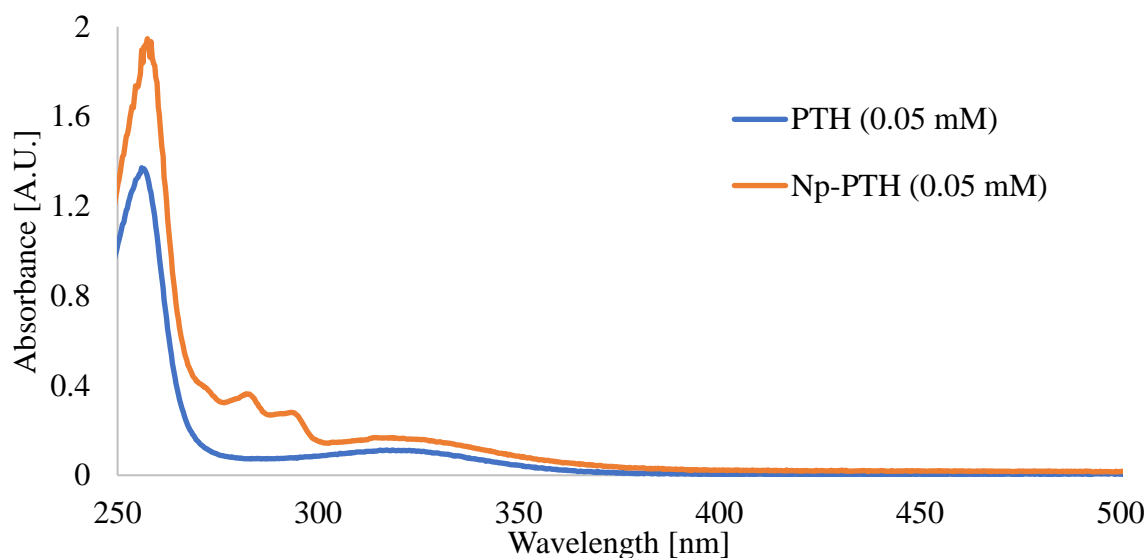
3.2 Reaction Optimisation

The reaction optimisation started with a screening of different irradiation wavelengths. 5 sets of LEDs ranging from 365 nm to 610 nm were available as well as white light LEDs. Table 4 summarizes the results of this screening, including one reaction where the LED power was set to 50%. The results are in perfect agreement with the absorption spectrum of PTH which is shown in Figure 7. The reaction works well when 365 or 385 nm UVA-LEDs are used, but when visible light LEDs are used the yield drops, to 51% at 405 nm, whereas at 485 or 610 nm the reaction did not proceed. In the case of reducing the light intensity to 50% only a moderate decrease in yield was observed. Although this was surprising at first, estimation of the light absorbance using the Beer-Lambert law showed that only 10 to 20% of the incident light is absorbed in the reaction medium, depending on whether 2.5 or 5 mol% of the catalyst is used (see Table 5). Therefore, it can be assumed that the reaction is not operating in a light-limited kinetic regime.

Table 4. Wavelength screening.

	<chem>N#Cc1ccc(Cl)cc1</chem> 2a $\xrightarrow[\text{MeCN (0.1 M), X nm LEDs, 20 }^\circ\text{C, 3.5 bar, } t_{\text{Res}} = 1 \text{ min, flow}]{\text{PTH (2.5 mol\%), CySH (5 mol\%), HCOOH (5 equiv), DIPEA (5 equiv)}}$ <chem>N#Cc1ccc(H)cc1</chem> 3					
Wavelength [nm]	365	365 ^[b]	385	405	485	610
Yield ^[a] [%]	78	64 ^[b]	75	51	no conv.	no conv.

^[a]Yield was determined by HPLC assay vs internal standard (biphenyl). ^[b]50% LED power.

**Figure 7.** UV/vis absorption spectra of PTH and Np-PTH catalysts.**Table 5.** Estimation of the light absorption at different catalyst loadings, using the Beer-Lambert law.

Catalyst loading [mol%]	Catalyst concentration [M]	Percentage of light absorbed in flow reactor
1	0.0001	4.2%
2.5	0.00025	10.3%
5	0.0005	19.5%

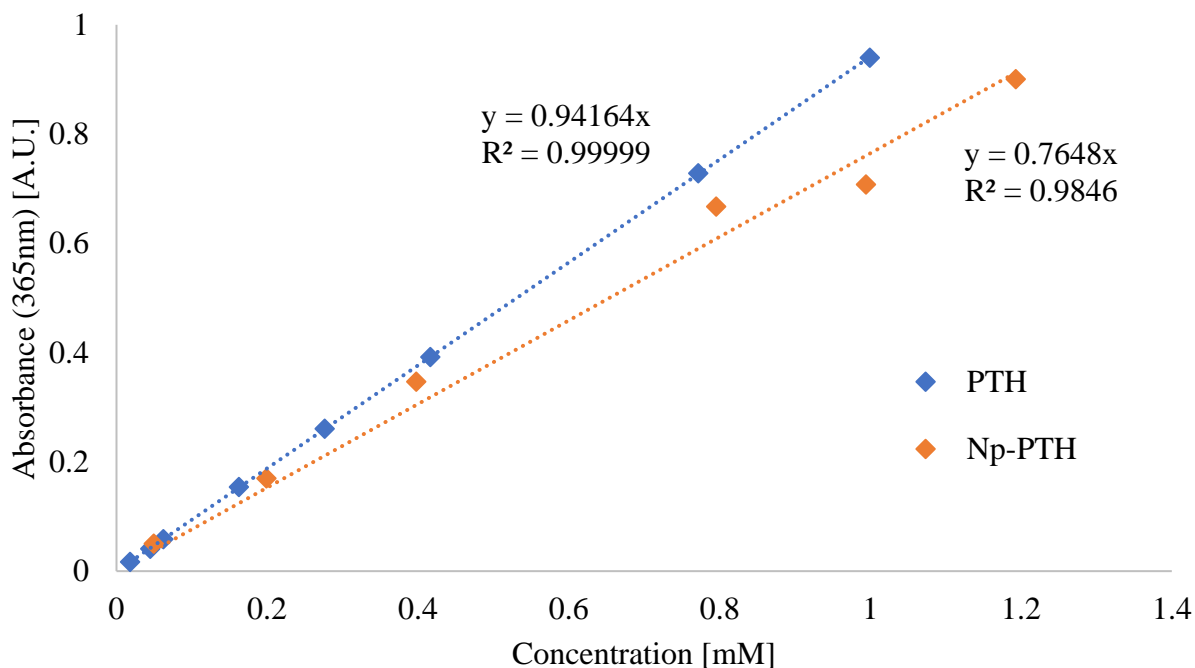


Figure 8. Plot of absorption at 365 nm vs concentration, for the determination of molar extinction coefficients (ϵ) for both PTH and Np-PTH catalysts in MeCN. Calculated extinction coefficients: $\epsilon_{(\text{PTH})} = 941.64 \text{ M}^{-1} \text{ cm}^{-1}$; $\epsilon_{(\text{Np-PTH})} = 764.8 \text{ M}^{-1} \text{ cm}^{-1}$.

3.2.1 Design of Experiment (DoE) Study

Since the conditions regarding the PC concentration and optimal irradiation had been established, the next step was the fine tuning of the reaction conditions and reagent loadings. To achieve this, a DoE study was performed. A factorial design, with three variables and 4 replicates of the centre point, was chosen and the order was randomised (see Table 6). The exact conditions as well as the experimental results are tabulated in Table 7.

Overall, the DoE study provided an excellent linear model. The results of the DoE are shown in Figure 9 and three trends can be extracted from the data: A higher thiol loading as well as a higher HCOOH/DIPEA loading are favourable whilst a higher substrate concentration gives lower yields. To further quantify those trends, the influence of the single factors as well as their products is plotted in Figure 10. According to this graph, the concentration has the highest influence on the yield, but the contribution is negative, which means lowering the concentration results in higher yields. The DIPEA/HCOOH loading as well as the CySH concentration have a positive contribution, the first one is significant while the latter has only minor contribution. The linear model fits the data perfectly, model statistics such as a R^2 of 0.9981, Q^2 of 0.9867, the model validity of 0.5543 and the reproducibility = 0.9985 which are shown in Figure 11 underscore that. The plot of the deleted studentised residuals (Figure 12) further shows that

none of the experimental data points can be considered an outlier. Figure 13 shows a near-perfect agreement between the observed and predicted results.

To summarise the study, the reaction works best under high DIPEA/HCOOH loading, high CySH loading and low substrate concentration, but to perform the reaction under practically favourable reaction conditions, the current conditions of 5 equivalent DIPEA/HCOOH, 5 mol% CySH and a concentration of 0.1 M were maintained.

Table 6. Design matrix for the DoE study.

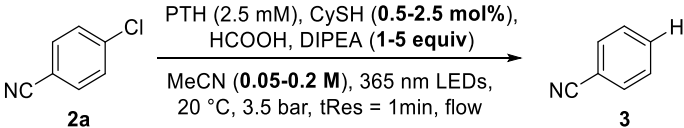
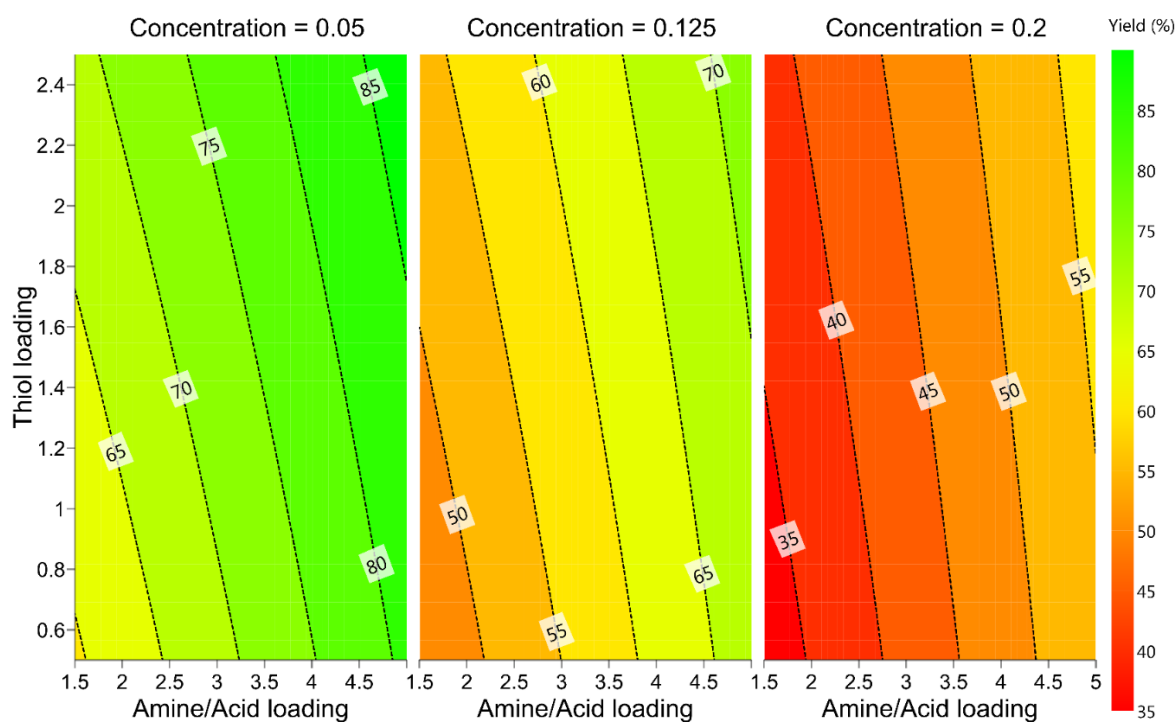
				
Experiment number	DIPEA/HCOOH loading [equiv]	Conc. [M]	CySH loading [mol%]	
1	-1	-1	1	
2	0	0	0	
3	1	-1	-1	
4	1	-1	1	
5	-1	1	-1	
6	1	1	1	
7	-1	-1	-1	
8	0	0	0	
9	1	1	-1	
10	0	0	0	
11	-1	1	1	
12	0	0	0	

Table 7. Conditions and results of the experiments run in the DoE study.

Entry	DIPEA/HCOOH loading [equiv]	Conc. [M]	CySH loading [mol%]	Yield ^[a]
1	1.5	0.05	2.5	69.6
2	3.25	0.125	1.5	59.0
3	5	0.05	0.5	81.1
4	5	0.05	2.5	87.0
5	1.5	0.2	0.5	32.5
6	5	0.2	2.5	58.1
7	1.5	0.05	0.5	59.6
8	3.25	0.125	1.5	58.6
9	5	0.2	0.5	54.2
10	3.25	0.125	1.5	59.3
11	1.5	0.2	2.5	37.8
12	3.25	0.125	1.5	60.0

^[a]Yield calculated by HPLC assay vs internal standard (biphenyl).

**Figure 9.** Contour plot showing the model's predicted yield under the examined conditions.

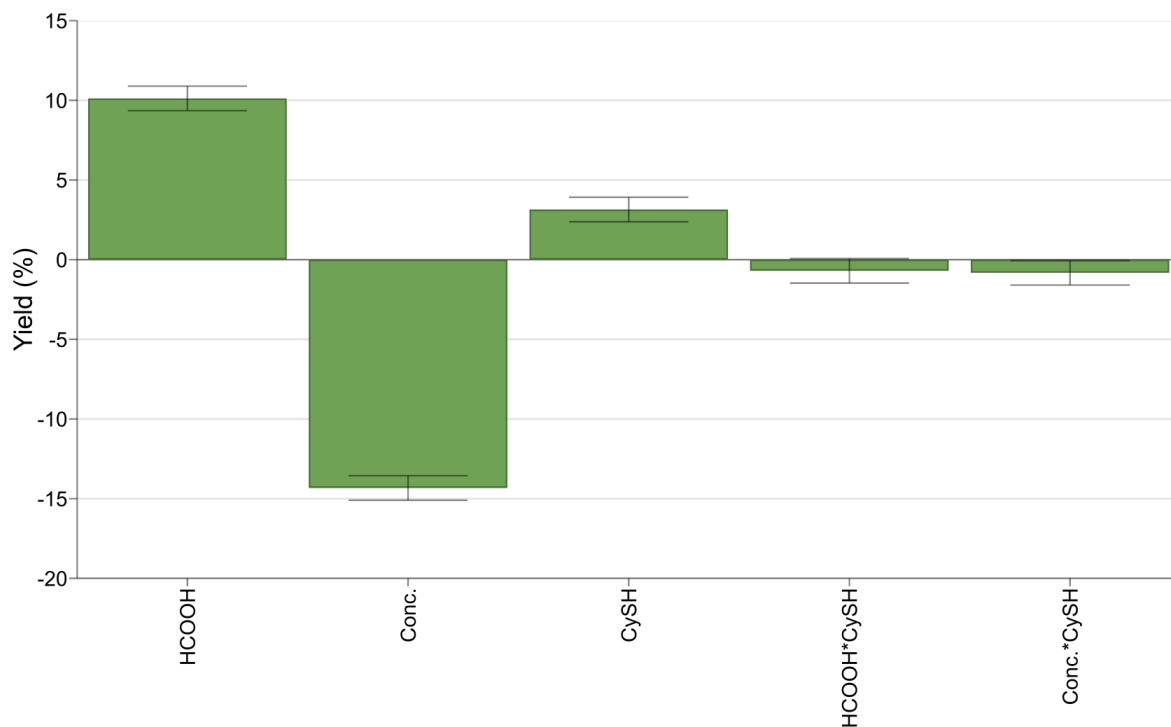


Figure 10. Plot showing the positive and negative contributions of each factor. HCOOH/DIPEA loading = significant positive; Concentration = significant negative; CySH loading = minor positive. 2-factor effects are insignificant

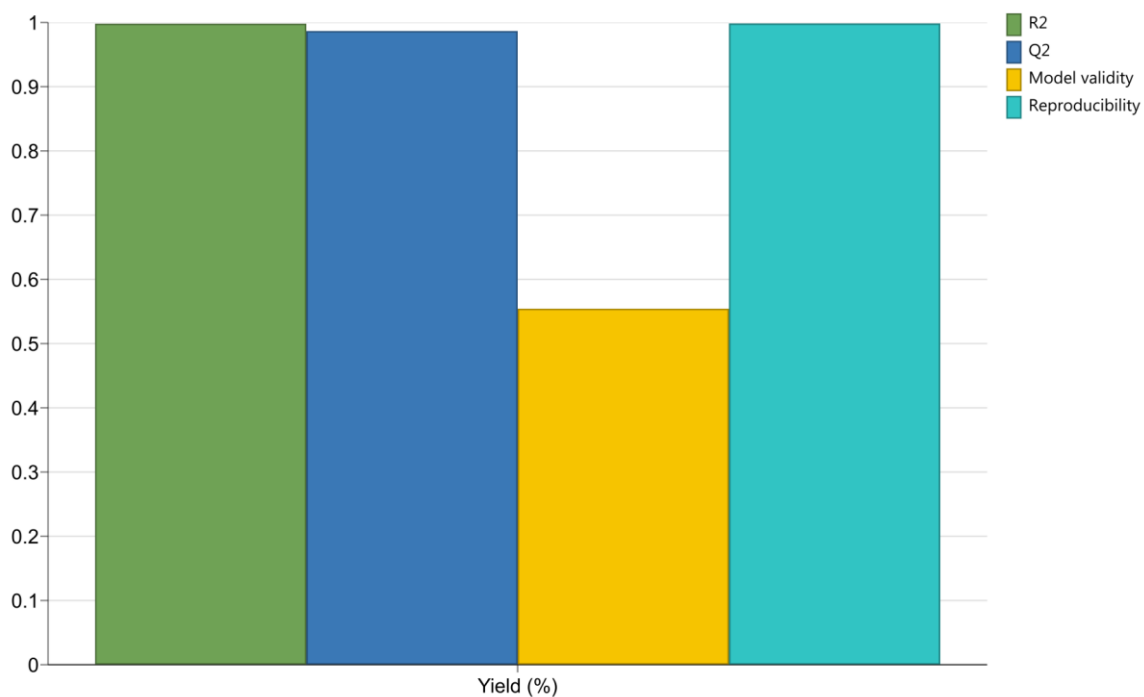


Figure 11. Plot showing the summary of the model statistics. $R^2 = 0.9981$; $Q^2 = 0.9867$; Model validity = 0.5543; Reproducibility = 0.9985. **Note:** "Model validity should be greater than 0.25 for a model free of statistically significant problems".

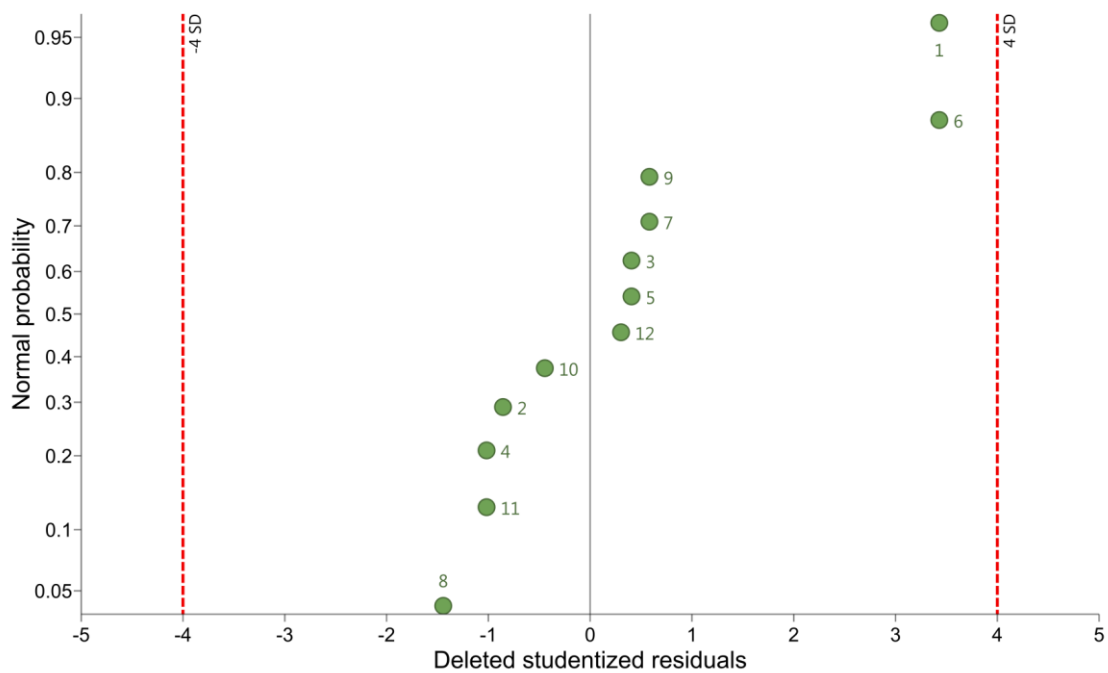


Figure 12. Plot of deleted studentised residuals, showing that none of the experimental points can be considered to be outliers.

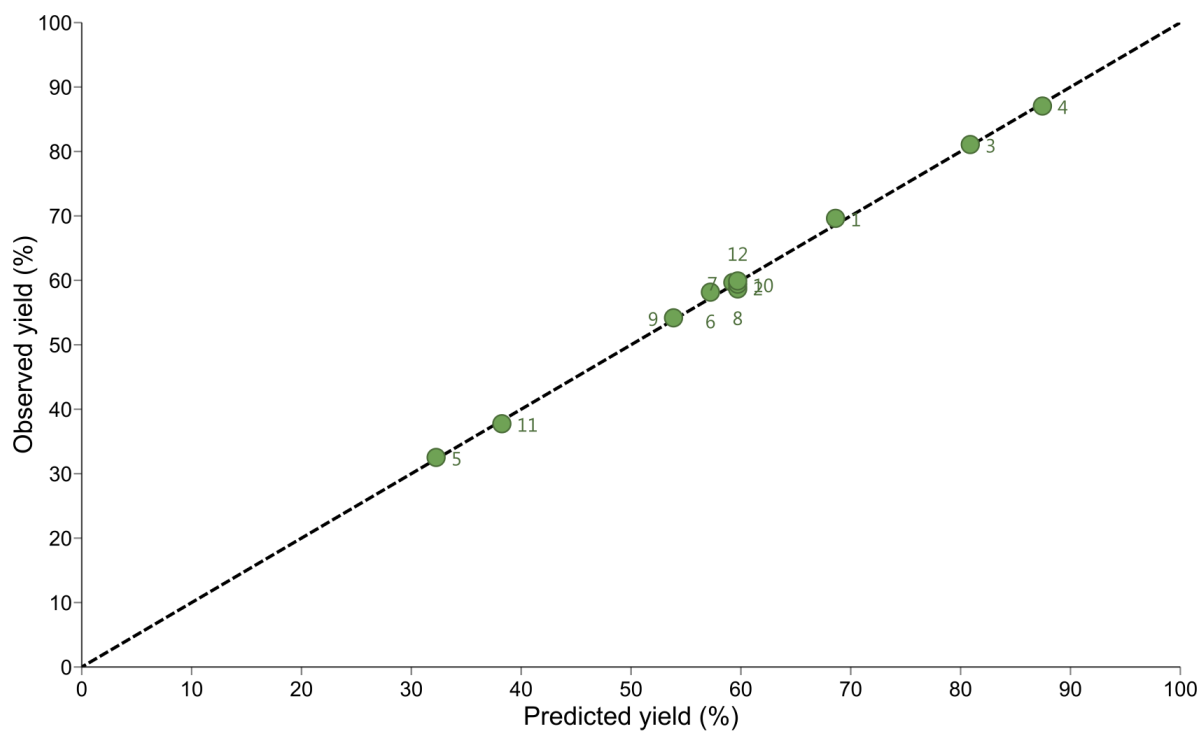
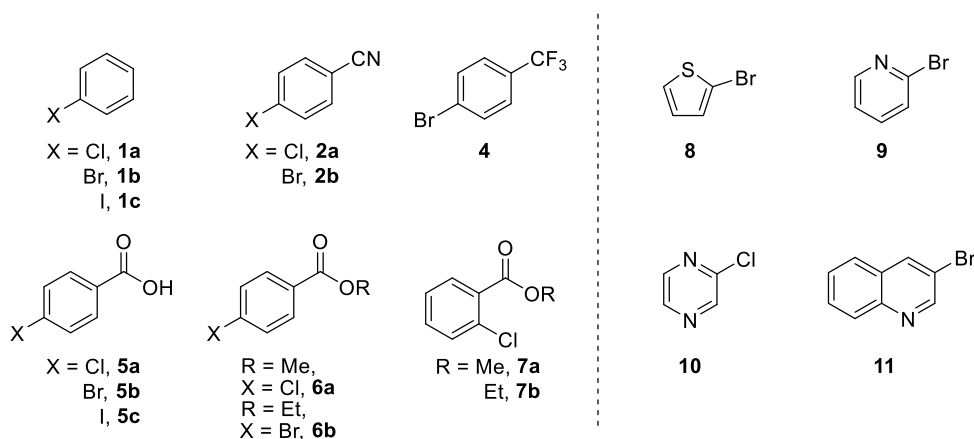


Figure 13. Graph of the model predicted yield versus observed yield in the experiments performed. The close fitting to the straight line observed here implies excellent agreement of the model with the experimental results.

3.3 Substrate Scope Dehalogenations

3.3.1 Mono Dehalogenations

Having the optimum conditions in hand, the reaction scope was investigated. An overview is given in Scheme 12.



Scheme 12. Overview of the substrate scope for mono dehalogenation reactions.

First, several aryl halides, including chlorides, bromides and iodides were tested. Not surprisingly, only iodobenzene **1c** of the group of unsubstituted aryl halides (Table 8, entries 1-3) was reactive when using the PTH catalyst. Using bromobenzene **1b** less than 5% conversion and in the case of the chlorobenzene **1a** no conversion was observed at all. Looking again at the data given in Table 2 and Scheme 11, namely the reduction potential of the excited state PTH (-2.10 V vs SCE) and the reduction potentials of **1c** (-1.91 V vs SCE), **1b** (-2.43 V vs SCE) and **1a** (-2.76 V vs SCE), it is apparent that PTH should only be able to reduce **1c** but not the other derivatives. Surprisingly, de Alaniz et al.^[18] reported the reduction of **1b** with PTH in 85% yield in 72 hours.

The second iodide, iodobenzoic acid **5c** (entry 9), also showed quantitative conversion in just 1 minute. Substituted aryl bromides, such as the model substrate **2b** and the para-substituted ester **6b** (entries 5 and 11) showed excellent yields in 1 and 5 minutes residence time whilst the p-trifluoromethylbromobenzene **4** and p-bromobenzoic acid **5b** (entries 6 and 8) were dehalogenated only with some success, yielding about 60% of the corresponding products in 28 minutes residence time. Interestingly, p-chlorobenzoic acid **5a** gave a higher yield of 83% in 28 minutes. Other chloride-containing substrates that were dehalogenated successfully were

the o- and p-chloro esters **6a**, **7a** and **7b** which yielded 94 to 99% in 1 to 3 minutes (entries 10, 12-13).

Some of those substrates can again be compared to literature, for example the methyl p-chloro benzoate **6a** (98% in 1 minute vs 94% in 72 hours) or the p-chlorobenzoic acid **5a** (83% in 28 minutes vs 62% in 72 hours).^[18]

Table 8. Substrate scope: mono dehalogenations of aryl halides.

Entry	Compound	R	X ₁	X ₂	Residence time	Yield ^[a]
1	1a	H	Cl	H	10 min	no conv.
2	1b	H	Br	H	10 min	<5% conversion
3	1c	H	I	H	1 min	99%
4	2a	-CN	Cl	H	3 min	96% ^[b]
5	2b	-CN	Br	H	1 min	97% ^[b]
6	4	-CF ₃	Br	H	28 min	63%
7	5a	-CO ₂ H	Cl	H	28 min	83% ^[c]
8	5b	-CO ₂ H	Br	H	28 min	59% ^[c]
9	5c	-CO ₂ H	I	H	1 min	98% ^[c]
10	6a	-CO ₂ Me	Cl	H	1 min	98%
11	6b	-CO ₂ Et	Br	H	5 min	99%
12	7a	-CO ₂ Me	H	Cl	1 min	94%
13	7b	-CO ₂ Et	H	Cl	3 min	99%

^[a]Yield was determined by HPLC assay vs internal standard (biphenyl). ^[b]For this reaction 5 mol% PTH loading was used. ^[c]For this reaction 6 equiv HCOOH was used.

Figure 14 shows the influence of the residence time on the dehalogenation of **5b** where the yield increased steadily to 59% over 28 minutes. Figure 15 illustrates details on the reaction of **5c**, showing that the reaction is not complete in 30 seconds and that quantitative yield is obtained in 1 and 5 minutes residence time. More interesting are the time courses given in Figure 16. The dehalogenations of the chloro and bromo esters **6a**, **7a** and **7b** get to a point of quantitative yield and conversion, but if irradiated for a longer time the yields drop, which might indicate reduction of the ester moiety.

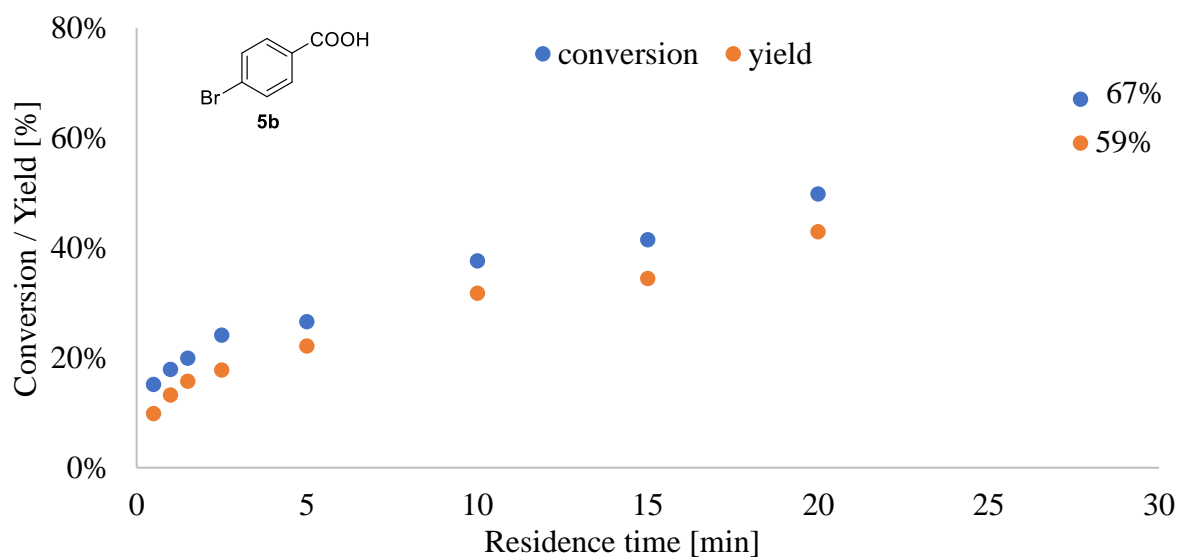


Figure 14. Graph showing the influence of residence time on the dehalogenation of 4-bromobenzoic acid **5b**. Yield was determined by HPLC assay vs internal standard (biphenyl).

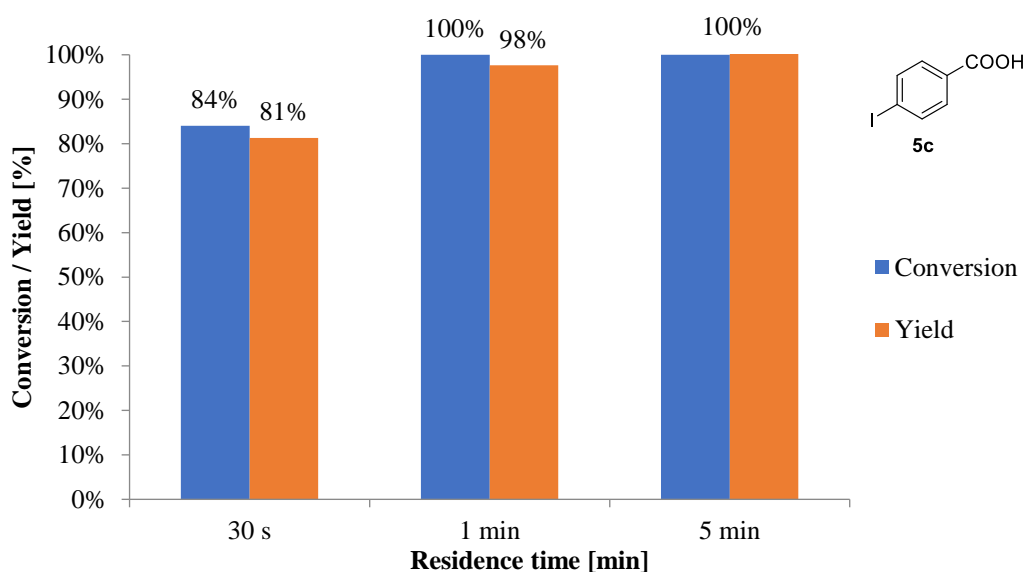


Figure 15. Influence of the residence time on the dehalogenation of 4-iodobenzoic acid **5c**. Yield was determined by HPLC assay vs internal standard (biphenyl).

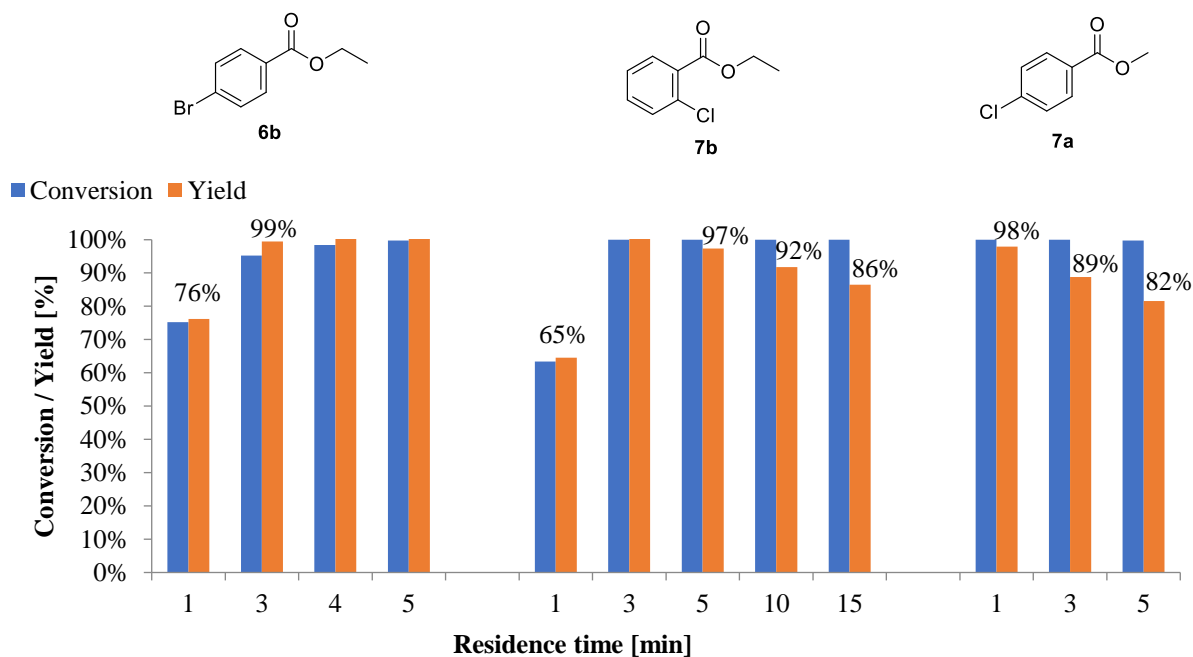
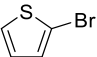
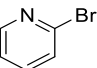
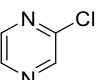
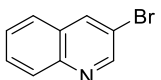


Figure 16. Graph showing the influence of residence time on the dehalogenation of bromo and chloro benzoates **6b**, **7b** and **7a**. Yield was determined by HPLC assay vs internal standard (biphenyl).

Also the mono dehalogenation of heteroaryl halides was attempted as shown in Table 9. 2-bromothiophene **8** (entry 1) was also reduced with some success, yielding 81% in 28 minutes. 2-bromopyridine **9** and 2-chloropyrazine **10** (entries 2 and 3) could not be reduced with this system. 3-bromoquinoline **11** (entry 4) was successfully reduced with quantitative yield in 5 minutes, the corresponding time course is shown in Figure 17, especially interesting because its product quinoline could also be reduced according to its reduction potential of -2.08 V vs SCE.^[66]

Table 9. Substrate scope: mono dehalogenations of heteroaryl halides.

		PTH (2.5 mol%), CySH (5 mol%), HCOOH (5 equiv), DIPEA (5 equiv) MeCN (0.1M), 365 nm LEDs, flow, 20 °C, 3.5 bar		
Het-X		→ Het-H		
Entry	Compound	Structure	Residence time	Yield
1	8		28 min	81% ^[a]
2	9		5 min	< 15% conversion ^[b]
3	10		15 min	< 10% conversion ^[b]
4	11		5 min	99% ^[a]

^[a]Yield was determined by HPLC assay vs internal standard (biphenyl). ^[b]Conversion was determined by HPLC: remaining starting material compared with initial, versus internal standard (biphenyl).

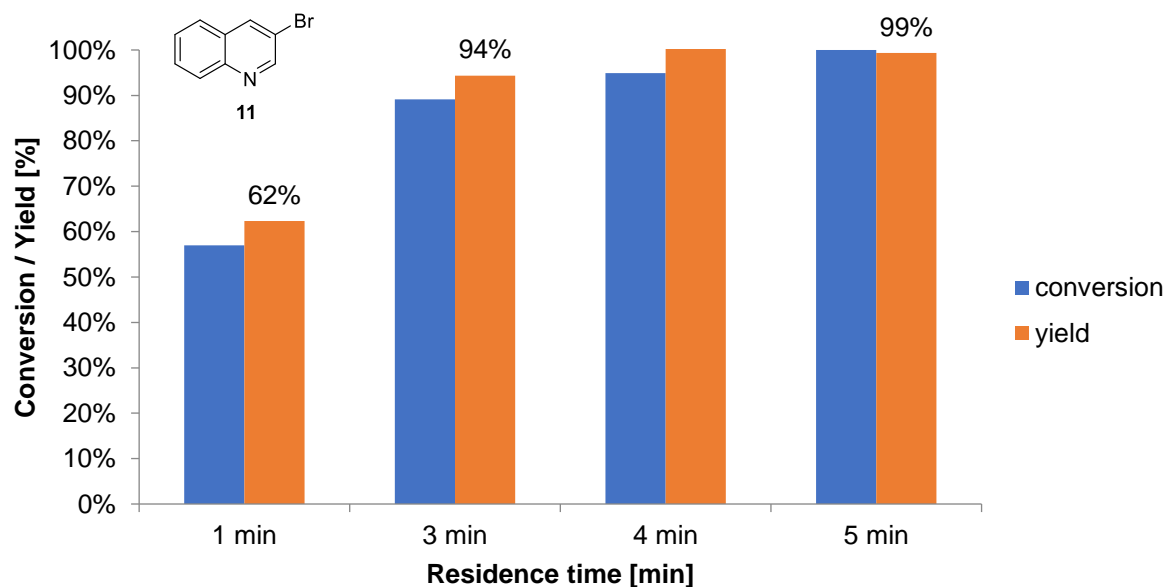
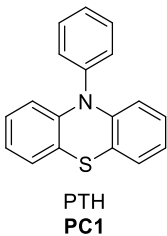
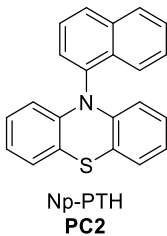
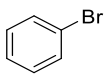
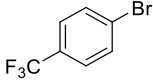
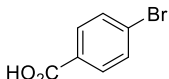
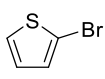


Figure 17. Graph showing the influence of residence time on the dehalogenation of 3-bromoquinoline **11**. Yield was determined by HPLC assay vs internal standard (biphenyl).

3.3.2 Comparison of the Photocatalysts: PTH vs Np-PTH

As mentioned above, the main issue in these reactions was the reduction potential of the substrates being too high for the chosen PC. However, the reduction potential of a certain PC can be modified by altering its structure. In the case of PTH (**PC1**) a promising derivative is Np-PTH (**PC2**), where the phenyl moiety is exchanged by a naphthyl group, which increases the reduction potential from -2.10 to -2.23 V vs SCE as has been shown in literature.^[59] Using this more potent catalyst, four challenging substrates were chosen for further investigations listed in Table 10: bromobenzene **1b**, p-trifluoromethylbromobenzene **4**, p-bromobenzoic acid **5b** and 2-bromothiophene **8**. As suggested by the reduction potential, **1b** (entry 1) showed only slightly better results, because its reduction potential is still much higher than the catalysts'. The other three substrates however showed significantly improved results. **4** was reduced in 96% yield in 20 minutes (entry 2) without cleaving C-F bonds (as shown to be possible by Wang and co-workers).^[59] **5b** was reduced in 96% yield in only 10 minutes (entry 3) and **8** was reduced in 90% yield in 20 minutes. Figure 18 directly compares the reaction time dependence of the reduction of **8** using PTH or Np-PTH.

Table 10. Comparison between the photocatalysts PTH and Np-PTH.

		 PTH PC1				 Np-PTH PC2	
Residence time	Yield ^[a]	Compound	Structure	Yield ^[a]	Residence time		
10 min	<5% conv.	1b		14%	15 min ^[b]		
28 min	63%	4		96%	20 min		
28 min	59%	5b		96%	10 min		
28 min	81%	8		90%	20 min		

^[a]Yield was determined by HPLC assay vs internal standard (biphenyl or 4-ethylbiphenyl).

^[b]Increasing the residence time to 28 min did not improve the yield.

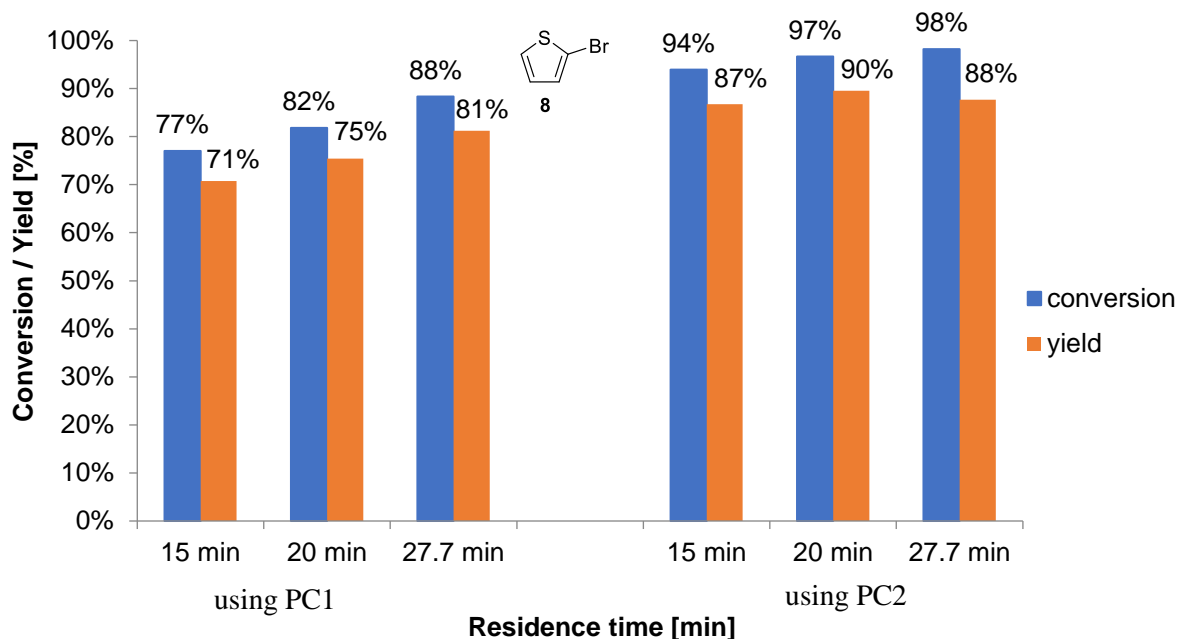


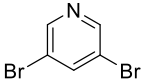
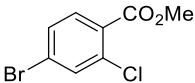
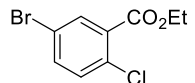
Figure 18. Influence of the residence time on the dehalogenation of 2-bromothiophene **8**. Yield was determined by HPLC assay vs internal standard (biphenyl).

3.3.3 Double Dehalogenations

Having already observed some reactivity differences between aryl chlorides and bromides, as well as the position of the halide on the ring, the selectivity of this dehalogenation protocol was tested on substrates containing two halogen atoms. Table 11 gives an overview of the three chosen substrates and the required conditions for selective mono dehalogenation (if achieved) and conditions for removal of both halogen atoms. In the case of the 3,5-dibromopyridine **12** (entries 1 and 2) removal of both bromine atoms could be achieved in 5 minutes residence time with 100% light power in 87% yield. However, if the residence time was reduced to 30 seconds and the light power to 25%, 3-bromopyridine could be selectively obtained with 91% yield.

Regarding the esters **13** and **14**, double dehalogenation could be achieved easily in 3 and 4 minutes residence time using 100% light power. When attempting to selectively cleave the Ar-Br bond, the difference in reactivity between the meta and para position becomes apparent. If the bromine atom is in the para position, as in compound **13**, selective dehalogenation could be achieved again by reducing the residence time to 30 seconds and the light power to 25%, as shown in entry 3. However, if the bromine atom is in the meta position, the reactivity is close to the reactivity of the chlorine in ortho position, and no selective debromination was observed (entry 5).

Table 11. Substrate scope: substrates containing two halogen atoms, including studies into selective monodehalogenation.

Entry	Substrate	Product	Residence Time / LED Power	Yield ^[a]
1		Ar-Br 19	0.5 min / 25%	91%
2	12	pyridine 10	5 min / 100%	87%
3		Ar-Cl 7a	0.5 min / 25%	91%
4	13	methyl benzoate 18	4 min / 100%	95%
5		Ar-Cl 7b	no selectivity, see Table 12 for details	
6	14	ethyl benzoate 16	3 min / 100%	84%

^[a]Yield was determined by HPLC assay vs internal standard (biphenyl or 4-ethylbiphenyl).

As shown in more detail in Table 12, selective dehalogenation could not be achieved, mixtures of the ethyl benzoate **16**, and its 2-chloro and 3-bromo derivatives (**7b** and **15**) were obtained. **Table 13** and **Table 14** show how the reaction was optimised to get the selective mono dehalogenation of **12** and **13** by reducing the residence time and light intensity, starting with the conditions of double dehalogenation. Additionally, reactions using only one equivalent of HCOOH and DIPEA to stop the reaction after removal of one halogen were examined. However, using 5 equivalents gives better selectivity whilst having a higher productivity due to the lower residence time.

Table 12. Detailed experimental results for the single- and double dehalogenation of dihalide **14**. Rows in bold are the results given in the overview above (Table 11).

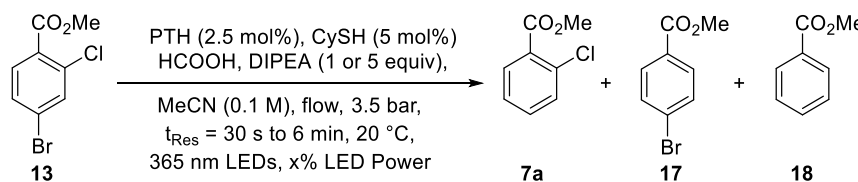
Reaction scheme showing the dehalogenation of dihalide **14** (1-bromo-4-chloro-2-ethoxycarbonylbenzene) to products **7b** (1-chloro-2-ethoxycarbonylbenzene), **15** (1-bromo-2-ethoxycarbonylbenzene), and **16** (ethyl benzoate). Reagents: PTH (2.5 mol%), CySH (5 mol%), HCOOH, DIPEA (1 or 5 equiv). Conditions: MeCN (0.1 M), flow, 3.5 bar, $t_{Res} = 30$ s to 3 min, 20 °C, 365 nm LEDs, x% LED Power.

Residence time	LED power	DIPEA + HCOOH	Conversion ^[a]	Yield		
				7b ^[b]	15 ^[b]	16 ^[c]
30 s	25%	5 equiv	100%	43%	25%	20%
1 min	10%	5 equiv	100%	44%	27%	18%
1 min	50%	5 equiv	100%	22%	5%	63%
1 min	100%	5 equiv	100%	13%	0%	77%
3 min	100%	5 equiv	100%	0%	0%	84%
1 min	100%	1 equiv	82%	30%	41%	5%
3 min	100%	1 equiv	91%	31%	47%	10%

^[a]Conversion was determined by remaining starting material **14**, compared with initial value, versus the internal standard (4-ethylbiphenyl). ^[b]Yield of products **7b** and **15** were determined by HPLC % Area.

^[c]Yield of product **16** was determined by HPLC assay vs internal standard (4-ethylbiphenyl).

Table 13. Detailed experimental results for the single- and double dehalogenation of dihalide **13**. Rows in bold are the results given in the overview above (Table 11).



Reaction conditions:
 PTH (2.5 mol%), CySH (5 mol%)
 HCOOH, DIPEA (1 or 5 equiv),
 MeCN (0.1 M), flow, 3.5 bar,
 t_{Res} = 30 s to 6 min, 20 °C,
 365 nm LEDs, x% LED Power

Residence time	LED power	DIPEA + HCOOH	Conversion	Yield ^[a]		
				7a	17	18
30 s	25%	5 equiv	94%	91%	<5%	1%
1 min	100%	5 equiv	100%	68%	<5%	30%
3 min	100%	5 equiv	100%	4%	<5%	89%
4 min	100%	5 equiv	100%	0%	<5%	95%
5 min	100%	5 equiv	100%	0%	<5%	96%
3 min	100%	1 equiv	85%	75%	<5%	1%
6 min	100%	1 equiv	86%	74%	<5%	1%

^[a]Conversion was determined by remaining starting material **13**, compared with initial value, versus the internal standard (4-ethylbiphenyl). ^[b]Yield of products **7a** and **17** were determined by HPLC %Area.

^[c]Yield of product **18** was determined by HPLC assay vs internal standard (4-ethylbiphenyl).

Table 14. Detailed experimental results for the single- and double dehalogenation of dihalide **12**. Rows in bold are the results given in the overview above (Table 11).

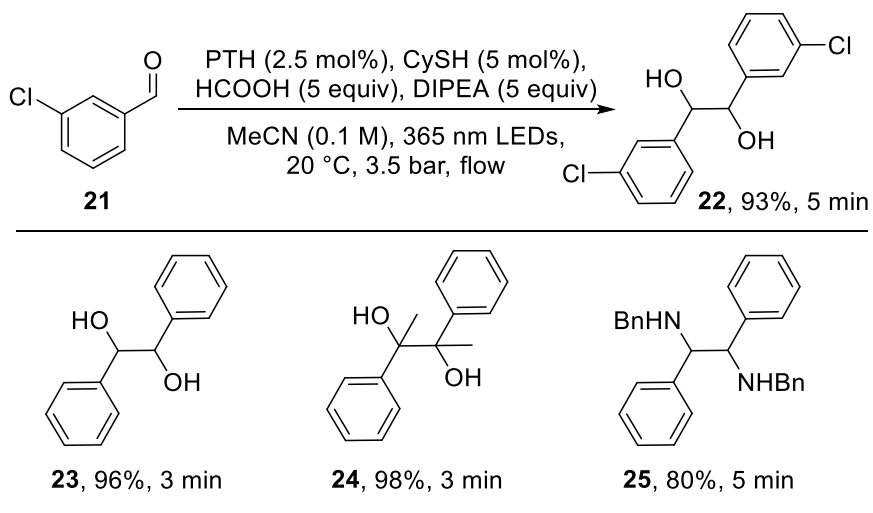
Residence time	LED power	Conversion ^[a]	Yield ^[b]	
			19	20
30 s	25%	81%	79%	7%
30 s	50%	100%	50%	50%
1 min	100%	100%	12%	88%
5 min	100%	100%	2%	98%

^[a]Conversion was determined by remaining starting material **12**, compared with initial value, versus the internal standard (biphenyl). ^[b]Yield of products **19** and **20** were determined by HPLC assay vs internal standard (biphenyl).

3.4 Further Reactions

3.4.1 Pinacol couplings

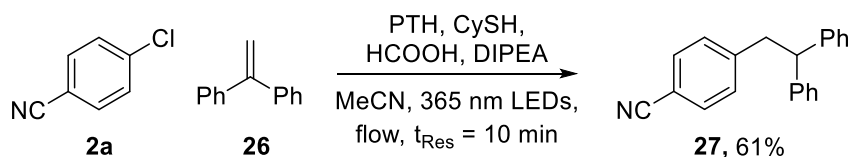
When analysing the substrate scope published by de Alaniz and co-workers^[18] it was observed that no aldehydes or ketones were included. Indeed, when reduction of 3-chlorobenzaldehyde **21** was attempted, instead of the desired benzaldehyde, the pinacol coupling product **22** was obtained. This was not unexpected behaviour since the redox potentials of aryl aldehydes and ketones (e.g. benzaldehyde $E_{1/2} = -1.93$ V vs SCE and acetophenone $E_{1/2} = -2.11$ V vs SCE)^[49] suggest direct reduction of the carbonyl group by the catalyst. Taking advantage of this reactivity, three more substrates were reduced, including an aromatic aldehyde, ketone and imine with complete selectivity and excellent isolated yields in residence times of only 3 to 5 minutes as shown in Scheme 13. This protocol is a significant improvement upon all previously reported photoredox pinacol couplings, which require much longer reaction times and provide lower yields.^[67–69]



Scheme 13. Pinacol couplings of aldehydes, ketones and imines. Isolated yields are shown.

3.4.2 Reductive styrene coupling

As discussed in some examples in the introduction, aryl radicals can also react with other functional groups, such as olefins. König and co-workers, for example, have shown such addition of aryl radicals to the styrene derivative **26** in reaction times of < 24 hours.^[51,55] The protocol presented in this work is capable of reducing the residence time to only 10 minutes, whilst maintaining a good yield of 61%.



Scheme 14. Reductive coupling of aryl chloride with a styrene derivative. Conditions: aryl chloride (0.85 mmol), 1,1-diphenylethylene (4.25 mmol), PTH (10 mol%), CySH (5 mol%), HCOOH (4.25 mmol), DIPEA (4.25 mmol), MeCN (0.1 M), 365 nm LEDs, 50 °C, conducted in flow with a 10 minute residence time, 3.5 bar back pressure, 0.85 mmol scale. Isolated yield is shown.

3.5 Mechanistic Studies

3.5.1 Fluorescence Quenching Studies

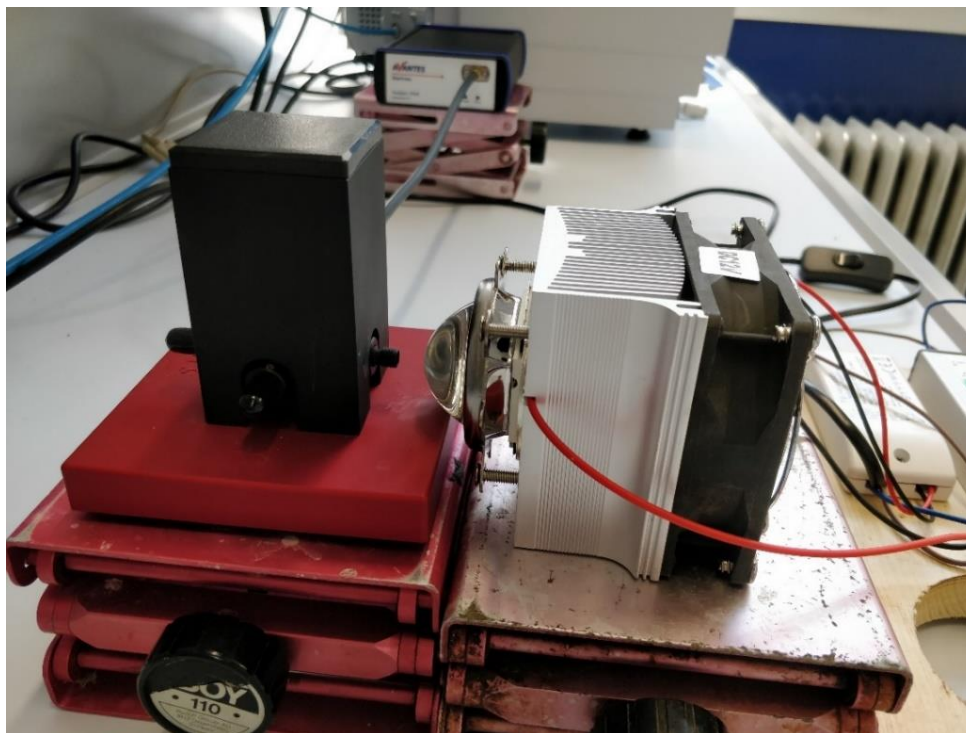


Figure 19. A photograph of the experimental setup used for fluorescence quenching experiments. A 50 W 365 nm LED was used as the light source (see general information p45 for details), fibre coupled to the detector (Avantes, see general information p45 for details).

To investigate fluorescence quenching, the 365 nm LED as used in the batch experiments (see general information p45 for details) was used to excite a 0.02 M PTH solution in acetonitrile. The fluorescence of the catalyst was measured in the presence of various concentrations of two selected substrates: iodobenzene **1c** and acetophenone **28**, as well as cyclohexanethiol and formic acid (Figure 20 to Figure 23). De Alaniz and co-workers have already shown that iodobenzene quenches the excited state of PTH whilst their base, triethylamine, does not.^[18] Since the HAT catalyst might change that, Figure 21 shows that the quenching behaviour is the same with and without CySH, which underscores the assumption that the aryl halide is directly reduced by the PC. Also acetophenone, as can be seen in Figure 20, quenches the catalyst indicating direct reduction by the PC. Quenching constants (k_q), calculated as shown in equation 1, are given in Table 15. For the quenching constant of acetophenone only low concentrations were used since it exhibits some absorbance at 365 nm. However, as the inset graph in Figure 20 shows, a linear relationship was obtained also at higher concentrations. Interestingly,

acetophenone ($k_q = 14.5 \times 10^9 \text{ M}^{-1}\text{s}^{-1}$) is a much better quencher of the PTH than iodobenzene ($k_q = 1.12 \times 10^9 \text{ M}^{-1}\text{s}^{-1}$). 4-Bromobenzonitrile, the model substrate of this study, fluoresces as well (see Figure 29), so no Stern-Volmer quenching studies could be done on this substrate. As can be seen in Figure 22 and Figure 23, the reagents CySH and HCOOH do not quench the catalyst's fluorescence.

Quenching constants were calculated using the Stern-Volmer relationship:

Equation 1:
$$\frac{I_f^0}{I_f} = 1 + k_q \tau_0 [Q]$$

Where I_f^0 = fluorescence intensity in absence of quencher; I_f = fluorescence intensity with quencher; k_q = quenching constant; $[Q]$ = quencher concentration and τ_0 = catalyst excited state lifetime (taken as 2.3 ns here).^[18]

Table 15. Experimentally determined quenching constants of selected substrates.

Quencher	Quenching constant k_q [$\text{M}^{-1} \text{s}^{-1}$]
Acetophenone	14.5×10^9
Iodobenzene	1.12×10^9

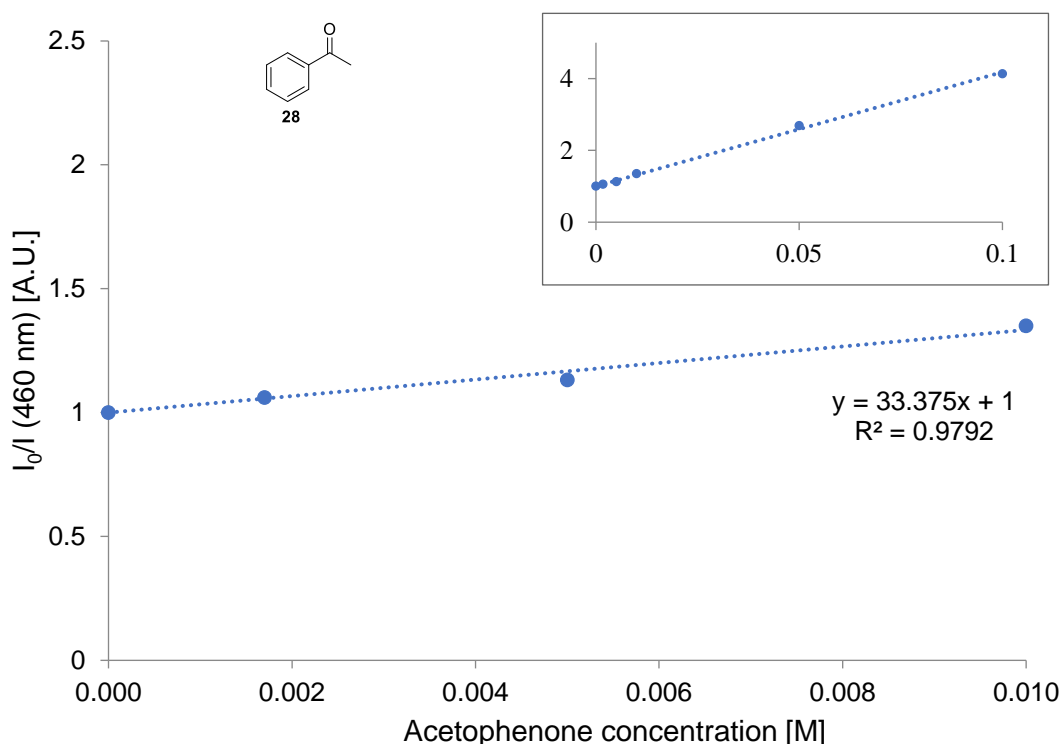


Figure 20. Fluorescence quenching of PTH (0.02 M) and acetophenone (quencher) in MeCN. **Inset:** quenching using higher concentrations of the quencher.

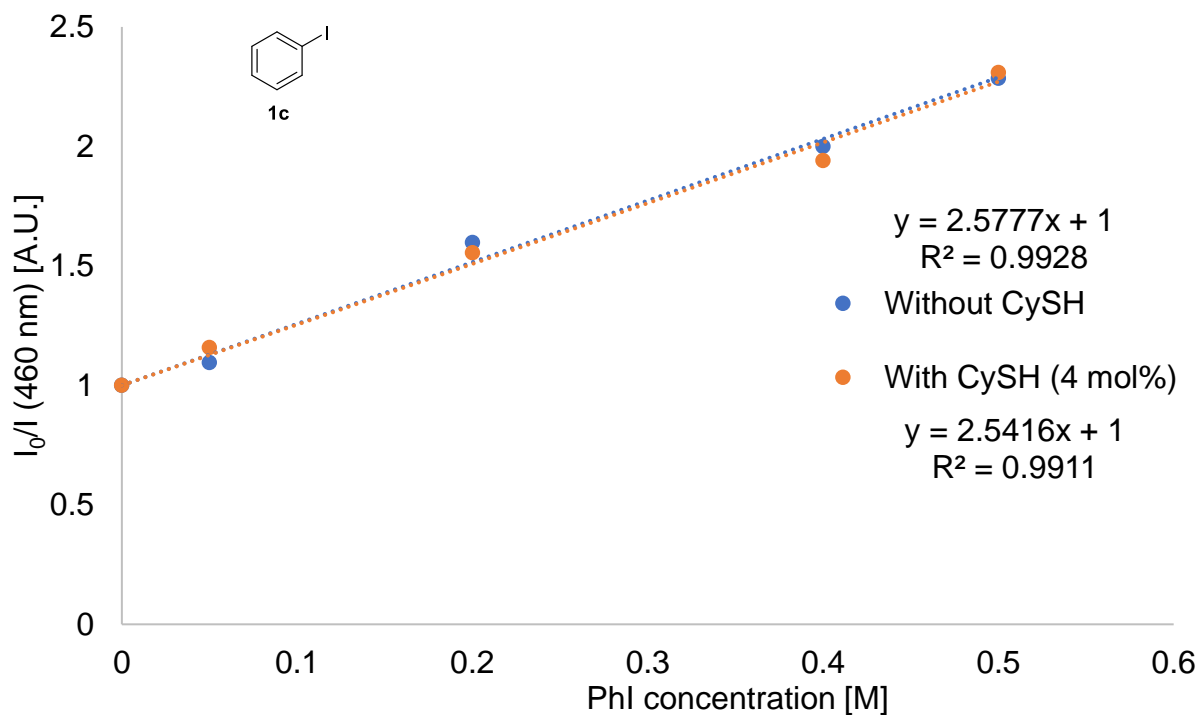


Figure 21. Fluorescence quenching of PTH (0.02 M) by iodobenzene with 4 mol% CySH (red) and without CySH (blue) in MeCN.

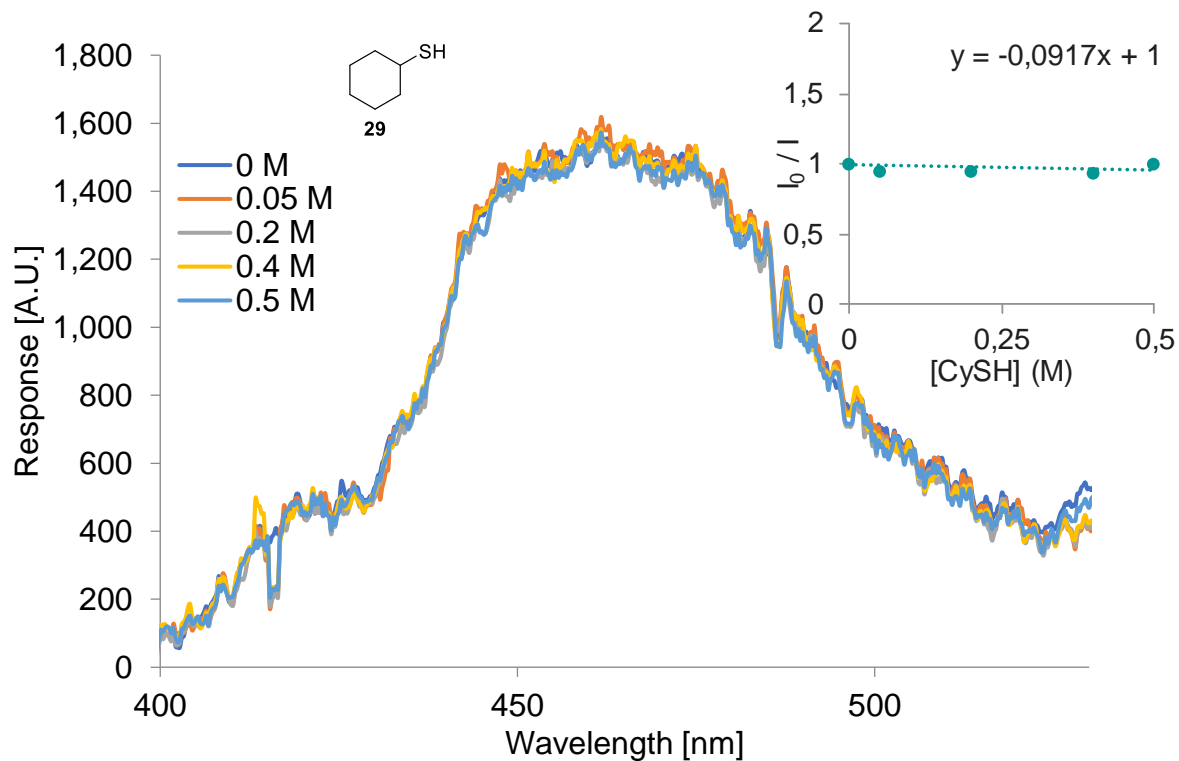


Figure 22. Emission spectra of PTH (0.02 M) in MeCN with CySH as quencher. **Inset:** Graphical representation of quenching.

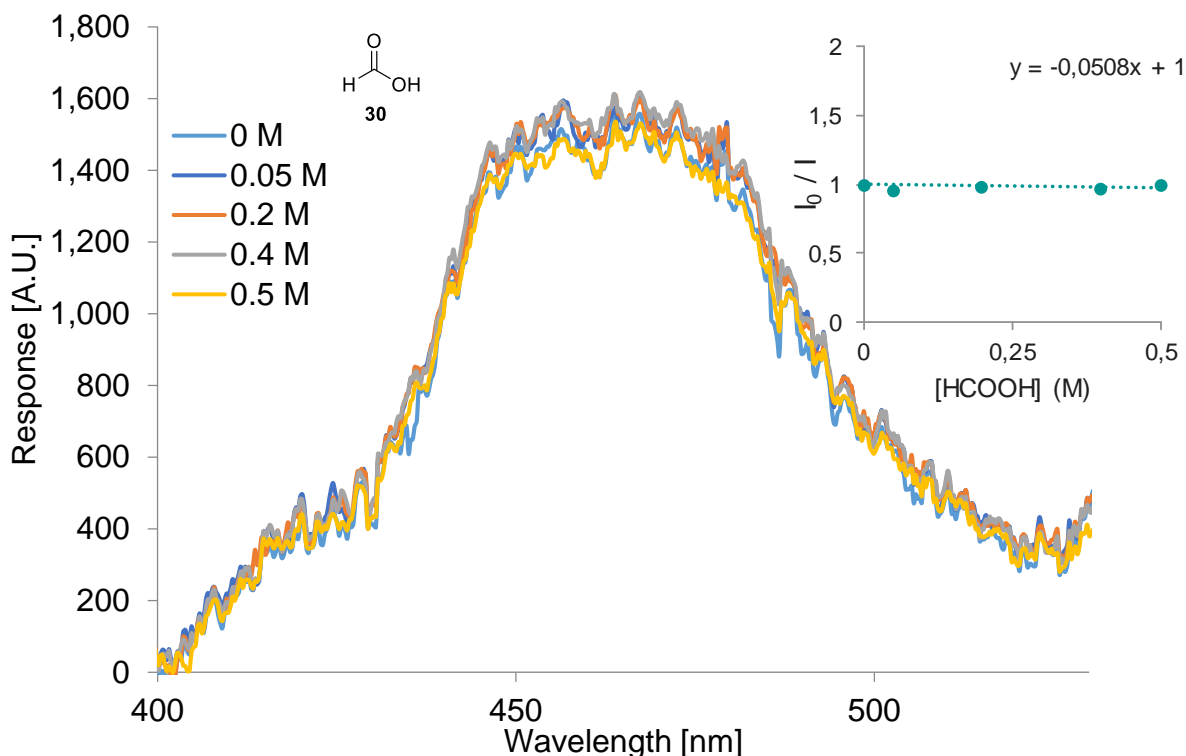
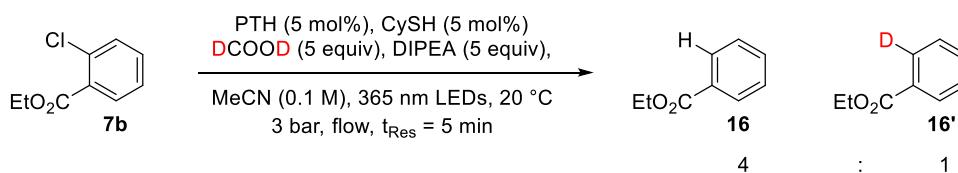


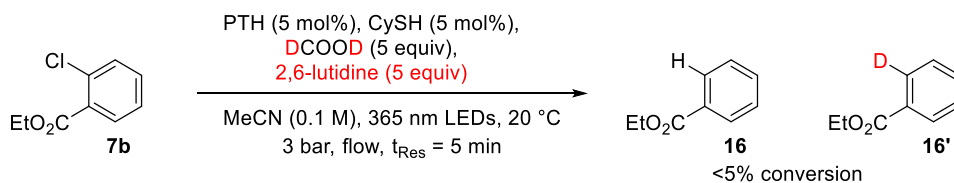
Figure 23. Emission spectra of PTH (0.02 M) in MeCN with formic acid as quencher. **Inset:** Graphical representation of quenching.

3.5.2 Deuterium Incorporation

To determine the main source of the hydrogen atom, deuteration studies using DCOOD in place of HCOOH were carried out following *General Procedure 1*. After removal of the solvent, NMR was used to analyse the product mixture and to calculate the amount of incorporated deuterium. Since only 20% of the product contained deuterium, the amine seems to be the major source of the hydrogen atoms as it was also observed without the HAT catalyst previously.^[18] When exchanging the base for 2,6-lutidine, an amine base not capable of donating hydrogen atoms in the same way (Scheme 16), the reaction did not proceed.



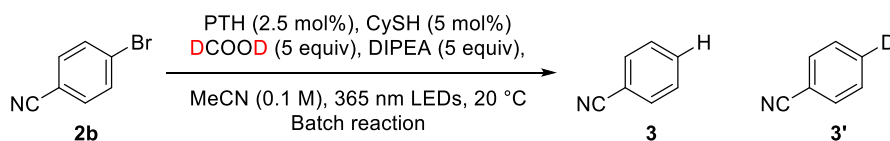
Scheme 15. Deuteration experiment showing very little deuterium incorporation



Scheme 16. Deuteration experiment with 2,6-lutidine as amine base shows very little reaction. This provides further evidence that under standard reaction conditions the amine acts as terminal H-atom source.

3.5.3 Kinetic Isotope Effect

A batch comparison between DCOOD and HCOOH was carried out as specified in *General Procedure 3*. The initial rates of the reactions, based on the first 3 minutes (equals 4 reaction points) were determined and are given in Table 16. The resulting kinetic isotope effect of 1.044 is negligible, thus C-H bond cleavage in the formic acid is likely not involved in the rate limiting step. The slower reaction rate towards the end of the reaction coincides with faster catalyst decomposition. A plausible explanation is the higher water content (5%) present in the DCOOD.



Scheme 17. Reaction conditions for the determination of the kinetic isotope effect using HCOOH or DCOOD.

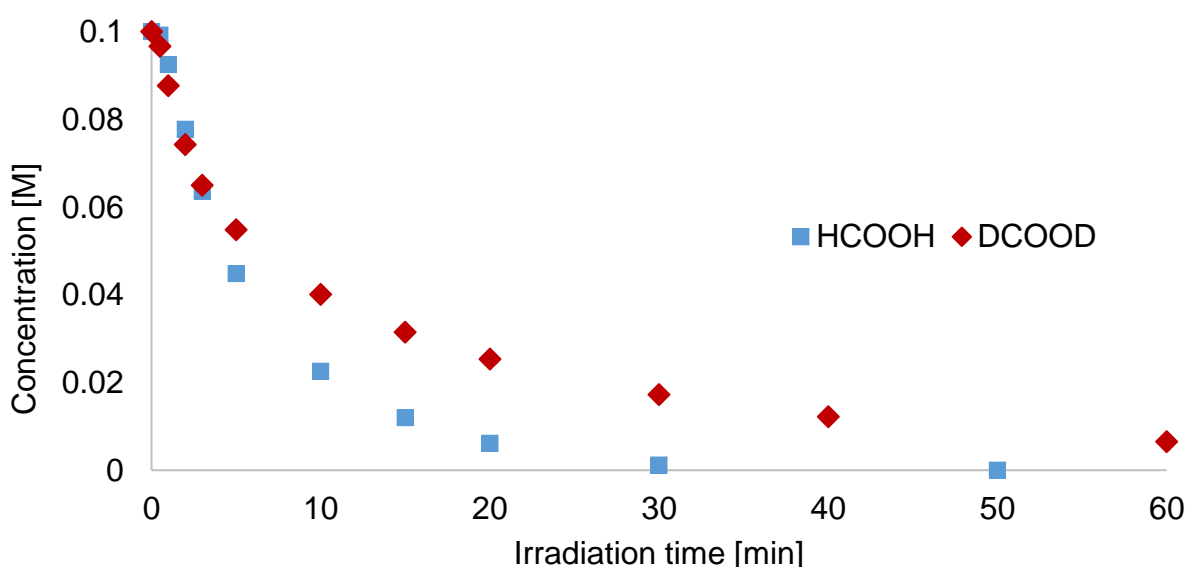


Figure 24. Comparative time course between HCOOH (blue) and DCOOD (red).

Table 16. Initial rates of the reduction of **2b** using HCOOH or DCOOD.

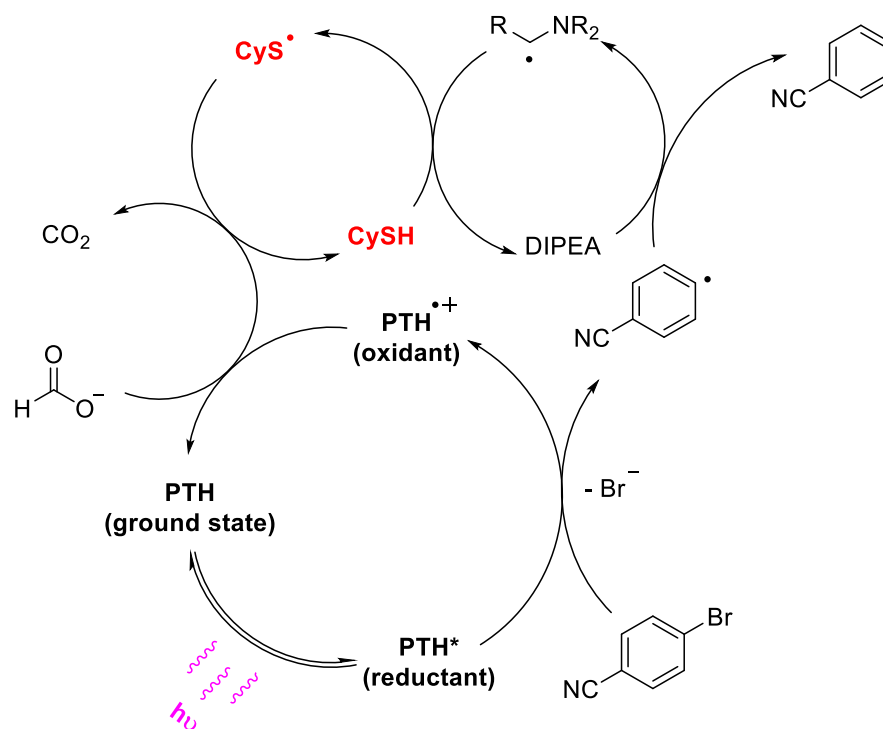
	Initial rate [M s^{-1}]	Linear R^2
HCOOH	2.14×10^{-4}	0.978
DCOOD	2.05×10^{-4}	0.988

3.5.4 Proposed Mechanism

No clear evidence on how the thiol accelerates the reaction was found in the deuterium incorporation experiments and the KIE experiments. Therefore, it was anticipated that the explanation could be an enhanced rate of quenching by interaction with the aryl halide. However, as shown above in Figure 21, the Stern-Volmer studies showed no change in quenching constant. Also, no quenching directly by the CySH (Figure 22) was observed. This implies that the thiol does not participate in quenching of the excited state of the PC.

Another probable explanation for the increased rate would be the formation of a donor-acceptor complex, which allows absorption of light of longer wavelengths and/or initiates the reaction. Those complexes are known in many photochemical transformations.^[70,71] UV/vis absorption spectra of the reaction components in the presence and absence of CySH were recorded in order to test for this effect. Since no change in absorption spectra was observed it was concluded that a complex involving the thiol component is not formed and therefore not responsible for the acceleration.

Scheme 18 shows a proposed mechanism based on the mechanistic studies described in this section. The proposed mechanism is analogous to the one published by Wang et al.^[59] It is proposed that the substrate is reduced by the excited state PTH and the formed aryl radical abstracts a hydrogen radical from the DIPEA to yield the desired product and an α -amino radical. The oxidised PTH radical cation is then regenerated by oxidation of formate, liberating CO_2 . This formate oxidation process is promoted by the thiyl radical, which itself is being generated by the amine radical, regenerating the DIPEA. Overall, CySH acts as a H-atom transfer mediator, which is proposed to be the reason for the increased rate of reaction.



Scheme 18. Proposed reaction mechanism based on the evidence described in this section, featuring HAT-assisted formate oxidation. An analogous mechanism is proposed for a related transformation elsewhere in the literature.^[59]

4. Conclusion

To sum up, the combination of the highly reducing photoredox catalyst PTH and the hydrogen atom transfer catalyst cyclohexanethiol, has led to a significantly improved system for reductive transformations of aryl halides and carbonyl compounds. Transferring this protocol to a continuous flow photoreactor further accelerated these transformations. Residence times as short as 1 minute resulted in full conversion for some substrates, including even aryl chlorides. In one case the productivity could be increased by a factor of >20. Selective mono- or bis-dehalogenation of dihalogenated (hetero-) aryl halides by simply tuning residence time and light intensity gave excellent results in some cases. Applying this photochemical protocol for the reduction of aldehydes, ketones and imines yielded the expected pinacol-type products, with significantly reduced residence times and increased yields compared to previous reports. Furthermore, the coupling of an aryl chloride to a styrene, which had not been demonstrated in literature before, showed good yield. Additionally, mechanistic studies were performed, ranging from fluorescence quenching to deuterium incorporation and kinetic isotope effects, to probe the proposed mechanism. Considering all mechanistic results, it was concluded that the thiol catalyst is likely involved in the regeneration of the ground state photocatalysts and does not interact with the excited state.

5. Experimental

5.1 General Information

All solvents and chemicals were obtained from standard commercial vendors (Sigma-Aldrich or TCI) and were used without any further purification, unless otherwise noted. The acetonitrile used as solvent was HPLC grade ($\geq 99.8\%$), obtained from VWR and was used without drying. Deuterated formic acid (DCOOD) was obtained from Acros Organics ($\geq 99\%$ D atom, 95% solution in D_2O).

NMR spectra: 1H NMR spectra were recorded on a Bruker 300 MHz instrument. ^{13}C NMR spectra were recorded on a Bruker 300 MHz instrument at 75 MHz. Chemical shifts (δ) are expressed in ppm downfield from TMS as internal standard. The letters s, d, dd, t, q, and m are used to indicate singlet, doublet, doublet of doublets, triplet, quadruplet, and multiplet. The prefix br denotes a broad peak.

HPLC: analysis was carried out on a C18 reversed-phase analytical column (150×4.6 mm, particle size $5 \mu m$) at $37^\circ C$ using mobile phases: **A** (water/MeCN 90:10 (v/v) + 0.1% TFA) and **B** (MeCN + 0.1% TFA) at a flow rate of 1.5 mL/min. The following gradient was applied:

Method 1:

Time [min]	Solvent B [%]
0	30
10	100

Method 2:

Time [min]	Solvent B [%]
0	3
3	5
7	30
10	100
12	100

UV/Vis: spectra were recorded using a fibre-coupled Avantes Starline AvaSpec-2048 spectrometer, with an Avantes AvaLight-DHc lamp as the light source. These spectra were processed using Avasoft 8.7 software.

Fluorescence quenching: spectra were recorded using a fibre-coupled Avantes Starline AvaSpec-2048 spectrometer, with a 365 nm 50 W LED (as used in batch reactions) as the light source. These spectra were processed using Avasoft 8.7 software.

Light source characterization: emission spectra were recorded using a fibre-coupled Avantes Starline AvaSpec-2048 spectrometer and were processed using Avasoft 8.7 software.

Microwave: Microwave experiments were performed using a Biotage Initiator+ Microwave Synthesizer, using 20 mL microwave vials (Biotage part# 355632).

Flash column chromatography: automated flash column chromatography was performed on a Biotage Isolera system using columns packed with KP-SIL, 60 Å (32-63 µm particle size) silica.

5.1.1 Flow Reactor Setup

The reactions were conducted in a commercial continuous-flow reactor: Corning AdvancedFlow Lab Photo Reactor (Figure 25).

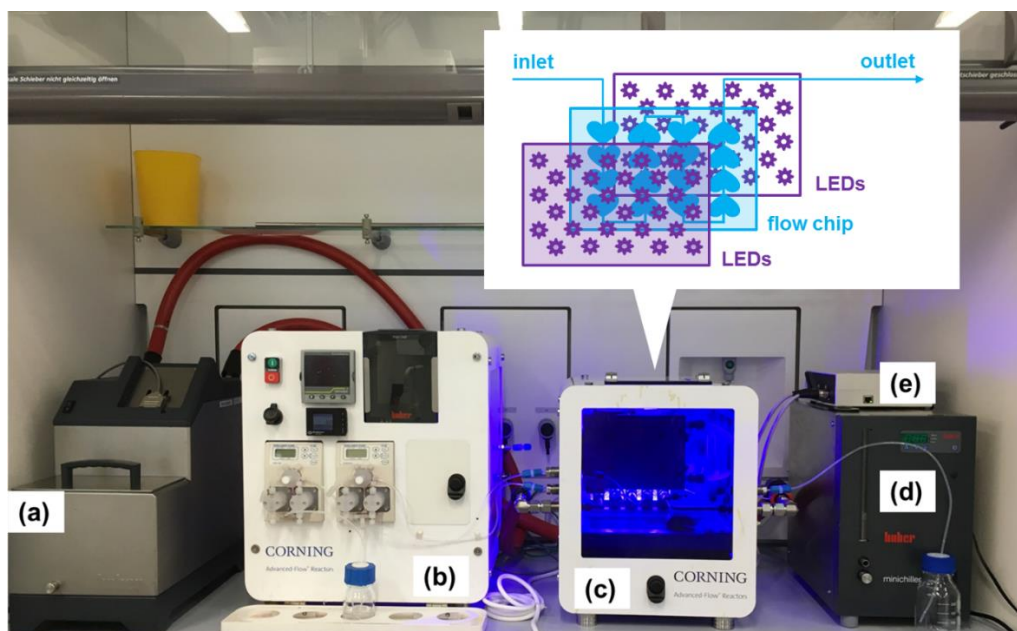


Figure 25. Photograph of commercial reactor setup: **a)** temperature control for reaction plate; **b)** control module, containing pumps, mass flow controller, Huber controller and data logger; **c)** fluidic module housing, with tinted plastic panels for light containment; **d)** temperature control for LED panels; **e)** wireless receiver for LED control.

Reactor module (G1 “low flow” fluidic module): The flow reactor used in this work consisted of a compact glass fluidic module (155 × 125 × 8 mm size, 0.4 mm channel depth, 2.8 mL internal volume), encased within a high capacity heat exchange channel (20 mL volume).

Light source: LED panels were mounted on both sides of the fluidic module (40 mm from the center of the process stream). Each LED panel was equipped with 20 LEDs of 6 different wavelengths (120 LEDs in total) and a heat exchanger ($T = 15\text{ }^{\circ}\text{C}$). The LED wavelength and intensity was controlled externally using a web-based interface, connected wirelessly to a router. The panel used in this study contains the following LEDs: 365, 385, 405, 485, 610 nm and “4000K” white light; see details on LED power and emission spectra below, Table 17 and Figure S2.

Table 17. Power of LEDs of various wavelengths used in this study.

Peak wavelength [nm]	Radiant flux per LED [W]	Total radiant flux [W]	Photon flux [mmol h ⁻¹]
365	1.09	43.6	477
385	1.34	53.6	619
405	1.42	56.8	690

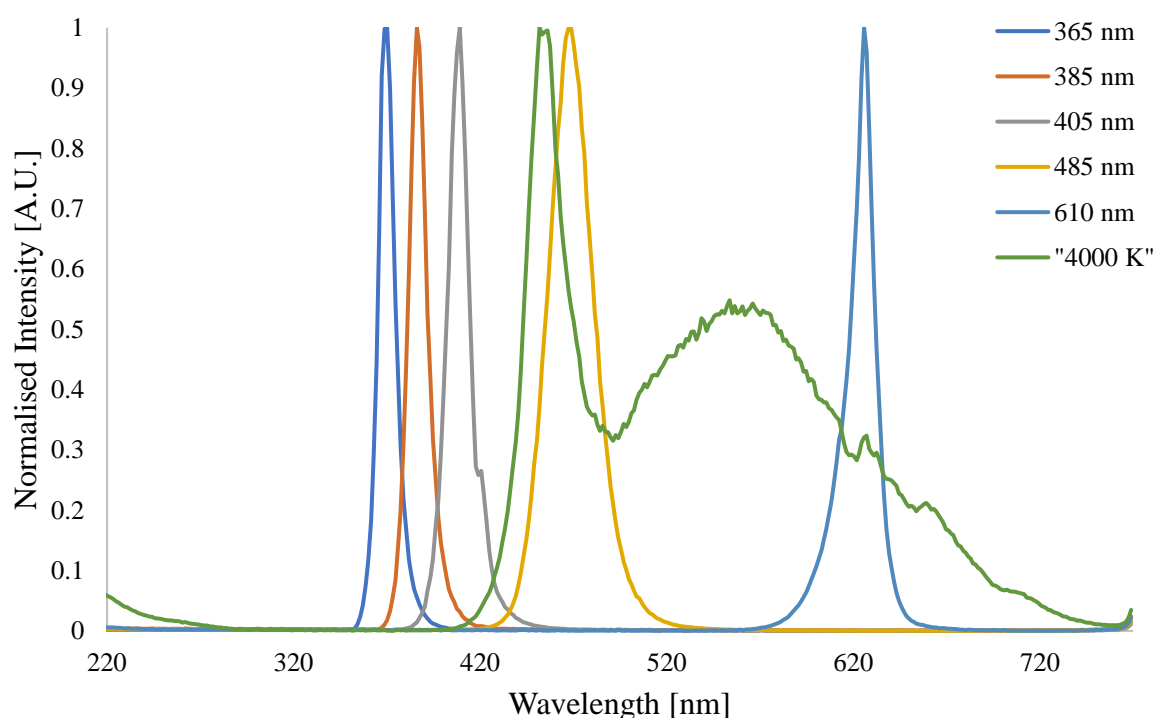


Figure 26. Emission spectra of LEDs on the panel used in this study.

Temperature control: Thermal regulation of the LED panels was carried out using a Huber Minichiller 280 filled with 30% ethylene glycol in water. Thermal regulation of the glass fluidic module was carried out using a Huber Ministat 230 filled with silicon oil (−20 °C to 195 °C).

Pumps: The feed solution was conveyed to the photoreactor using a FLOM UI 22-110DC HPLC pump (0.01-10 mL/min; wetted-parts: PTFE, PCTFE, FFKM and ruby).

Backpressure regulator: A dome-type backpressure regulator (BPR-10, Zaiput Flow Technologies) was installed after the reactor exit with a set point of 3.5 bar for all flow experiments.

General connections: Connection between the pumps, fluidic module input and output was achieved using 1/8" (external diameter) PFA tubing (Swagelok), using metal-free connectors (Swagelok MS-GC-2 swaging system). Other connections used 1/16" (external diameter) PFA tubing, with PEEK fittings.

Sample loop: An Upchurch 6-way switching valve was used to inject the reaction mixture (part # V-450, <https://www.idex-hs.com/store/injection-valve-2-position-6-port-040-black.html>), with a 5 mL (for scoping experiments) or 8.5 mL (for isolation experiments) sample loop (made from 1/16" outer diameter, 0.8 mm inner diameter PFA tubing) installed.

5.1.2 General Procedure 1 for Scoping Experiments in Flow

The substrate (2.5 mmol), photocatalyst (0.0625 mmol), and internal standard (biphenyl, 0.25 mmol) were added to a 25 mL volumetric flask. Acetonitrile was added to dissolve the reagents, followed by DIPEA (12.5 mmol), HCOOH (12.5 mmol) and CySH (0.125 mmol). The flask was topped up with acetonitrile, then sealed with a septum and parafilm and the solution was sparged with argon for 5 min using a balloon (and outlet needle). The reactor was turned on (LEDs, pump and thermostats) the system was given 15 min to equilibrate. The 5 mL sample loop was charged with the degassed solution and injected into the reactor. To account for any dilution effects at the edges of the injected sample, the central fraction (~1 mL) was collected for analysis by HPLC.

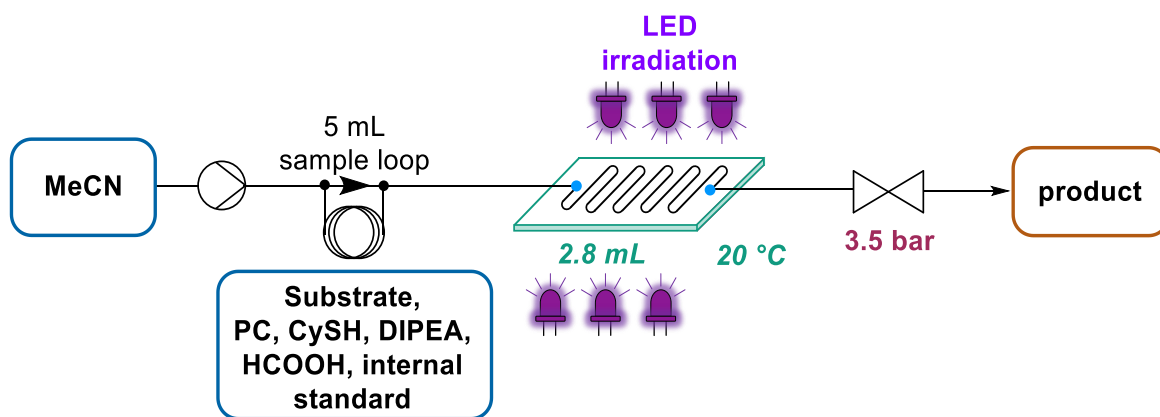


Figure 27. A schematic representation of the flow setup used in these experiments

5.1.3 General Procedure 2 for Isolation Experiments in Flow

The substrate (1 mmol) and photocatalyst (0.025 mmol) were added to a 10 mL volumetric flask. Acetonitrile was added to dissolve the reagents, followed by DIPEA (5 mmol), HCOOH (5 mmol) and CySH (0.05 mmol). The flask was topped up with acetonitrile, then sealed with a septum and parafilm and the solution was sparged with argon for 5 min using a balloon (and outlet needle). The reactor was turned on (LEDs, pump and thermostats) the system was given 15 min to equilibrate. The 8.5 mL sample loop was charged with the degassed solution and injected into the reactor. At least 25 mL of reactor outlet was collected, to ensure that no product was lost due to dilution effects. The solvent was evaporated, and the product was purified by column chromatography, as specified in each example.

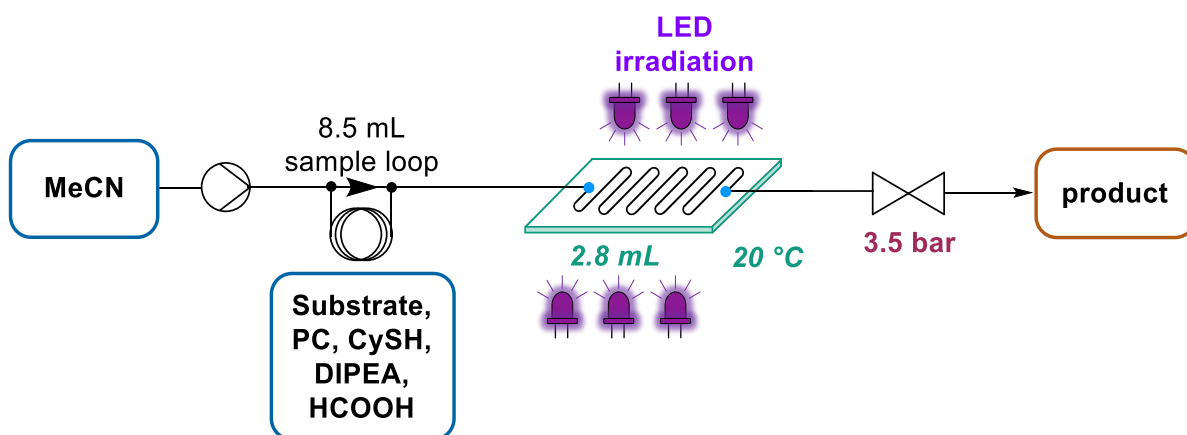


Figure 28. A schematic representation of the flow setup used in these experiments.

5.1.4 General Procedure 3 for Batch Reactions

4-Bromobenzonitrile **2b** (91 mg, 0.5 mmol), PTH (3.4 mg, 0.0125 mmol) and internal standard (biphenyl, 7.7 mg, 0.05 mmol) were added to a microwave vial, equipped with a stirrer bar. MeCN (4.47 mL), DIPEA (434 μ L, 2.5 mmol) and HCOOH (94 μ L, x mmol) were added, followed by CySH (3 μ L, 0.025 mmol) if required. The vial was sealed with a septum and the reaction mixture degassed by sparging with a balloon of argon (and outlet needle) for 5 min. The LED was turned on, and the reaction mixture sampled at intervals for HPLC analysis. Note: during sampling, the LED was turned off and reaction time paused.

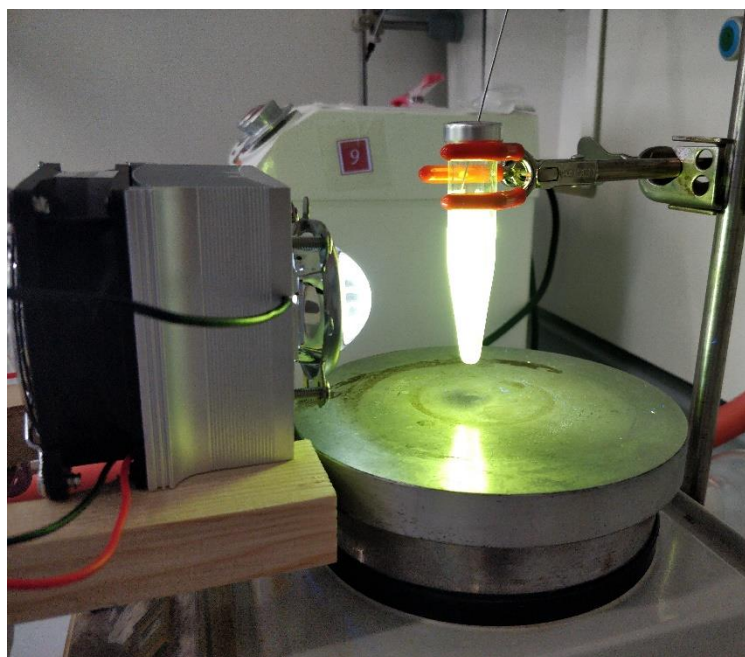
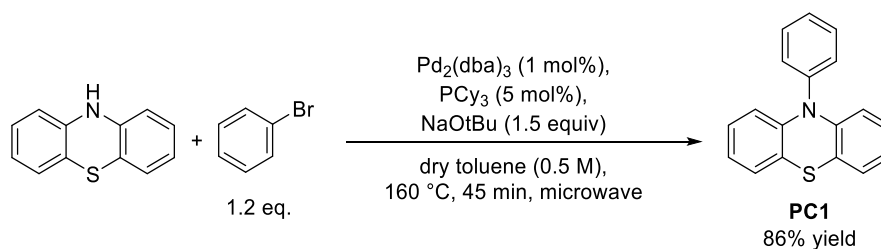


Figure 29. Reaction set-up of batch reactions, using a 365 nm LED as light source, with the reaction mixture in a crimp cap Biotage microwave vial (Biotage part #354625). **Note:** the observable yellow colour is caused by fluorescence of the 4-bromobenzonitrile substrate **2b**.

5.2 Catalyst Synthesis

10-Phenylphenothiazine (PTH, **PC1**):

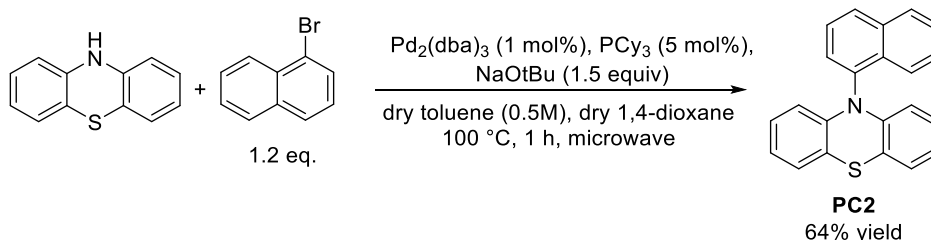


A 20 mL microwave vial equipped with a magnetic stir bar was charged with phenothiazine (1.0 g, 5 mmol), NaOtBu (720 mg, 7.5 mmol), $\text{Pd}_2(\text{dba})_3$, CHCl_3 (52 mg, 0.05 mmol) and PCy_3 (70 mg, 0.25 mmol). The vial was capped and flushed with argon before adding dry toluene (10 mL). After addition of anhydrous bromobenzene (942 mg, 628 μL , 6 mmol) the mixture/suspension was heated in the microwave to 160 °C for 45 min. The remaining solids were removed by filtration, the solvent removed *in vacuo*. The crude product was purified by flash chromatography on silica using 40-60 petroleum ether and ethyl acetate as eluent (gradient: 0-5% EtOAc over 13 column volumes) to yield 1.19 g (86%) of the desired product as a white solid.

^1H NMR (300 MHz, DMSO) δ 7.67 (t, $J = 7.6$ Hz, 2H), 7.54 (t, $J = 7.4$ Hz, 1H), 7.42 (d, $J = 7.2$ Hz, 2H), 7.08 (dd, $J = 7.4, 1.7$ Hz, 2H), 6.96 – 6.83 (m, 4H), 6.16 (dd, $J = 8.1, 1.2$ Hz, 2H).
 ^{13}C NMR (75 MHz, DMSO) δ 144.0, 140.8, 131.5, 130.8, 128.9, 127.7, 127.1, 123.2, 119.8, 116.5.

The NMR data is in agreement with previous reports.^[18]

N-(1-Naphthyl)-phenothiazine (Np-PTH, **PC2**):



A 20 mL microwave vial equipped with a magnetic stir bar was charged with phenothiazine (500 mg, 2.5 mmol), NaOtBu (360 mg, 3.75 mmol), $\text{Pd}_2(\text{dba})_3$, CHCl_3 (23 mg, 0.025 mmol) and PCy_3 (35 mg, 0.125 mmol). The vial was capped and flushed with argon before adding dry toluene (5 mL) and dry 1,4-dioxane (1 mL). After addition of 1-bromonaphthalene (420 μL ,

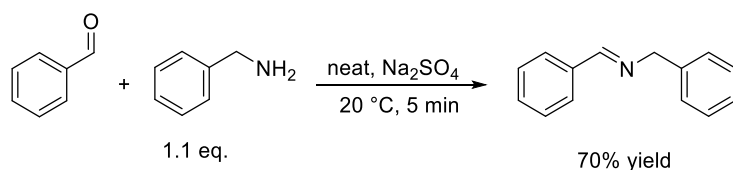
3 mmol) the mixture was heated in the microwave to 100 °C for 1 h. The remaining solids were removed by filtration and the solvent removed *in vacuo*. The crude product was purified by flash chromatography on silica using 40-60 petroleum ether and ethyl acetate as eluent (gradient: 0-5% EtOAc over 25 column volumes) to yield 520 mg (64%) of the desired product as a white solid.

^1H NMR (300 MHz, DMSO) δ 8.24 – 8.06 (m, 2H), 7.97 (d, J = 8.3 Hz, 1H), 7.83 – 7.72 (m, 2H), 7.57 (dddd, J = 19.3, 8.3, 6.9, 1.4 Hz, 2H), 7.17 – 7.03 (m, 2H), 6.91 – 6.72 (m, 4H), 6.07 – 5.91 (m, 2H). ^{13}C NMR (75 MHz, DMSO) δ 143.1, 136.0, 135.2, 130.4, 129.9, 129.0, 127.6, 127.4, 126.9, 126.8, 126.6, 122.7, 122.5, 118.8, 115.5.

The NMR data is in agreement with previous reports.^[72]

5.3 Substrate Synthesis

N-Benzylideneaniline:

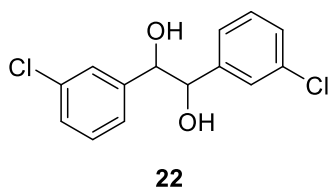


A 100 mL round bottom flask was charged with benzaldehyde (2.7 g, 25.6 mmol). Benzylamine (3.0 mg, 28.2 mmol) was added, followed by Na_2SO_4 1 min later. After shaking for 5 min the reaction mixture was diluted with DCM. The solids were removed by filtration and the filtrate was concentrated under reduced pressure to yield 4.5 g crude product which contained about 10% benzylamine. The excess amine was removed by adding 20 mL diethyl ether and washing with water (3×50 mL). Drying with Na_2SO_4 followed by evaporation of the ether under reduced pressure yielded 3.5 g (70%) of the desired product as a pale-yellow oil.

^1H NMR (300 MHz, CDCl_3) δ 8.41 (s, 1H), 7.80 (m, 2H), 7.44 – 7.24 (m, 8H), 4.84 (s, 2H). ^{13}C NMR (75 MHz, CDCl_3) δ 173.4, 135.6, 135.0, 131.1, 129.6, 128.9, 128.6, 128.3, 127.9, 43.9.

The NMR data is in agreement with previous reports.^[73]

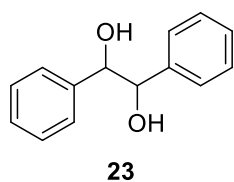
5.4 Pinacol Coupling Reactions



1,2-bis(3-chlorophenyl)ethane-1,2-diol (**22**) was synthesized following *General Procedure 2* using 3-chlorobenzaldehyde (0.85 mmol), PTH (2.5 mol%), HCOOH (5 equiv), DIPEA (5 equiv) and CySH (5 mol%) in 3 min residence time. After concentrating the crude reaction mixture under reduced pressure, the product was purified by flash chromatography on silica using 40-60 petroleum ether and ethyl acetate (with 1% v/v formic acid) as eluent (gradient: 0-60% EtOAc over 15 column volumes). The resulting product was dissolved in EtOAc (25 mL) and washed with saturated sodium bicarbonate (3×5 mL). The organics were dried over Na₂SO₄, filtered and solvent removed under reduced pressure to yield 121 mg (93% yield) of the desired product **22** as a pale yellow solid, ratio *dl:meso* = 1.07 : 1.

¹H NMR (300 MHz, CDCl₃) δ 7.30 – 7.14 (m, 12H), 7.09 – 7.02 (m, 2H, *meso*), 6.96 – 6.89 (m, 2H, *dl*) 4.81 (s, 2H, *meso*), 4.64 (s, 2H, *dl*), 2.55 (br s, 4H). ¹³C NMR (75 MHz, CDCl₃) δ 141.7, 141.6, 134.40, 134.37, 129.57, 129.55, 128.5 (2C), 127.3, 127.1, 125.4, 125.3, 78.4, 77.3.

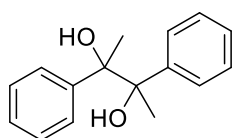
The NMR data is in agreement with previous reports.^[74]



1,2-diphenylethane-1,2-diol (**23**) was synthesized following *General Procedure 2* using benzaldehyde (0.89 mmol), PTH (2.5 mol%), HCOOH (5 equiv), DIPEA (5 equiv) and CySH (5 mol%) in 3 min residence time. After concentrating the crude reaction mixture under reduced pressure, the product was purified by flash chromatography on silica using 40-60 petroleum ether and ethyl acetate (with 1% v/v formic acid) as eluent (gradient: 0-100% EtOAc over 15 column volumes). The resulting product was dissolved in EtOAc (25 mL) and washed with saturated sodium bicarbonate (3×5 mL). The organics were dried over Na₂SO₄, filtered and solvent removed under reduced pressure to yield 91 mg (96% yield) of the desired product **23** as a white solid, ratio *dl:meso* = 1.25 : 1.

¹H NMR (300 MHz, CDCl₃) δ 7.35 – 7.30 (m, 6H), 7.29 – 7.23 (m, 10H), 7.16 – 7.11 (m, 4H, *dl*), 4.83 (s, 2H, *meso*), 4.70 (s, 2H, *dl*), 2.62 (br s, 4H). ¹³C NMR (75 MHz, CDCl₃) δ 140.0, 139.9, 128.3, 128.2 (2C), 128.0, 127.2, 127.1, 79.2, 78.2.

The NMR data is in agreement with previous reports.^[67]

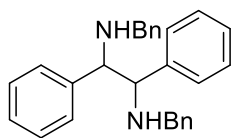
**24**

2,3-diphenylbutane-2,3-diol (**24**) was synthesized following *General Procedure 2* using acetophenone (0.87 mmol), PTH (2.5 mol%), HCOOH (5 equiv), DIPEA (5 equiv) and CySH (5 mol%) in 3 min residence time.

After concentrating the crude reaction mixture under reduced pressure the product was purified by flash chromatography on silica using 40-60 petroleum ether and ethyl acetate as eluent (gradient: 0-10% over 20 column volumes) to yield 103 mg (98% yield) of the desired product **24** as a white solid, ratio *dl:meso* = 1.5 : 1.

^1H NMR (300 MHz, CDCl_3) δ 7.29 – 7.20 (m, 25H, 10H *meso* and 1.5 x 10H *dl*), 2.63 (br s, 1.5 x 2H *dl*), 2.02 (br s, 2H, *meso*), 1.61 (s, 6H, *meso*), 1.53 (s, 1.5 x 6H, *dl*). ^{13}C NMR (75 MHz, CDCl_3) δ 143.9, 143.5, 127.5, 127.4, 127.3, 127.2, 127.1 (2C), 79.0, 78.7, 25.3, 25.1.

The NMR data is in agreement with previous reports.^[67]

**25**

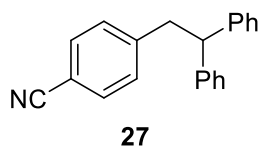
N,N-dibenzyl-1,2-diphenylethane-1,2-diamine (**25**) was synthesized following *General Procedure 2* using *N*-benzyl-1-phenylmethanimine (0.85 mmol), PTH (2.5 mol%), HCOOH (5 equiv), DIPEA (5 equiv) and CySH (5 mol%) in 5 min residence time. After concentrating the crude

reaction mixture under reduced pressure the product was purified by flash chromatography on silica using 40-60 petroleum ether and ethyl acetate (with 1% v/v Et_3N) as eluent (gradient: 0-15% over 15 column volumes) to yield 132 mg (80% yield) of the desired product **25** as an off-white solid, ratio *dl:meso* = 1.5 : 1.

^1H NMR (300 MHz, CDCl_3) δ 7.35 – 6.94 (m, 20H, 10H *meso* and 1.5 x 10H *dl*), 3.75 (s, 1.5 x 2H, *dl*), 3.71 (s, 2H, *meso*), 3.66 (d, $J=13.3$ Hz, 2H, *meso*), 3.54 (d, $J=13.7$ Hz, 1.5 x 2H, *dl*), 3.48 (d, $J=13.3$ Hz, 2H, *meso*), 3.30 (d, $J=13.7$ Hz, 1.5 x 2H, *dl*), 1.97 (br s, 2H *meso* and 1.5 x 2H *dl*).

The NMR data is in agreement with previous reports.^[67]

5.5 Reductive Styrene Coupling



4-(2,2-diphenylethyl)benzonitrile (**27**) was synthesized following **General Procedure 2**, but with the flow reactor heated to 50 °C by the thermostat, using 4-chlorobenzonitrile (0.85 mmol), 1,1-diphenylethylene (4.25 mmol), PTH (10 mol%), HCOOH (5 equiv), DIPEA (5 equiv) and CySH (5 mol%) in 10 min residence time. After concentrating the crude reaction mixture under reduced pressure the product was purified by flash chromatography on silica using 40-60 petroleum ether and ethyl acetate as eluent (gradient: 0-10% over 20 column volumes) to yield 145 mg (61% yield) of the desired product **27** as a green/yellow oil.

^1H NMR (300 MHz, DMSO- d_6) δ 7.63 (d, J = 8.2 Hz, 2H), 7.39 – 7.31 (m, 6H), 7.25 (t, J = 7.6 Hz, 4H), 7.13 (tt, J = 7.2, 2.2 Hz, 2H), 4.39 (t, J = 8.1 Hz, 1H), 3.47 (d, J = 8.1 Hz, 2H). ^{13}C NMR (75 MHz, DMSO- d_6) δ 146.5, 144.1, 131.8, 130.1, 128.4, 127.8, 126.2, 118.9, 108.6, 51.4, 40.4. IR (ATR, neat, cm^{-1}): 2954, 2923, 2853, 2226, 1452, 1052, 1026, 1007. HRMS (ESI, positive mode) calculated for $\text{C}_{21}\text{H}_{18}\text{N}$ $[\text{M}+\text{H}]^+$: 284.1439, found: 284.1428.

6. References

- [1] T. Mirkovic, E. E. Ostroumov, J. M. Anna, R. Van Grondelle, Govindjee, G. D. Scholes, *Chem. Rev.* **2017**, *117*, 249–293.
- [2] D. Y. Goswami, S. M. Besarati, *World Energy Resources: Solar*, **2013**.
- [3] B. Obama, *Science* **2017**, *355*, 126–129.
- [4] G. Nebbia, G. B. Kauffman, *Chem. Educ.* **2007**, *12*, 362–369.
- [5] H. D. Roth, *Angew. Chemie - Int. Ed.* **1989**, *28*, 1193–1207.
- [6] H. Klinger, *Berichte der Dtsch. Chem. Gesellschaft* **1886**, *19*, 1862–1870.
- [7] H. Klinger, O. Standke, *Berichte der Dtsch. Chem. Gesellschaft* **1891**, *24*, 1340–1346.
- [8] J. Schramm, *Monatshefte für Chemie* **1888**, *9*, 842–853.
- [9] G. Ciamician, *Science* **1912**, *36*, 385–394.
- [10] A. Albini, M. Fagnoni, *Handbook of Synthetic Photochemistry*, Wiley-VCH, Weinheim, **2010**.
- [11] N. Hoffmann, *Chem. Rev.* **2008**, *108*, 1052–1103.
- [12] B. D. A. Hook, W. Dohle, P. R. Hirst, M. Pickworth, M. B. Berry, K. I. Booker-Milburn, *J. Org. Chem.* **2005**, *70*, 7558–7564.
- [13] M. D. Lainchbury, M. I. Medley, P. M. Taylor, P. Hirst, W. Dohle, K. I. Booker-Milburn, *J. Org. Chem.* **2008**, *73*, 6497–6505.
- [14] I. Ryu, Y. Manabe, K. Fukase, M. Nagasaki, Y. Hino, T. Fukuyama, Y. Kitawaki, H. Matsubara, *Chem. - A Eur. J.* **2014**, *20*, 12750–12753.
- [15] B. D. Ravetz, A. B. Pun, E. M. Churchill, D. N. Congreve, T. Rovis, L. M. Campos, *Nature* **2019**, *565*, 343–346.
- [16] M. H. Shaw, J. Twilton, D. W. C. MacMillan, *J. Org. Chem.* **2016**, *81*, 6898–6926.
- [17] J. D. Williams, M. Nakano, R. Gérardy, J. A. Rincón, Ó. De Frutos, C. Mateos, J. C. M. Monbaliu, C. O. Kappe, *Org. Process Res. Dev.* **2019**, *23*, 78–87.
- [18] E. H. Discekici, N. J. Treat, S. O. Poelma, K. M. Mattson, Z. M. Hudson, Y. Luo, C. J. Hawker, J. R. De Alaniz, *Chem. Commun.* **2015**, *51*, 11705–11708.

- [19] N. J. Turro, V. Ramamurthy, J. C. Scaiano, *Principles of Molecular Photochemistry: An Introduction*, University Science Books, **2009**.
- [20] N. A. Romero, D. A. Nicewicz, *Chem. Rev.* **2016**, *116*, 10075–10166.
- [21] P. Esser, B. Pohlmann, H.-D. Scharf, *Angew. Chemie - Int. Ed.* **1994**, *33*, 2009–2023.
- [22] Y. Muramoto, M. Kimura, S. Nouda, *Semicond. Sci. Technol.* **2014**, *29*, 084004.
- [23] K. N. Loponov, J. Lopes, M. Barlog, E. V. Astrova, A. V. Malkov, A. A. Lapkin, *Org. Process Res. Dev.* **2014**, *18*, 1443–1454.
- [24] H. E. Bonfield, J. D. Williams, W. X. Ooi, S. G. Leach, W. J. Kerr, L. J. Edwards, *ChemPhotoChem* **2018**, *2*, 938–944.
- [25] S. Meyer, D. Tietze, S. Rau, B. Schäfer, G. Kreisel, *J. Photochem. Photobiol. A Chem.* **2007**, *186*, 248–253.
- [26] D. Ziegenbalg, G. Kreisel, D. Weiß, D. Kralisch, *Photochem. Photobiol. Sci.* **2014**, *13*, 1005–1015.
- [27] M. Sender, D. Ziegenbalg, *Chemie-Ingenieur-Technik* **2017**, *89*, 1159–1173.
- [28] Y. Su, N. J. W. Straathof, V. Hessel, T. Noël, *Chem. - A Eur. J.* **2014**, *20*, 10562–10589.
- [29] F. Politano, G. Oksdath-Mansilla, *Org. Process Res. Dev.* **2018**, *22*, 1045–1062.
- [30] M. B. Plutschack, B. Pieber, K. Gilmore, P. H. Seeberger, *Chem. Rev.* **2017**, *117*, 11796–11893.
- [31] K. Kalyanasundaram, *Coord. Chem. Rev.* **1982**, *46*, 159–244.
- [32] N. Emmanuel, C. Mendoza, M. Winter, C. R. Horn, A. Vizza, L. Dreesen, B. Heinrichs, J. C. M. Monbaliu, *Org. Process Res. Dev.* **2017**, *21*, 1435–1438.
- [33] D. M. Hedstrand, W. H. Kruizinga, R. M. Kellogg, *Tetrahedron Lett.* **1978**, *19*, 1255–1258.
- [34] C. K. Prier, D. A. Rankic, D. W. C. MacMillan, *Chem. Rev.* **2013**, *113*, 5322–5363.
- [35] H. Cano-Yelo, A. Deronzier, *Tetrahedron Lett.* **1984**, *25*, 5517–5520.
- [36] C. Pac, M. Ihama, M. Yasuda, Y. Miyauchi, H. Sakurai, *J. Am. Chem. Soc.* **1981**, *103*, 6495–6497.
- [37] D. H. R. Barton, M. A. Csiba, J. C. Jaszberenyi, *Tetrahedron Lett.* **1994**, *35*, 2869–2872.
- [38] Nobel Media AB, NobelPrize.org, “The Nobel Prize in Chemistry 2010,” can be found

- under <https://www.nobelprize.org/prizes/chemistry/2010/summary/>, **2019**.
- [39] I. Ghosh, L. Marzo, A. Das, R. Shaikh, B. König, *Acc. Chem. Res.* **2016**, *49*, 1566–1577.
- [40] C. S. Wang, P. H. Dixneuf, J. F. Soulé, *Chem. Rev.* **2018**, *118*, 7532–7585.
- [41] X. Pan, C. Fang, M. Fantin, N. Malhotra, W. Y. So, L. A. Peteanu, A. A. Isse, A. Gennaro, P. Liu, K. Matyjaszewski, *J. Am. Chem. Soc.* **2016**, *138*, 2411–2425.
- [42] N. J. Treat, H. Sprafke, J. W. Kramer, P. G. Clark, B. E. Barton, J. Read De Alaniz, B. P. Fors, C. J. Hawker, *J. Am. Chem. Soc.* **2014**, *136*, 16096–16101.
- [43] F. Mo, G. Dong, Y. Zhang, J. Wang, *Org. Biomol. Chem.* **2013**, *11*, 1582–1593.
- [44] M. Anselmo, A. Basso, S. Protti, D. Ravelli, *ACS Catal.* **2019**, *9*, 2493–2500.
- [45] D. P. Hari, P. Schroll, B. König, *J. Am. Chem. Soc.* **2012**, *134*, 2958–2961.
- [46] D. P. Hari, T. Hering, B. König, *Org. Lett.* **2012**, *14*, 5334–5337.
- [47] T. Hering, D. P. Hari, B. König, *J. Org. Chem.* **2012**, *77*, 10347–10352.
- [48] L. Gu, C. Jin, J. Liu, *Green Chem.* **2015**, *17*, 3733–3736.
- [49] H. G. Roth, N. A. Romero, D. A. Nicewicz, *Synlett* **2016**, *27*, 714–723.
- [50] I. Ghosh, T. Gosh, J. I. Bardagi, B. König, *Science* **2014**, *346*, 725–728.
- [51] I. Ghosh, B. König, *Angew. Chemie - Int. Ed.* **2016**, *55*, 7676–7679.
- [52] R. S. Shaikh, S. J. S. Düsel, B. König, *ACS Catal.* **2016**, *6*, 8410–8414.
- [53] L. Marzo, I. Ghosh, F. Esteban, B. König, *ACS Catal.* **2016**, *6*, 6780–6784.
- [54] J. I. Bardagi, I. Ghosh, M. Schmalzbauer, T. Ghosh, B. König, *European J. Org. Chem.* **2018**, *2018*, 34–40.
- [55] I. Ghosh, R. S. Shaikh, B. König, *Angew. Chemie - Int. Ed.* **2017**, *56*, 8544–8549.
- [56] A. U. Meyer, T. Slanina, A. Heckel, B. König, *Chem. - A Eur. J.* **2017**, *23*, 7900–7904.
- [57] R. Matsubara, T. Yabuta, U. Md Idros, M. Hayashi, F. Ema, Y. Kobori, K. Sakata, *J. Org. Chem.* **2018**, *83*, 9381–9390.
- [58] S. O. Poelma, G. L. Burnett, E. H. Discekici, K. M. Mattson, N. J. Treat, Y. Luo, Z. M. Hudson, S. L. Shankel, P. G. Clark, J. W. Kramer, et al., *J. Org. Chem.* **2016**, *81*, 7155–7160.
- [59] H. Wang, N. T. Jui, *J. Am. Chem. Soc.* **2018**, *140*, 163–166.

- [60] F. D. Lu, D. Liu, L. Zhu, L. Q. Lu, Q. Yang, Q. Q. Zhou, Y. Wei, Y. Lan, W. J. Xiao, *J. Am. Chem. Soc.* **2019**, *141*, 6167–6172.
- [61] K. C. Harper, E. G. Moschetta, S. V. Bordawekar, S. J. Wittenberger, *ACS Cent. Sci.* **2019**, *5*, 109–115.
- [62] Y. Su, K. Kuijpers, V. Hessel, T. Noël, *React. Chem. Eng.* **2016**, *1*, 73–81.
- [63] J. D. Williams, Y. Otake, G. Coussanes, I. Saridakis, N. Maulide, C. O. Kappe, *ChemPhotoChem* **2019**, *3*, 229–232.
- [64] R. J. Enemærke, T. B. Christensen, H. Jensen, K. Daasbjerg, *J. Chem. Soc. Perkin Trans. 2* **2001**, 1620–1630.
- [65] C. P. Seath, D. B. Vogt, Z. Xu, A. J. Boyington, N. T. Jui, *J. Am. Chem. Soc.* **2018**, *140*, 15525–15534.
- [66] K. Daasbjerg, P. Frøyen, S. Gronowitz, A. Hallberg, J. Alvhäll, R. Svenson, M. Greune, J. Weidlein, A. Nasiri, Y. Okada, *Acta Chem. Scand.* **1993**, *47*, 398–402.
- [67] M. Nakajima, E. Fava, S. Loescher, Z. Jiang, M. Rueping, *Angew. Chemie - Int. Ed.* **2015**, *54*, 8828–8832.
- [68] S. Okamoto, K. Kojiyama, H. Tsujioka, A. Sudo, *Chem. Commun.* **2016**, *52*, 11339–11342.
- [69] A. Gualandi, G. Rodeghiero, E. Della Rocca, F. Bertoni, M. Marchini, R. Perciaccante, T. P. Jansen, P. Ceroni, P. G. Cozzi, *Chem. Commun.* **2018**, *54*, 10044–10047.
- [70] B. Liu, C. H. Lim, G. M. Miyake, *J. Am. Chem. Soc.* **2017**, *139*, 13616–13619.
- [71] Q.-Q. Ge, J.-S. Qian, J. Xuan, *J. Org. Chem.* **2019**, *84*, 8691–8701.
- [72] X. Pan, M. Lamson, J. Yan, K. Matyjaszewski, *ACS Macro Lett.* **2015**, *4*, 192–196.
- [73] L. G. Marinescu, C. M. Pedersen, M. Bols, *Tetrahedron* **2005**, *61*, 123–127.
- [74] J. Li, Z. Lin, N. Qi, T. Li, *Synth. Commun.* **2004**, *34*, 4339–4348.

7. Appendix

7.1 Abbreviations

aq	aqueous	IC	internal conversion
Ar	aryl	IR	infrared spectroscopy
ATR	attenuated total reflection	ISC	intersystem crossing
ATRA	atom transfer radical addition	LED	light emitting diode
BPR	back pressure regulator	LUMO	lowest unoccupied molecular orbital
bpy	2,2'-bipyridine	MeCN	acetonitrile
CySH	cyclohexanethiol	MeOH	methanol
DIPEA	<i>N,N</i> -diisopropylethylamine	NADH	nicotinamide adenine dinucleotide
DMF	<i>N,N</i> -dimethylformamide	NMR	nuclear magnetic resonance
DMSO	dimethylsulfoxide	Np-PTH	<i>N</i> -(1-naphthyl)-phenothiazine
DoE	design of experiment	PC	photoredox catalyst
dtbbpy	4,4-di- <i>tert</i> -butyl-2,2'-bipyridine	PDI	perylene diimide
equiv	equivalents	ppy	2-phenylpyridine
ESI	electrospray ionization	PS	photosensitizer
ET	energy transfer	PTH	<i>N</i> -phenylphenothiazine
HAT	hydrogen atom transfer	r.t.	room temperature
HOMO	highest occupied molecular orbital	Rh-6G	rhodamine 6G
HPLC	high performance liquid chromatography	SCE	saturated calomel electrode
HRMS	high resolution mass spectrometry	SET	single electron transfer
		UV	ultraviolet

7.2 Calibration Data for HPLC Assays

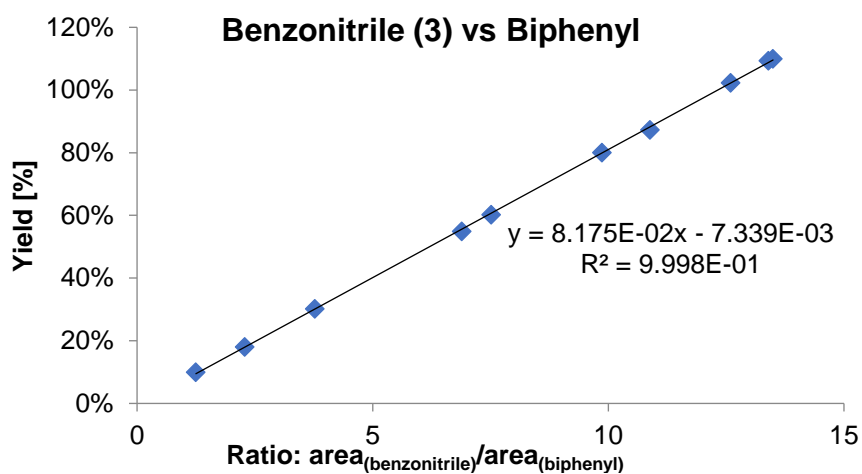


Figure 30. HPLC calibration curve: benzonitrile **3** vs biphenyl at 230 nm using HPLC method 1.

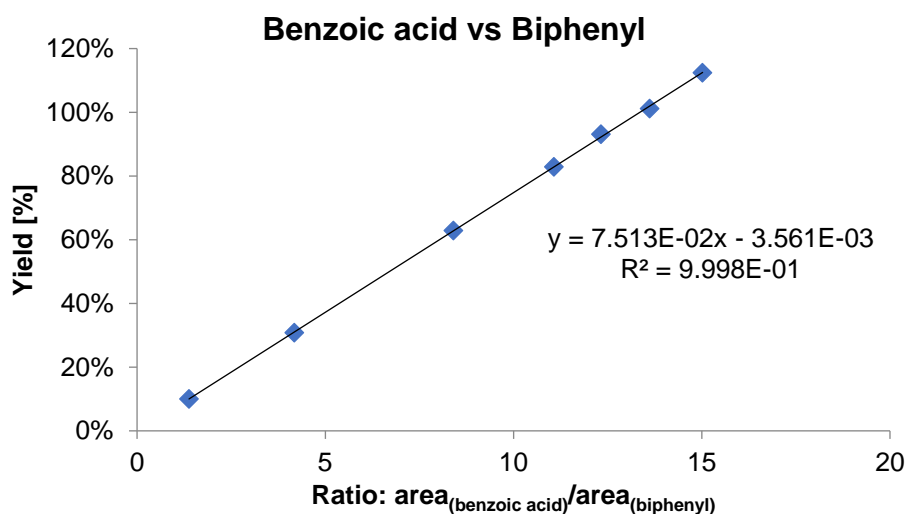


Figure 31. HPLC calibration curve: benzoic acid vs biphenyl at 230 nm using HPLC method 1.

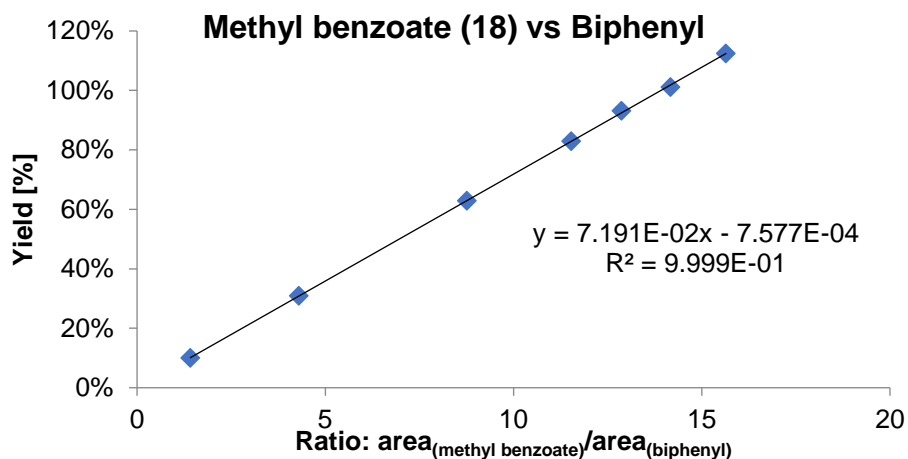


Figure 32. HPLC calibration curve: methyl benzoate **18** vs biphenyl at 230 nm using HPLC method 1.

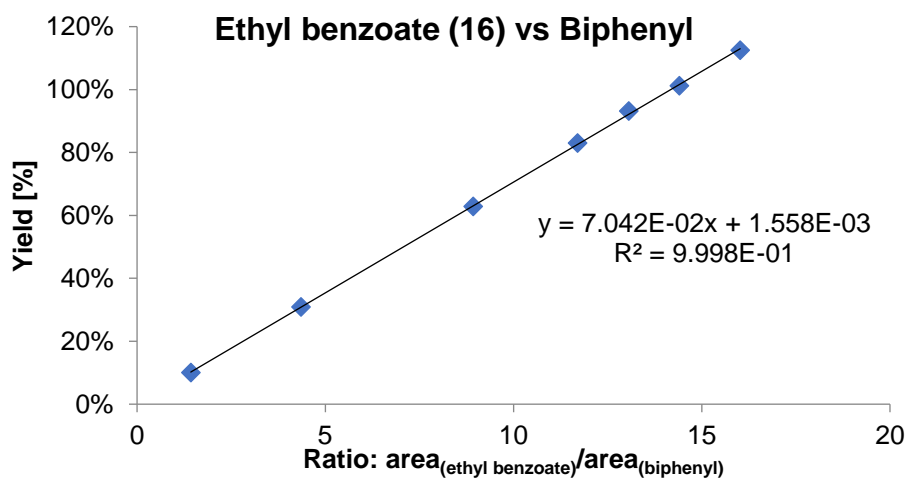


Figure 33. HPLC calibration curve: ethyl benzoate **16** vs biphenyl at 230 nm using HPLC method 1.

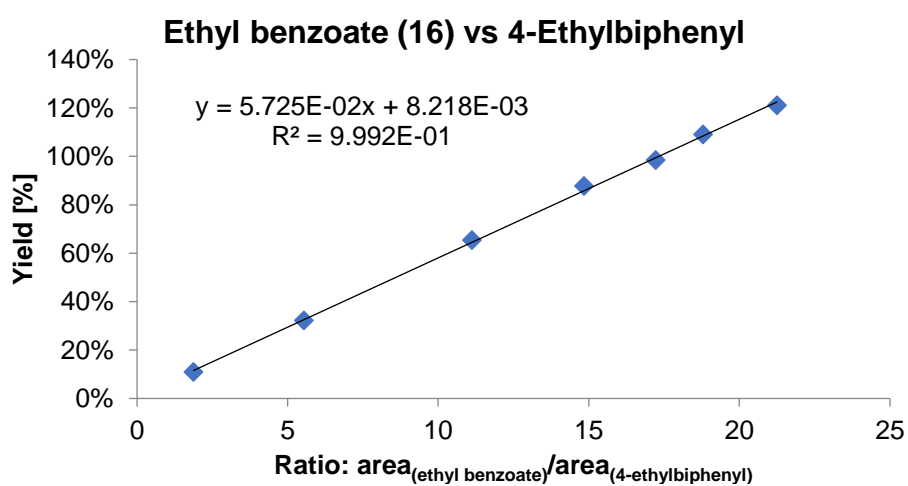


Figure 34. HPLC calibration curve: ethyl benzoate **16** vs 4-ethylbiphenyl at 230 nm using HPLC method 1.

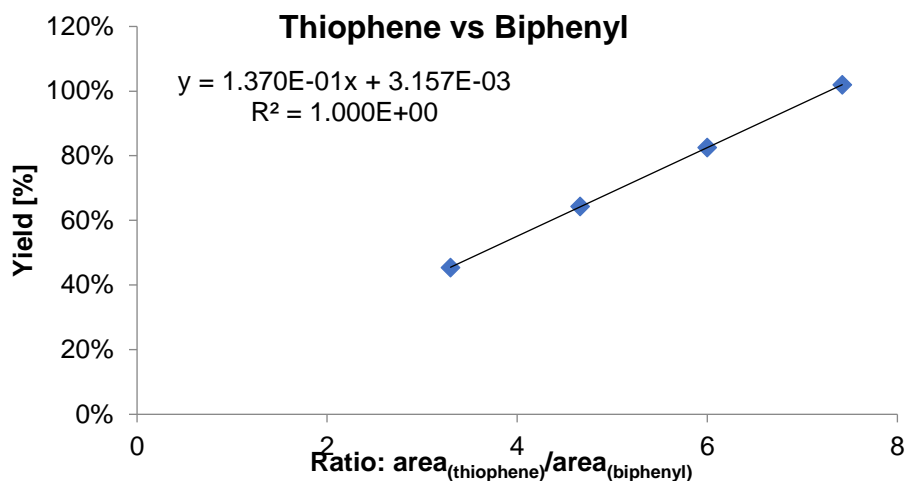


Figure 35. HPLC calibration curve: thiophene vs biphenyl at 230 nm using HPLC method 1.

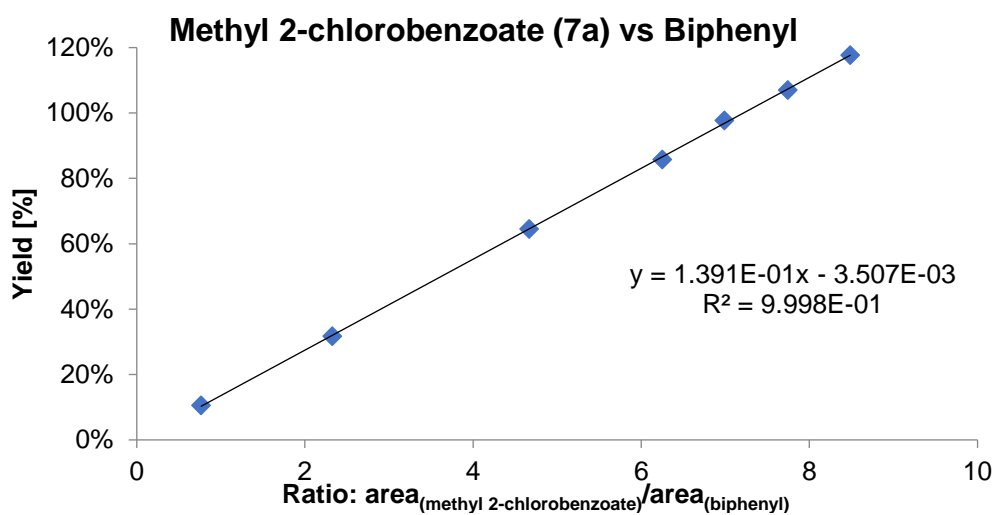


Figure 36. HPLC calibration curve: methyl 2-chlorobenzoate 7a vs biphenyl at 230 nm using HPLC method 1.

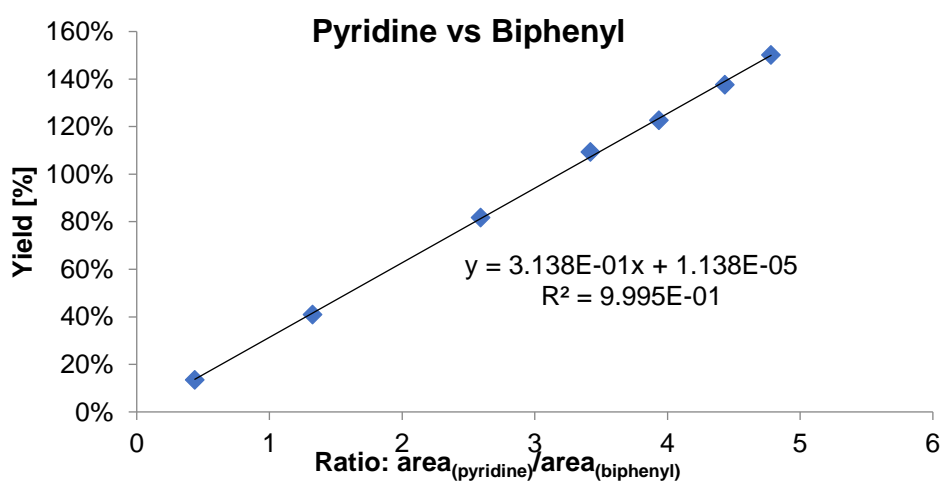


Figure 37. HPLC calibration curve: pyridine vs biphenyl at 254 nm using HPLC method 2.

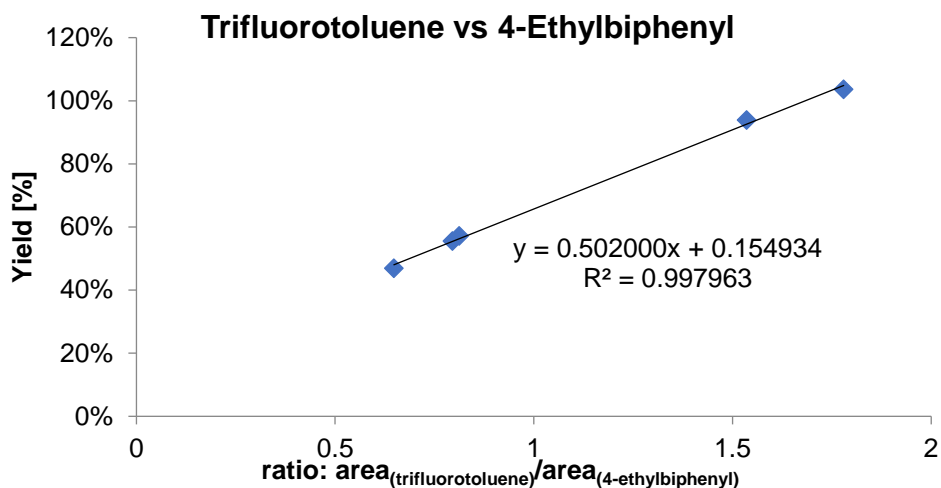


Figure 38. HPLC calibration curve: trifluorotoluene vs 4-ethylbiphenyl at 190 nm using HPLC method 1.

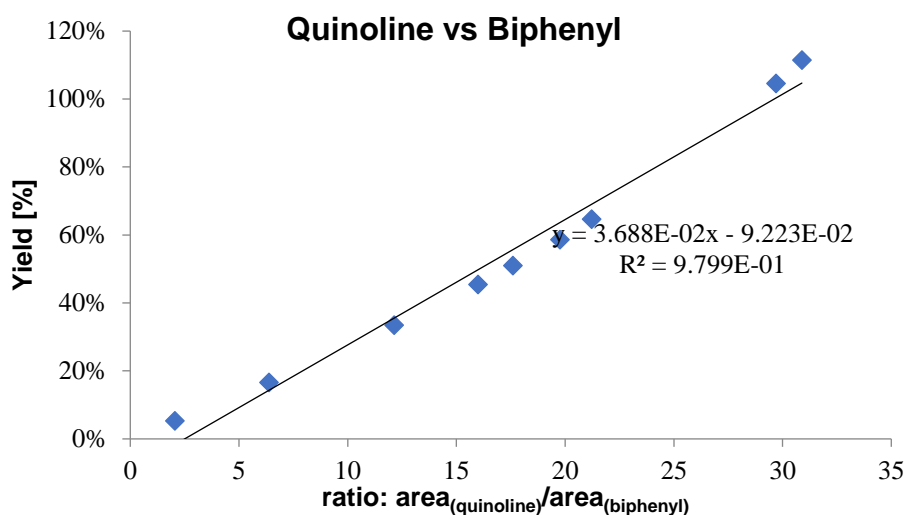


Figure 39. HPLC calibration curve: quinoline vs biphenyl at 230 nm using HPLC method 1.

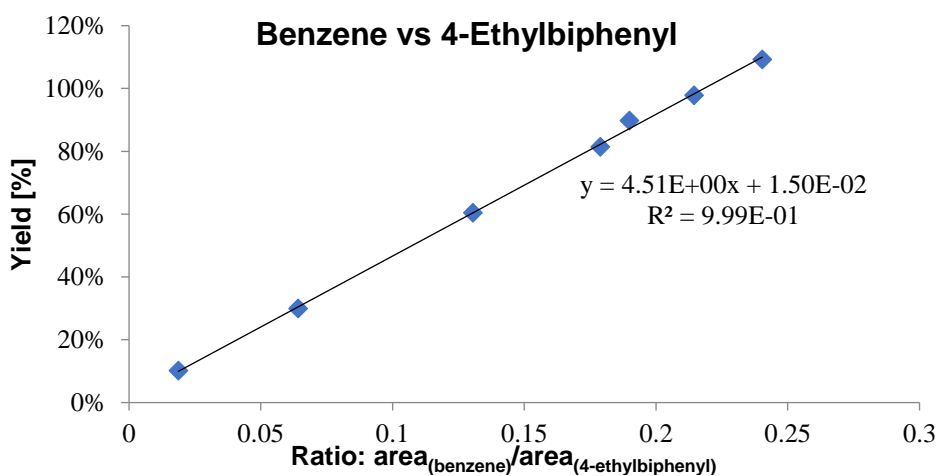
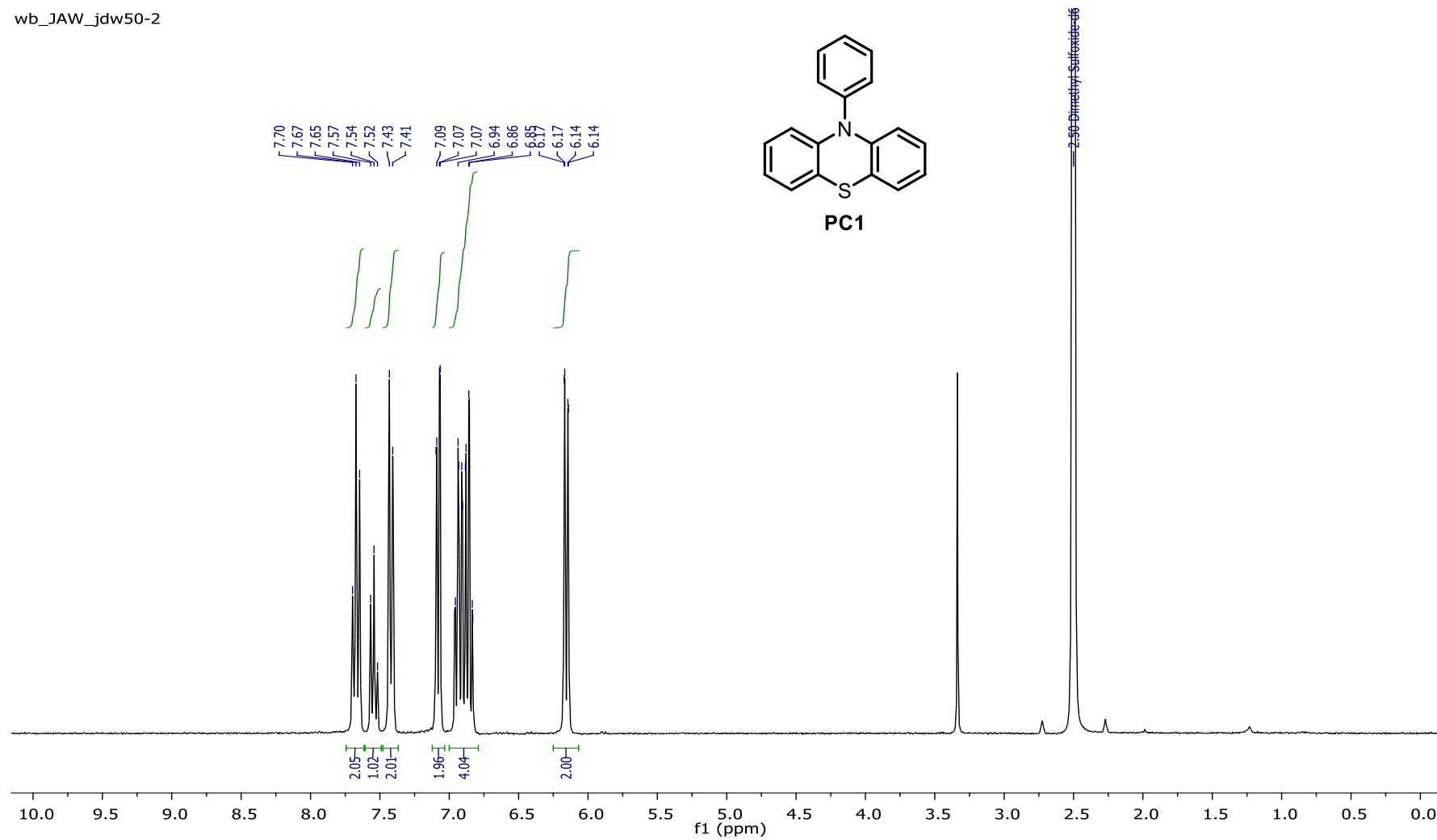


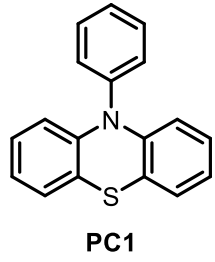
Figure 40. HPLC calibration curve: benzene vs 4-ethylbiphenyl at 215 nm using HPLC method 1.

7.3 NMR Spectra

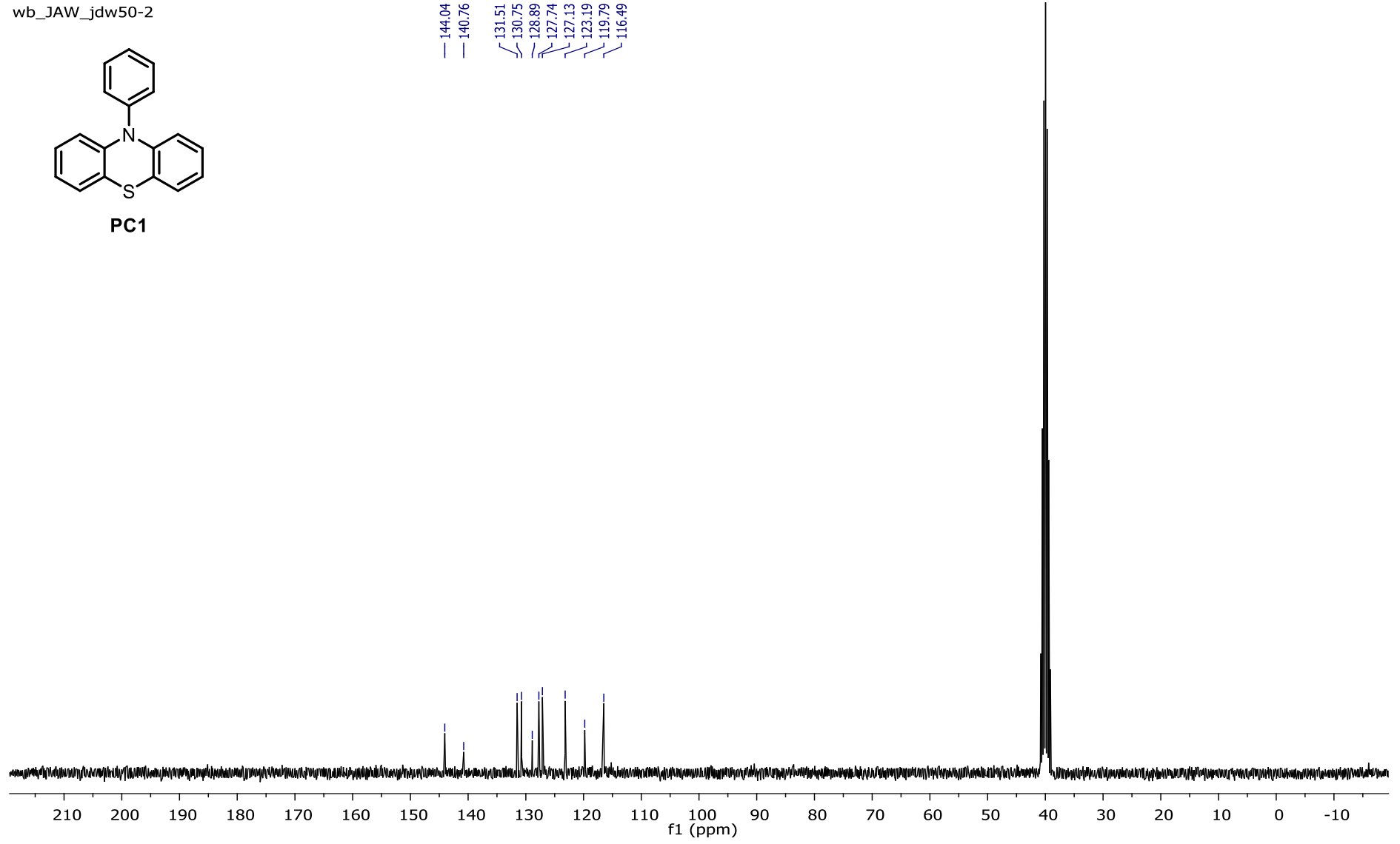
wb_JAW_jdw50-2

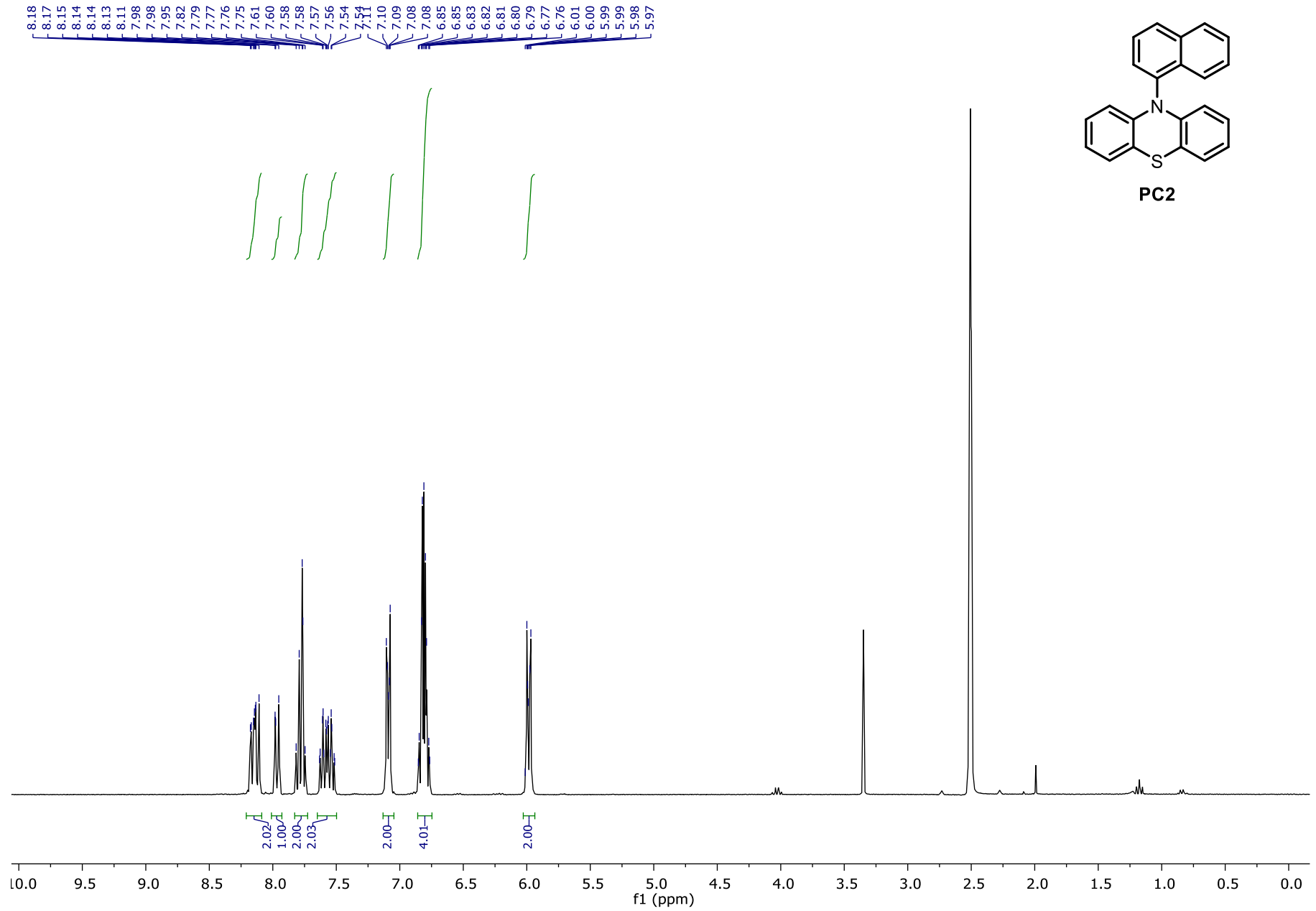


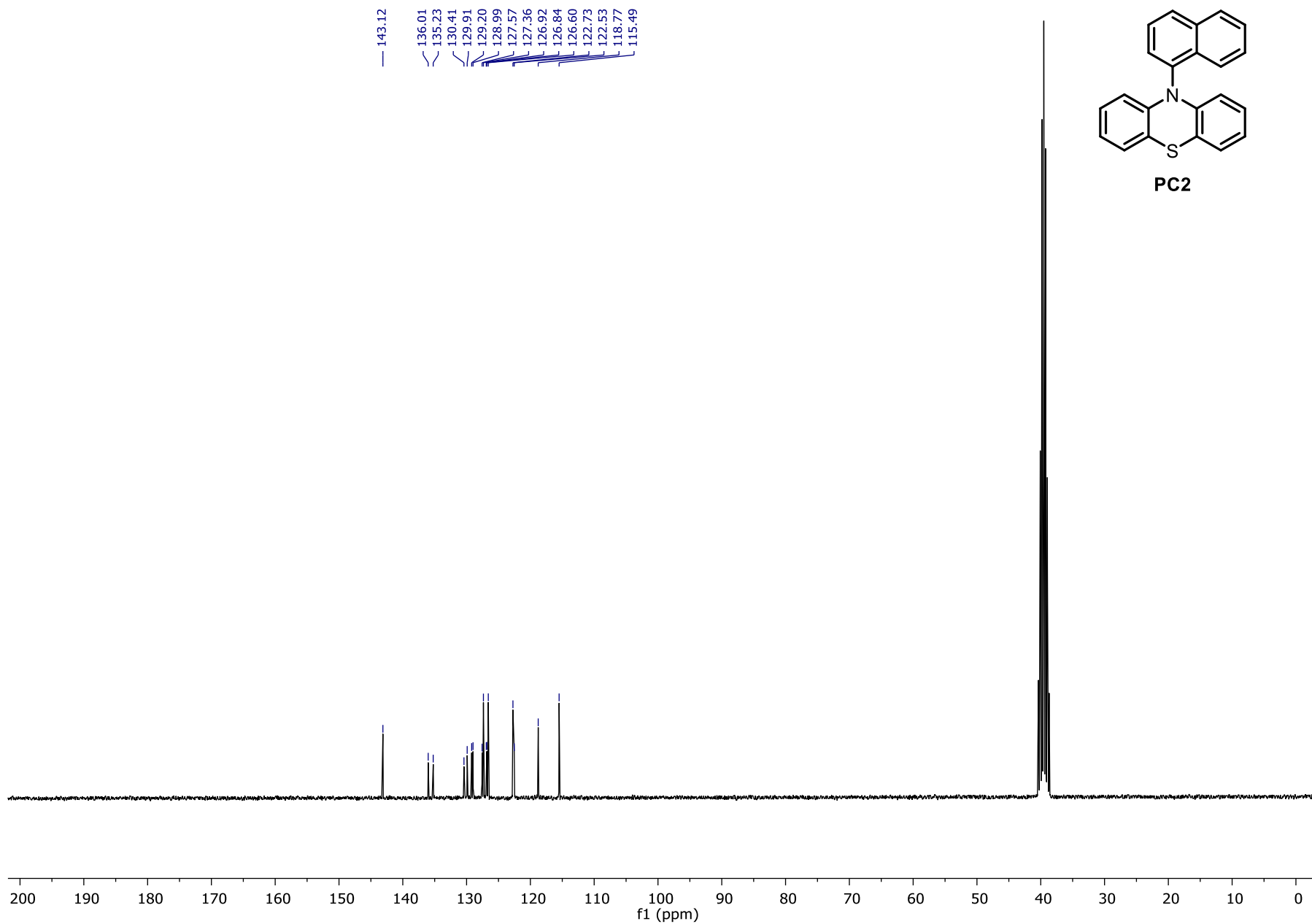
wb_JAW_jdw50-2



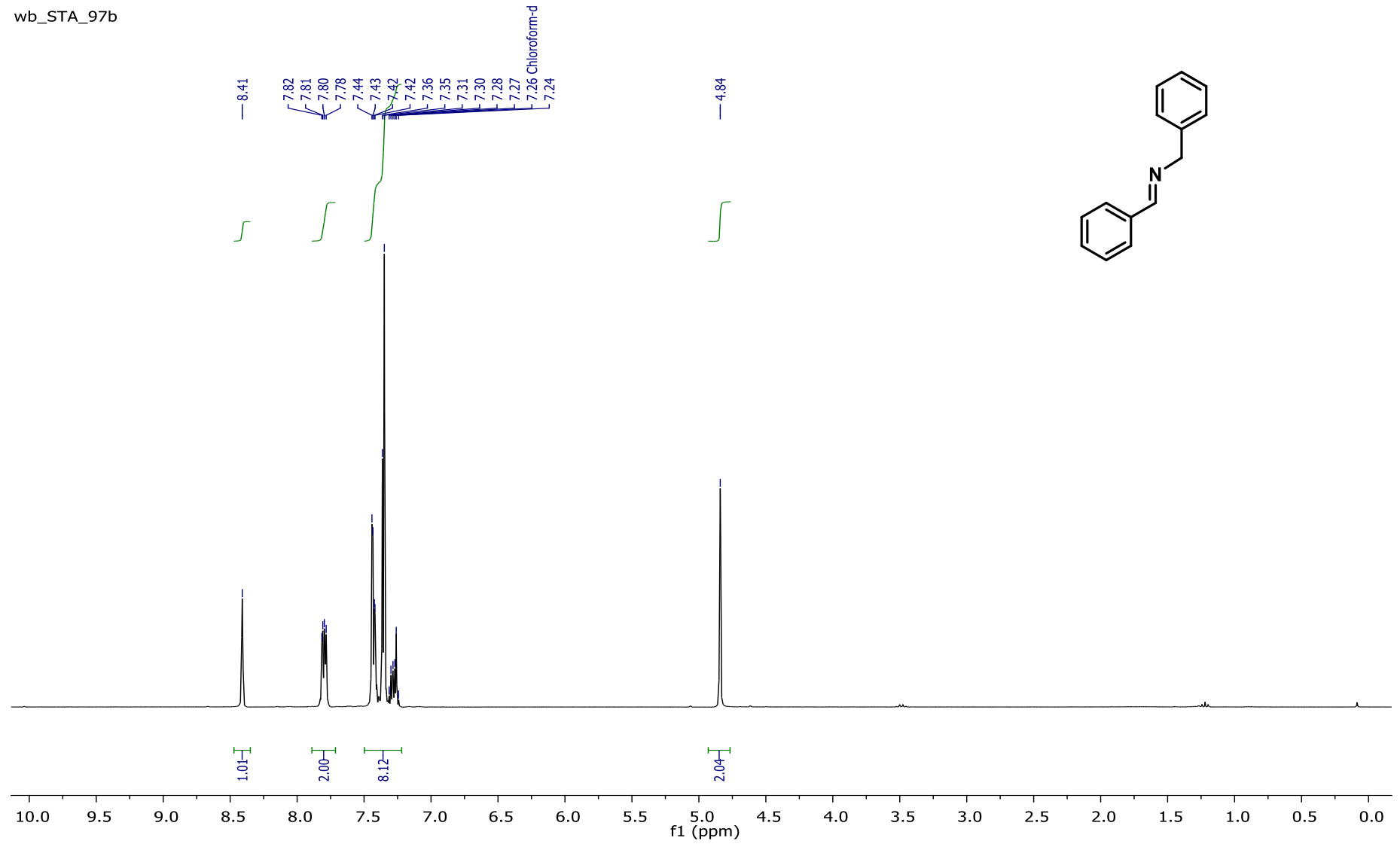
— 144.04
— 140.76
/ 131.51
/ 130.75
/ 128.89
/ 127.74
/ 127.13
/ 123.19
/ 119.79
/ 116.49



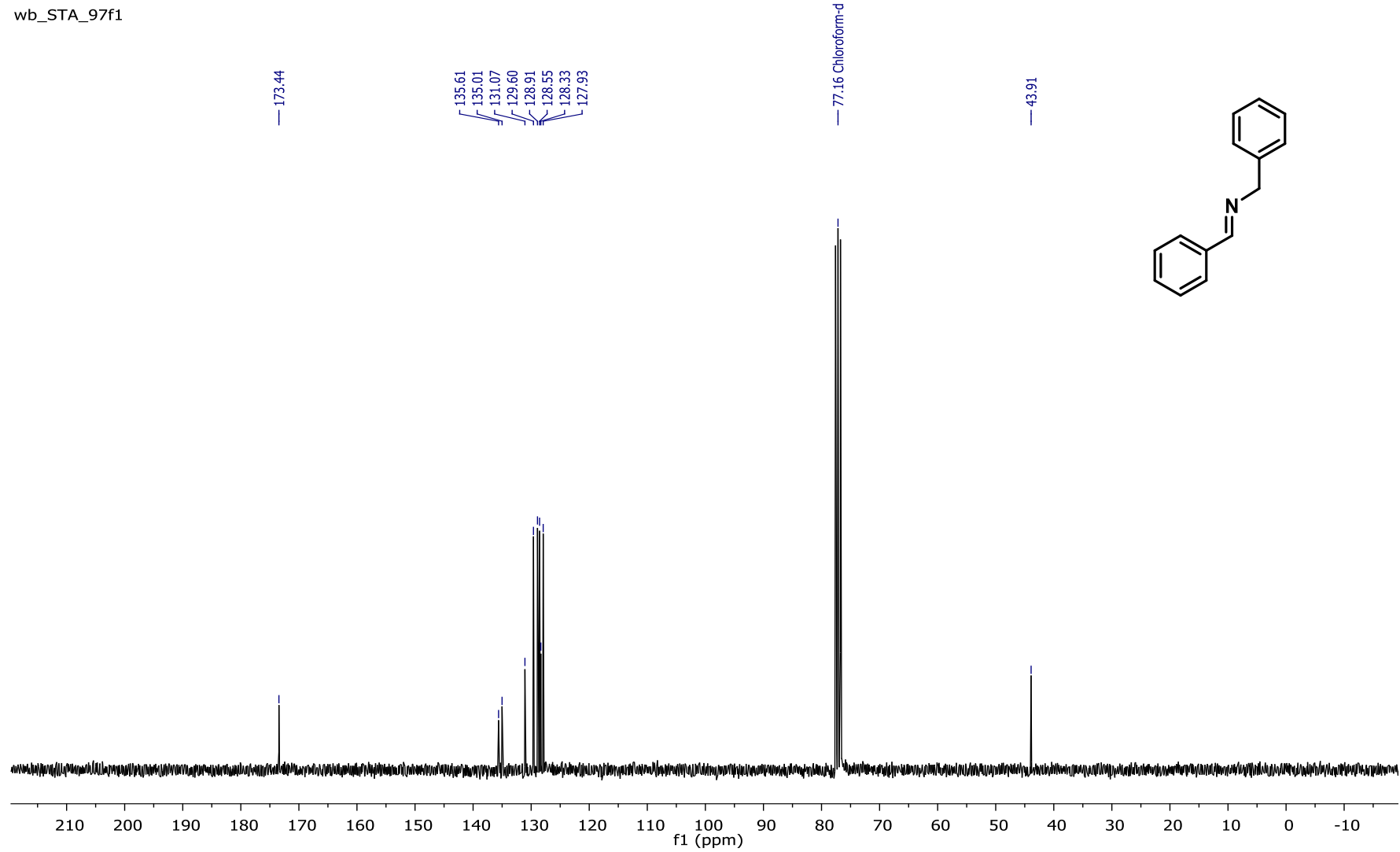


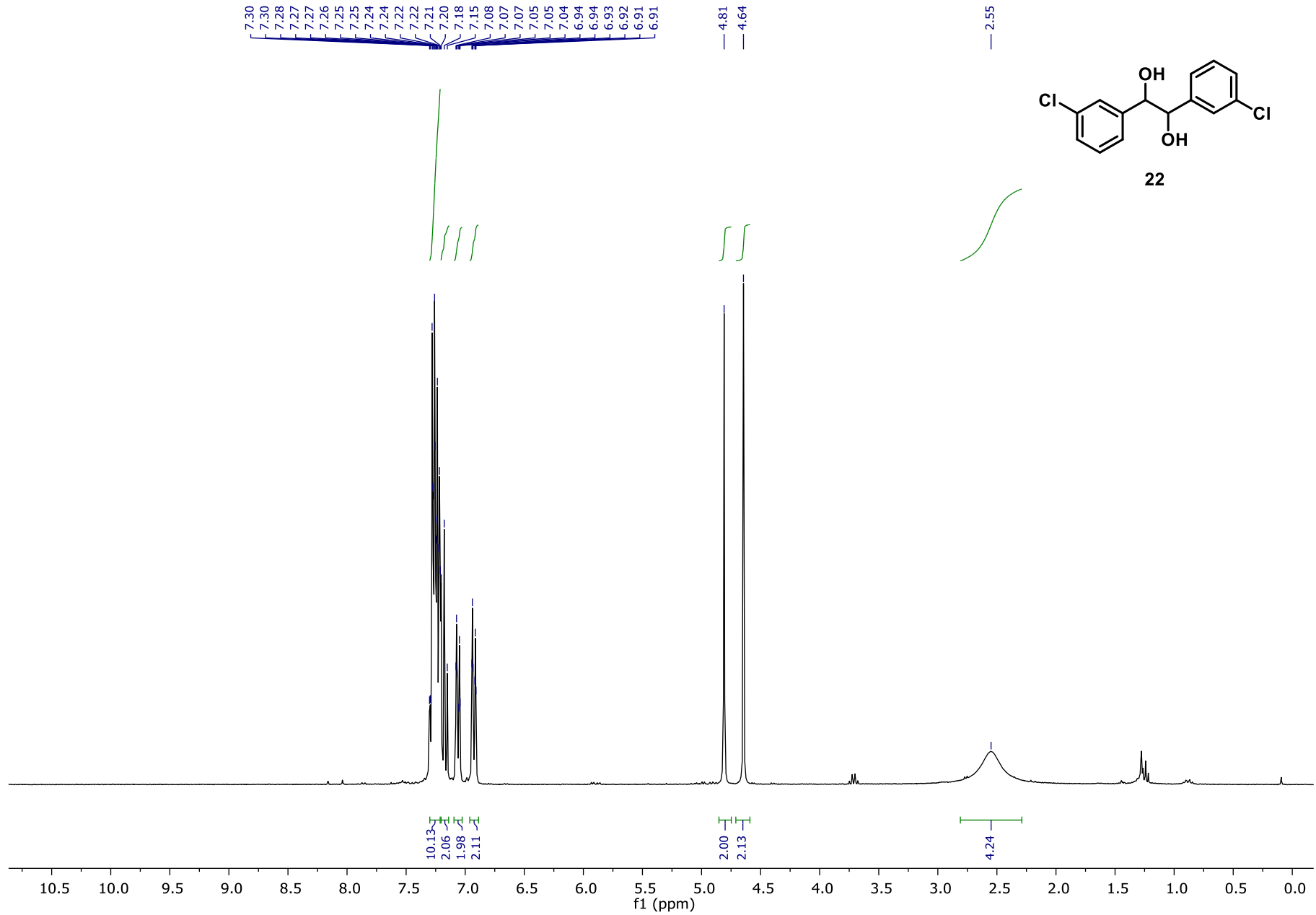


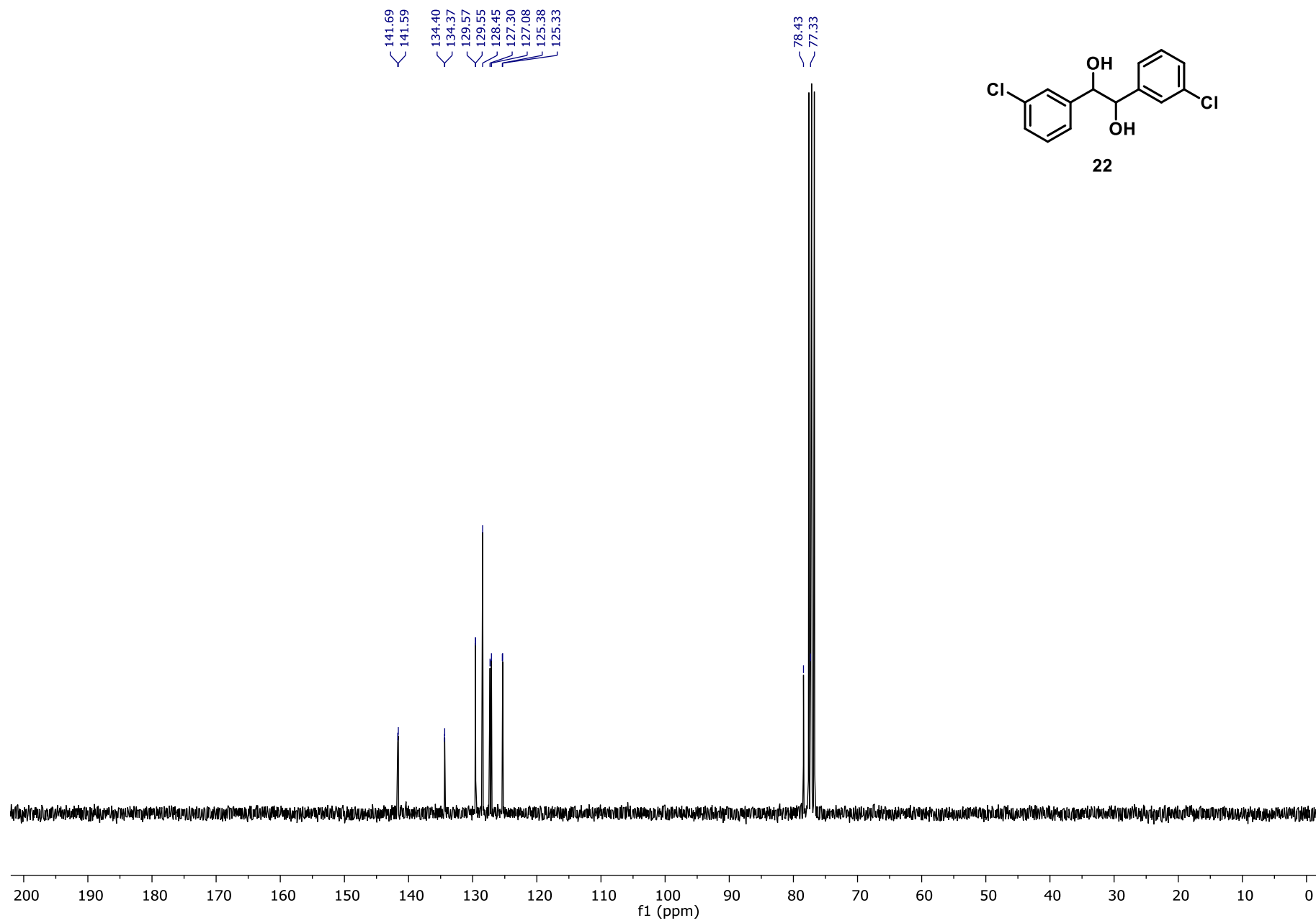
wb_STA_97b



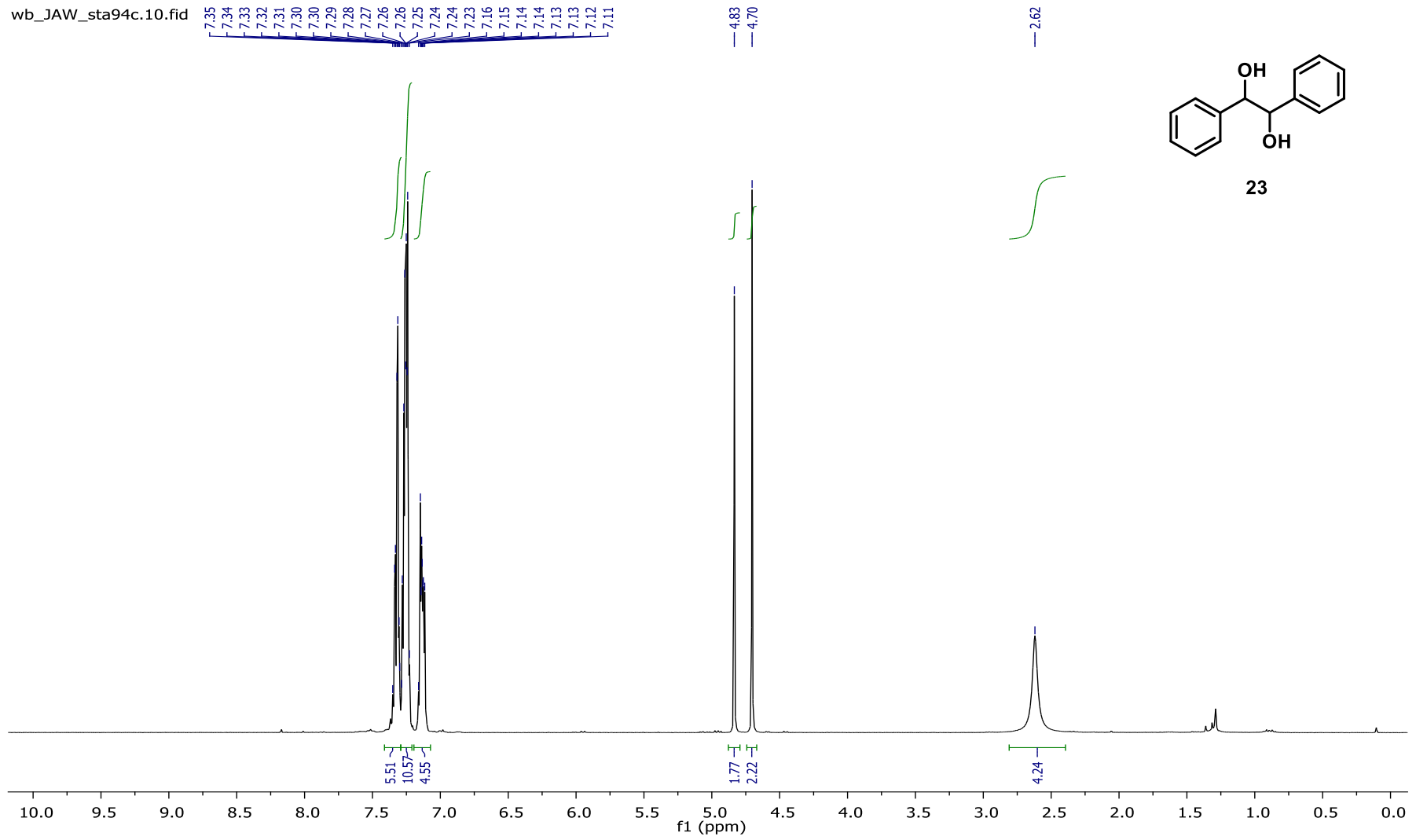
wb_STA_97f1



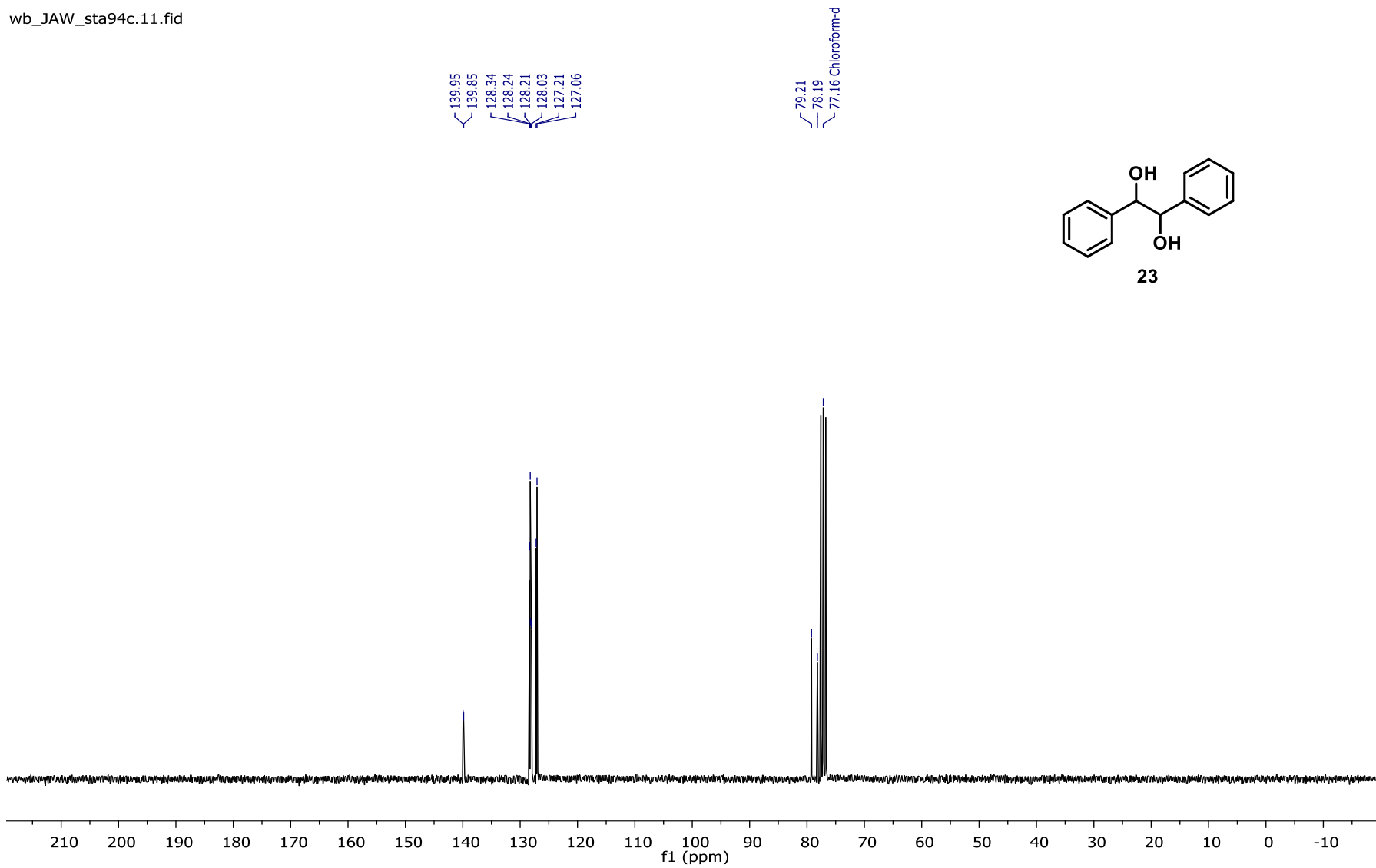




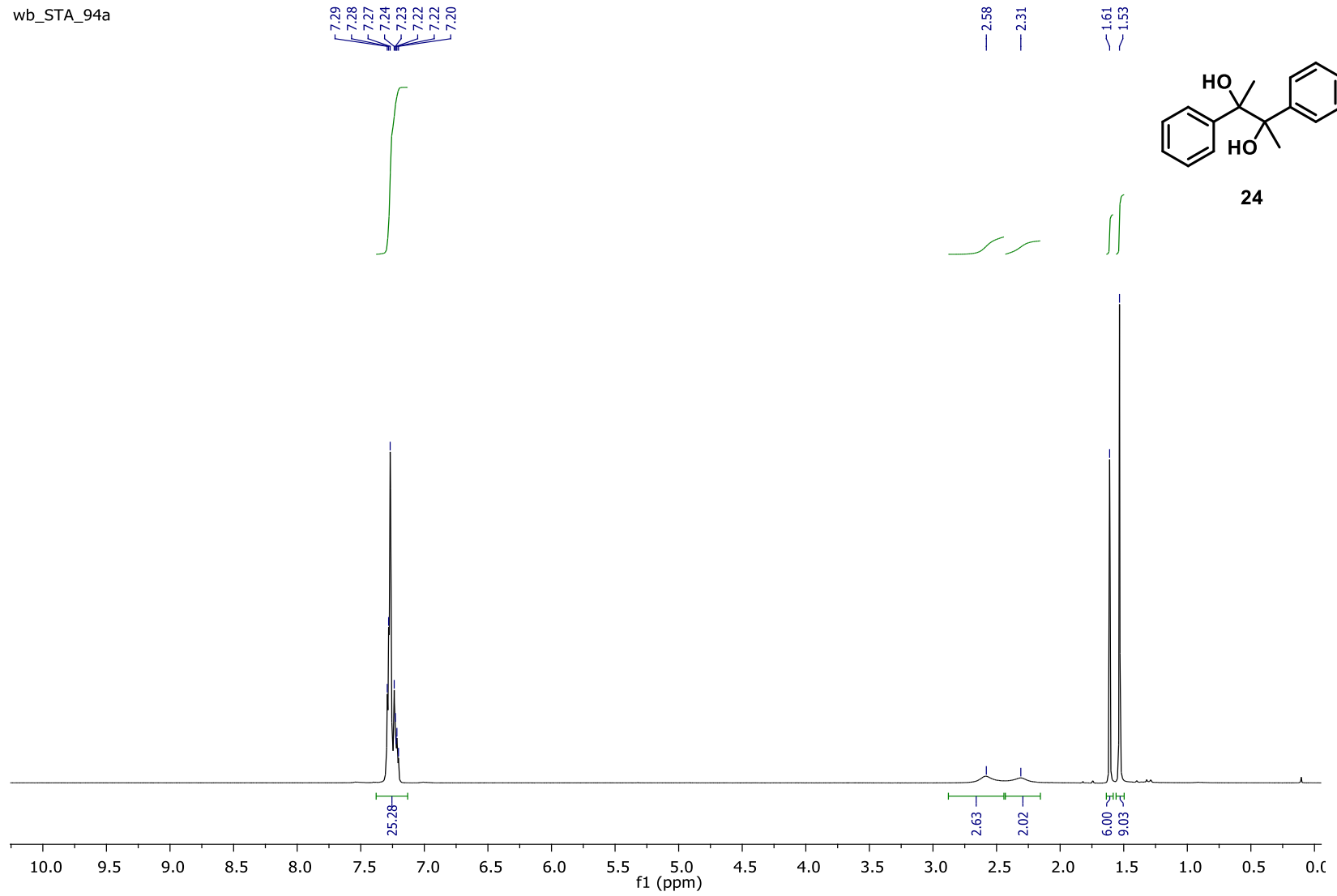
wb_JAW_sta94c.10.fid



wb_JAW_sta94c.11.fid



wb_STA_94a



wb_STA_94a

